EXHIBIT 405

STATE OF CALIFORNIA
California Energy Commission

In the Matter of: The Application for Certification for the **CALICO SOLAR PROJECT** (formerly SES Solar One)	Docket No. 08-AFC-13

REBUTTAL TESTIMONY OF BORIS POFF ON BEHALF OF CALIFORNIA UNIONS FOR RELIABLE ENERGY ON SOIL AND WATER RESOURCES FOR THE CALICO SOLAR PROJECT

July 29, 2010

Loulena A. Miles
Tanya A. Gulesserian
Adams Broadwell Joseph & Cardozo
601 Gateway Boulevard, Suite 1000
South San Francisco, CA 94080
(650) 589-1660 Voice
(650) 589-5062 Facsimile
lmiles@adamsbroadwell.com
tgulesserian@adamsbroadwell.com

Attorneys for the CALIFORNIA UNIONS FOR RELIABLE ENERGY

2309-076a

INTRODUCTION

The following rebuttal testimony is in response to the Supplemental Staff Assessment (SSA) prepared by CEC Staff (July, 2010), Opening Testimony prepared by the Applicant (June 30, 2010) and their attachments.

RESPONSE TO CEC'S SUPPLEMENTAL STAFF ASSESSMENT

The SSA fails to address several crucial aspects of the Soil and Water issues in the project area. As such, my comments on the SSA are focused on (1) the inadequate description and understanding of the affected environment in which the project is located (desert pavement and cryptobiotic crust); (2) the potential on and off-site impacts to these environments once disturbed; (3) the inadequate data collection, testing and modeling of these disturbances and impacts; (4) inadequate data from which to evaluate the impacts to the transmission upgrades required for the project; (5) insufficient data on the project water supply; and (6) insufficient consideration of the effects of climate change on the before mentioned areas of concern.

RESPONSE TO OPENING TESTIMONY BY APPLICANT (EXHIBITS 56, 74, 77)

Exhibits 56, 74 and 77 of the applicant's opening testimony are concerned with the water resources of the project. In particular exhibit 56 is the discussion and analysis of water supply in the Supplement to AFC, originally submitted on 5/14/10. Exhibit 76 is the testimony by RK Scott, which discusses the Applicant's proposed primary water source, the testing performed on that well, and the potential for significant adverse impacts on the local ground water. However, as mentioned below and pointed out in the SSA, important facts assumed therein are not supported by the exhibits. Exhibit 74, which is the testimony by M. Moore and provides a description of the surface water hydrologic setting for the project, inadequately addresses soils and water quality impacts due to erosion and sedimentation and proposes changes to the Conditions of Certification Soil&Water 3. The proposed changes to only monitor and inspect after year 10-year event could allow undesired and unacceptable erosion to go unchecked and unnoticed. Instead I believe that the Conditions of Certification proposed in the SSA provide enough guidance to mitigate those impacts Staff has envisioned. However, because of the gross inadequacy of the description of the affected environment and consequently inadequate description of the potential impacts, most of the Conditions of Certification are inadequate as well.

INADEQUACY IN DESCRIPTION OF THE AFFECTED ENVIRONMENT

Elements of the environmental setting were grossly inadequate, and as such, limited the description of the project impacts, hindered the impact analyses, and ultimately undermined the adequacy of the proposed mitigation. As pointed out in the SSA the "current soil survey data is limited in much of the Mojave Desert due to the lower potential for agricultural use. Detailed soil mapping has not been performed by NRCS for the site. However, soil mapping in the general area is being conducted by NRCS." I happen to be on the steering committee for the NRCS mapping effort in the Mojave National Preserve, which is located mostly east of the project site. Two environmental settings that are found on the project site and are of special concern to the NRCS because they are poorly understood are:

1. Desert pavement and its influence on hydrologic and sedimentation processes (which was not acknowledged or analyzed); and
2. Cryptobiotic crust and its influence on hydrologic and sedimentation processes (which was not acknowledged).

DESERT PAVEMENT

It is my opinion that the physical properties of the desert pavement at the site have neither been adequately nor correctly characterized by the Applicant or Staff. Any alterations to the desert pavement and distinct geomorphic surfaces across the project site have the potential to dramatically affect infiltration and runoff compared to the existing conditions (Sharifi et al. 1999, Okin et al. 2000, Okin 2002) (also see Figures 1 and 2) resulting in potentially significant impacts to water quality, sedimentation and biological processes through the degradation of the washes. The applicant is relying on information on the formation of desert pavement from a *biology* report (PWA 2010). This report incorrectly describes the formation of desert pavement as "fine sediment [that] has been selectively scoured away by wind or water action over time." Instead of erosion, desert pavement is created by the slow accumulation of soil below the evolving stone pavement, as described in a series of papers in the scientific literature (e.g., McFadden et al. 1987, Wells et al. 1995. Anderson et al. 2002) which studied the development of desert pavements in the Mojave Desert (along Kelbaker Road between Kelso and Baker, San Bernardino County in the Cima volcanic field just north of the project site).

It is important to fully understand the existing conditions in order to be able to identify the potential impacts, which will be dramatically different in a "crust" that evolved from erosion compared to top layer that is created by accumulation. A crust that was created through erosion will just erode further once disturbed. Whereas a crust formed by accumulation will cease to accumulate once disturbed and begin erosion instead, and drastically add sediment to the run-off process. Further, the proper understanding of the evolution of desert pavement directly ties into the understanding of its resilience and self healing abilities to minor anthropogenic disturbances. Major disturbances, such as those related to construction and corresponding erosion may lead to the crossing of thresholds where desert pavement may never again recover. However, minor disturbances may restore themselves over centuries if the mature Av horizon (eolian material that accumulates at the surface of desert soils, most often beneath a desert pavement) remains intact (Pelletier et al. 2007). In the context of project construction and subsequent maintenance activities (i.e., servicing the Power Conversion Unit, monthly mirror washing, etc.), this is unlikely to occur. Even shallow grading, as proposed in this project, will disturb the desert pavement and leave the Av horizon exposed to erosion (Okin et al. 2000). Under such a condition, while it has been observed that there are no statistical differences in the short term runoff characteristics with the clast cover removed (Chen et al. 2009), it has been observed that sediment production from the impacted surface can be significant over time (see Figures 1 and 2).

The increased sedimentation from the grading activities as well as from the placement of solar arrays directly in the washes would significantly impact the morphology of the washes, and subsequent delivery of runoff laden with very fine sediments (i.e., clays and silts) farther downstream. There, this fine material is likely to be picked up and transported off-site by winds (Okin et al 2000). Additionally, deep grading, another potential impact of the proposed project, will likely destroy the Av horizon and locally increase infiltration, decrease runoff, increase transmission losses, and significantly impact the movement of soluble salts from the leach zone beneath the desert pavement. Depending on the desert pavement type and the level of disturbance to the leach zone (climate change or human disturbance), increased infiltration and transmission losses could drive soluble salts downward into the groundwater, thereby increasing groundwater salinity (Graham et al. 2008). Furthermore, disturbance of the desert pavement could have significant indirect impacts on neighboring pavement types and established vegetation, since vegetation is linked to pavement type, clast cover, and influenced by proximity to leached soluble salts (Wood et al. 2005).

CRYPTOBIOTIC CRUST

Although a detailed surface soils assessment, including identification of the presence of a cryptobiotic crust, was not undertaken, it is highly likely that cryptobiotic crust is widespread across the site. Cryptobiotic crust, which is very common and widely distributed across desert landscapes, plays an important role in making nitrogen available to desert plants (Wohlfahrt et al. 2007). I have personally encountered cryptobiotic crust at similar elevations and in locations comparable and close to the project site as well as in other areas throughout the Mojave Desert. In my opinion the impacts to the cryptobiotic crust were not analyzed, nor were mitigation techniques provided.

The cryptobiotic crust[1] is a highly specialized community of cyanobacteria, mosses, and lichen and are prevalent in the project area. The living organisms present in the desert soils create a surface crust of soil particles bound together by organic material. The thickness of these crusts can reach up to 10 cm. The crusts are important members of the desert ecosystem and contribute to the well-being of other plants by stabilizing sand and dirt, promoting moisture retention, and fixing atmospheric nitrogen. Because of their thin, fiberous nature, cryptobiotic soils are extremely fragile systems. Some species in the soil can recover within a few years of disturbance, but slow growing species may require more than a century to recover.

Disruption of the crust will result in decreased organism diversity, soil nutrients, stability, and organic matter. The crusts significantly aid infiltration of precipitation and anthropogenic disturbance can dramatically increase surface runoff and increase the rate of soil loss by an order of magnitude. These increases in sediment laden runoff could significantly impact the morphology of the existing washes. Also, wind erosion is substantially more prevalent with disruption of the crust. Crusts that may remain intact downstream of the project site will inevitably be buried (and therefore permanently impacted) through windblown and water transported erosion.

INADEQUACY IN DESCRIPTION OF PROJECT IMPACTS

The applicant and the SSA failed to adequately analyze or describe project impacts. This failure is partially due to the failure to consider and describe important elements of the project setting.

Sedimentation and Morphology

The SSA concluded that morphological impacts to the washes would be significant due to increased sedimentation from the solar arrays from soil erosion due to grading impacts and subsequent changes to the sediment transport character of the washes to include scour effects, created by the solar dish towers. Further the SSA pointed out that:

> "[T]he applicant's Draft Drainage, Erosion, and Sedimentation Control Plan [DESCP] may mitigate the potential on site project-related storm water and sediment impacts. However, the calculations and assumptions used to evaluate potential storm water and sedimentation impacts in the Draft Plan are imprecise and have limitations and uncertainties associated with them such that the magnitude of potential impacts that could occur cannot be determined precisely."

While staff drafted Conditions of Certification **SOIL&WATER-1, -2** and **-3** to define specific methods of design analysis, development of best management practices, and monitoring and reporting procedures to mitigate impacts related to flooding, erosion, sedimentation, and stream morphological changes, these Conditions of Certification do not take into consideration the potential increases in surface runoff from damaged desert pavement and cryptobiotic crust as described above. The consequences of their manipulation are either poorly understood or simply ignored by the applicant and the Staff. Hence, the

[1] http://www.soilcrust.org/crust.pdf.

SSA failed to adequately address the impacts of environmental modification and its potential to significantly change hydrologic characteristics (i.e., runoff duration, frequency, volume), which, in turn, can significantly degrade the washes.

However, in the SSA, Staff recognizes - and I concur - that while "the DESCP provides the plan for the use of BMPs to mitigate erosion and sedimentation impacts caused by site grading…the measures discussed in the DESCP… are generally effective on most projects, [and] Staff believes that the circumstances of the proposed project are unusual and require additional mitigation. Specifically, this is a very large project that will be constructed on active alluvial fans, which dramatically increases the potential for soil erosion."

If a developer were to put in 10 subdivisions (and this project site is larger), a standard project, DESCP would not be adequate to mitigate the impacts either for several reasons. The principle hazards associated with alluvial fan flooding are high velocity, debris-laden floods and debris flows with highly uncertain flow paths. The dynamic geologic nature and consequent unpredictability of alluvial fan flooding presents unique challenges in designing a DESCP. Highly erosive soils mixed with water, rocks and boulders can travel at speeds recorded at over 50 miles per hour (Miller 1989). Undeveloped alluvial fans permit the overland flow of large amounts of flood water and sediment. When an almost entire alluvial fan is converted into a huge industrial site with metal poles the dynamic of the flow paths and debris flow will change and should be adequately modeled before any effective DESCP can be conceived.
Further, Staff pointed out that:

> "[B]asins or other forms of flood protection have not been addressed for the three drainages that traverse private property near the center of the project and enter the proposed solar array. Impacts due to flooding in these areas are potentially significant without adequate mitigation. This leaves portions of the project subject to significant adverse impact due to flooding."

It should also be noted that *so far no designs to mitigate these potential flood-related impacts have been proposed*.

Additionally, the effective percent impervious cover (PIC) will increase under project conditions, in the aggregate, as a combination of site infrastructure (i.e., paved roads, building pads, solar disc footings), access road compaction, destruction of desert pavement and cryptobiotic crust, and application of soil binders. These aggregate changes in PIC were not adequately considered and can have a significant impact on the morphology of the washes. While small increases in effective PIC were perceived to be negligible in the SSA, small changes in effective PIC can result in significant impacts to onsite and offsite resources if not properly accounted for in the analyses supporting the project.

Air/Water Quality
The applicant and Staff did not consider the water quality impacts of runoff laden with sediment from degraded desert pavement and cryptobiotic crust delivered downstream and offsite, as well as the potential for the increased sediments to be transported offsite by wind.

The large-scale disturbance that is to occur on the geomorphic surfaces of the Project will lead to extensive new aeolian activity. Given the predominant southwestern wind direction, this will mean that a plume of sand, eroded from the disturbed area, will begin to extend from the southern edge of the Project. Okin et al. (2001a, 2001b, 2006, and 2009) have investigated the impacts of this sort of sand plume originating from disturbed soils on nearby vegetation communities that were not directly disturbed.

Of course, any disturbance of the soil surface that encourages increased aeolian activity in a soil with dust-sized (< 50 um) particles will also lead to the production of dust. The potential for the wind-driven impact on the area immediately downwind of the Project is a significant impact that was not considered.

INADEQUACY IN ANALYSIS OF DISTURBANCES AND IMPACTS

It is my opinion that the core analyses conducted by the applicant and integrated into the SSA are insufficient to adequately analyze the impacts. Therefore, there is no adequate basis to compare impacts to soil and water resources in the various alternatives.

The applicant completed a hydrologic study and hydraulic modeling of the major stream channels on the project site. The applicant has proposed the construction of large debris basins in channels upstream of the proposed solar array. The most recently-submitted design indicates that dams will be constructed to temporarily retain flows in the basins. The applicant has not submitted the comprehensive detail that staff would need to analyze the ability of the basins to retain maximum flows and protect the project from flooding. As a result, staff has recommended adoption of Conditions of Certification **GEO-2** and **-3**, which contain performance standards that ensure that the design of the debris basin dams will comply with current engineering practices and existing regulations and prevent significant impacts. Further, Staff states that any proposed design must comply with requirements set forth in Conditions of Certification **SOIL&WATER-1**, **-2**, **-3** and **-8**, to ensure that no adverse impacts due to flooding will occur. However, because the analysis of the disturbances and impacts are inadequate, these proposed Conditions of Certification are inadequate as well and should be expanded on.

Additional Surveys, Data Collection and Analysis Required

I believe that the current level and type of analysis provided by the applicant is insufficient. Failure to undertake additional surveys, data collection and analysis, and design of appropriate mitigation actions as described below will result in significant unmitigated impacts to the desert pavement and cryptobiotic soils, with corresponding dramatic increases in sediment and wind erosion, and significant impacts:

1. Perform rainfall/runoff/sediment yield plot studies on different geomorphic surfaces (perhaps at multiple proposed solar sites) under existing and project (with and without BMPs) conditions.
2. Justify and/or quantify desert pavement, cryptobiotic crust, and BMP effectiveness (especially the soil binders given their proposed broad application) on stabilizing soils and runoff generation, using empirical data if available, site testing, or sensitivity modeling.
3. Revise the soil loss calculations, using a GIS-based approach (several examples exist in the literature), and use the information (from the above recommendations) as input into the sediment transport model.
4. Confirm whether solar dish runoff under intense runoff will not concentrate below the bottom lip of the solar dish and initiate gully erosion.
5. Confirm whether access road cuts will not intercept and concentrate runoff, inducing gully erosion, especially if they coincide with backfilled trenches.
6. The sediment transport modeling must be completed with the appropriate inputs. 2D or 3D sediment transport modeling should be undertaken for existing and project conditions, to include all representative project elements (i.e., BMP effectiveness, solar dish towers in the washes, etc.). If this does not occur, there is not sufficient modeling to conclude that impacts from the project will be less than significant with proposed mitigation.

7. Long-term changes in fluvial morphology should be assessed within and downstream of the project site as a result of the project and also as a result of climate change. Long-term hydrologic simulations that may be required as short-term (or design flood) outcomes only provide a "snapshot" from the starting condition. The long term degradation of the project site as well as downstream washes is therefore likely to be underestimated.
8. Until further detailed sediment transport analyses suggest no significant impact, solar dish towers should not be constructed in the washes.

SOIL BINDERS AND LINEAR SEDIMENT BARRIERS

Soil binders are proposed to be used to treat soil erosion by wind and water. The erosion control plans in the DESCP suggest extensive use of soil binders throughout the project site with little specifics on the placement of linear sediment barriers. The potential impacts of the soil binders on the natural characteristics of the desert pavement (specifically soil infiltration, runoff generation, and soil erosion), in addition to specifics on binder deterioration and reapplication rates, and downslope flow convergence leading to gully erosion, was not investigated nor stated. As such, more information is needed pertaining to the use of soil binders.

It is noted here that placement of linear sediment barriers on a project of this scope is better left to the final phases of the design. However, the effectiveness of these treatments at controlling sediment needs to be quantified during the identification and analysis of Project impacts for use in the soil loss calculations. Final designs are not required to quantify the expected effectiveness of these treatments.

Transmission Lines

Another impact that was inadequately addressed by the Applicant and Staff is the proposed transmission corridor needed to transmit the power generated at Calico. The applicant identified 346 drainage features that would cross the existing and/or proposed transmission corridor simply sing Google Earth aerial images (SES 2008). The amount of actual drainages is likely higher. While transmission lines themselves, aside from their foundation and required lay-down areas for construction, do not usually impact the desert environment significantly, the roads associated with these transmission lines potentially do, especially when crossing desert pavement, drainage features and mountain ranges. These roads have the potential to alter drainage patterns, vegetation patterns and habitats (as a consequence of hydrologic alterations) (Belnap et al. 2008) and should be evaluated accordingly.

PROJECT WATER SUPPLY

I agree with the Staff that there is significant uncertainty in the long-term reliability of the proposed water supply. The applicant states in Exhibit 56 that "…the aquifer penetrated by the well can support water demands for the Calico Solar site during construction and the lifespan of its operations, and pumping of the well at the prescribed rates will have no significant impact to water levels in the area." However, this statement is based on inadequate and insufficient testing and mere speculation.

Specifically, on page 2-2 in Exhibit 56, URS states that a) the boundary of the aquifer "basin to the east is *not well documented*; the mountains may only provide a partial groundwater barrier"; and b) "Because there are no records of other wells or borings drilled to this depth in the basin, *the areal extent of the aquifer is not known*." c) "Natural recharge into the basin is estimated to be about 300 afy and the storage capacity of the aquifer has been estimated to be approximately 270,000 acre-feet (af). However, *little data exists to confirm these estimated values*…" Thus, the SSA does not provide any estimates of the aquifer's storage capacity due to the lack of data.

As shown in Soil & Water Table 2, Staff points out that the 300 afy of recharge used by the applicant is a number of unknown origin. However, staff opts to use the recharge figures of 200 – 400 afy as suggested by the USGS, using a GIS model. Further, staff chooses - for this particular project - to ignore the recharge value of 0 afy using Maxey-Eakin Method, which is a very commonly used method for the Mojave Desert. Basic aquifer basin balance mathematics suggests that output equals input. Given that there is 0 output, it would suggest that there is also 0 input. It is my professional opinion that the Maxey-Eakin Method is well established and should not be ignored just because the results are inconvenient for this Project.

In the Drawdown Analysis (Section 5.2.3 on page 5-4 in Exhibit 56) URS qualifies its conclusion by stating that "the geology in the area appears to be *variable and additional drawdown may occur* as a result of *long-term pumping effects*." Further, URS believes that "it is likely that the aquifer penetrated by Well #3 is not confined." While the rate at which Well #3 was tested (100 gpm - gallons per minute) was appropriate since the peak rate of water extraction for the project would be 93 gpm (for five years) (93 gpm = 150 acre feet/year) and 100 gpm is within the suggested +/- 10 percent of the pump rate, the duration for the test should have been 72 hrs for an unconfined aquifer instead of 24 hrs. The pump test for Well #1 (a step test up to 8 gpm instead of the expected Project usage of at least 93 gpm) was utterly inadequate for the project's water requirements.

Based upon the information provided in Exhibit 56, it is my professional opinion that it is irresponsible to consider Well #3 a reliable and primary water source for the Calico Solar project until additional monitoring wells on and offsite, in addition to adequate pump tests – as described above – can confirm the assumptions made by the applicant. It is my opinion that there are serious questions regarding the long-term viability of this water supply. I would recommend that this Project not be permitted without a back-up water supply and monitoring of the groundwater supply, as suggested by Staff's **SOIL&WATER-9**.

Further, although the Applicant did consider impacts to the zone of influence from potential groundwater drawdown as a result of Project pumping, the Applicant did so using inadequate and insufficient data as described above. Although the Applicant concluded that water extraction would have negligible impacts on water quantity, the Applicant failed to look at impacts relating to long-term water availability in the region and the need for a back-up water supply. Finally, none of these issues have been considered under a climate change scenario.

Cadiz Water Supply

I will not be providing an analysis of the Cadiz water supply, because the Applicant had asked the CEC not to consider this water supply in the application. However, should the Applicant change their mind I will submit testimony at that time.

CLIMATE CHANGE

Climate change can have an influential role in shaping the project's impacts on the environment in terms of hydrologic response and soil erosion. Provided that intense summer storms are responsible for a majority of the runoff that occurs at the project site, the Nature Conservancy Climate Wizard (http://www.climatewizard.org/) would suggest that summer rainfall in southeastern California may increase by as much as 50% by 2080 in the summer, which could be accompanied by significant increases in rainfall intensity and erosivity (Angel et al. 2005). Significant increases in rainfall quantity, intensity, and erosivity will have a profound impact on the landscape, especially on the morphology of the washes where solar dishes are proposed. Changes to the morphology of the washes would significantly impact the structural stability and flood preparedness of the solar dishes placed in the washes, coupled with increased sedimentation from the graded service roads as well as solar arrays. This large scale erosion will subsequently have significant air quality impacts to downwind resources if project design and BMPs

don't adequately incorporate the best scientific data available about future changes in the region's climate.

While rainfall intensity is predicted to increase, at the same time recharge is predicted to decrease for several reason. (1) Aquifer recharge in the Mojave Desert occurs mostly in the winter when rainfall events are low in intensity and long in duration. However, the shift from precipitation events occurring less in the winter and more in the summer will lead to more run-off and less infiltration, which equals less recharge. (2) Increased temperatures will lead to increased evapotranspiration, even if precipitation remains unchanged (Seager et al. 2007, Diffenbaugh 2008, Kerr 2008). See Figures 3 and 4. As shown in Figure 5, the increase in variability in precipitation patterns are already noticeable. While there have been distinct wet (1910s and 1940s) and dry (1920s and 1950s) periods over the past century, the wettest and driest years have already occurred this century (within the past 10 years).

Climate change, and its potential to amplifying project-related impacts on disturbed desert pavement, crytpobiotic crust and the project's water supply was not considered. In particular, for the project's water supply this could mean that the estimates for the aquifer recharge should be approximately 50% lower towards the end of the project lifespan.

Climate change, and its potential to amplify downstream/wind project-related impacts, such as erosion, sedimentation and dust creation, was not considered. Neither were the implications of less aquifer recharge by the predicted decrease in precipitation/infiltration. Amplification of project-related impacts means the impacts will be more severe and long-lasting under potential climate change scenarios.

REFEFRENCES CITED

Anderson, K., S. Wells, R. Graham. 2002. Pedogenesis of vesicular horizons: Cima Volcanic Field, Mojave Desert, California, *Soil Science Society of America Journal* 66:878-887.

Angel, J.R., M.A. Palecki, S.T. Hollinger. 2005. Storm precipitation in the United States. Part II: soil erosion characteristics. *J Applied Meteorology* 44:947-959.

Belnap, J. , Webb, R.H., Miller, D.M., Miller, M.E., DeFalco, L.A., Medica, P.A., Brooks, M.L., Esque, T.C., and Bedford, D.R. 2008. Monitoring ecosystem quality and function in arid settings of the Mojave Desert: U.S. Geological Survey Scientific Investigations Report 2008-5064, 119 p.

Chen, Li, J. Yin, J. Miller, M. Young. 2009. The role of the clast layer of desert pavement in rainfall-runoff processes. *In World Environmental and Water Resources Congress 2009.*

Diffenbaugh, N. S., F. Giorgi, J. S. Pal. 2008. Climate change hotspots in the United States. *Geophys. Res. Lett.*, 35

Graham, R.C., D.R. Hirmas, Y.A. Wood, C. Amrhein. 2008. Large near-surface nitrate pools in soils capped by desert pavement in the Mojave Desert, California. *Geology* 36:259-262.

Kerr R.A. 2008. Global Warming Climate Change Hot Spots Across the United States. *Sci.* 321:909

McFadden, L.D., S.G. Wells, M.J. Jercinovich. 1987. Influences of eolian and pedogenic processes on the origin and evolution of desert pavements. *Geology* 15:504-508.

Miller. 1989. *USGS Bulletin 1847.*

Okin, G.S., B. Murray, W.H. Schlesiger. 2000. Degradation of sandy arid shrubland environments: observations, process modelling , and management implication. *J Arid Environments*, 46: 000-000, doi: 10.1006/jare.2000.0711, available online at http://www.ideallibrary.com.

Okin, G. S., B. Murray, and W. H. Schlesinger. 2001a. Desertification in an arid shrubland in the southwestern United States: Process modeling and validation, in Land Degradation: Papers Selected from Contributions to the Sixth meeting of the *International Geographical Union's Commission on Land Degradation and Desertification*, Perth, Western Australia, 20-28 September 1999, edited by A. Conacher, pp. 53-70, Kluwer Academic Publishers, Dordrecht.

Okin, G. S., B. Murray, and W. H. Schlesinger. 2001b. Degradation of sandy arid shrubland environments: observations, process modelling, and management implications, *J Arid Environments* 47:123-144.

Okin, G.S. 2002. Toward a Unified View of Biophysical Land Degradation Processes in Arid and Semi-arid Lands, in *Global Desertification: Do Humans Cause Deserts?* J.F. Reynolds & D.M. Stafford Smith, eds. Dahlem University Press, Berlin, pp. 95-109.

Okin, G. S., J. E. Herrick, and D. A. Gillette (2006), Multiscale controls on and consequences of aeolian processes in landscape change in arid and semiarid environments, *J Arid Environments* 65:253-275.

Okin, G. S., A. J. Parsons, J. Wainwright, J. E. Herrick, B. T. Bestelmeyer, D. P. C. Peters, and E. L. Fredrickson. 2009. Do changes in connectivity explain desertification? *Bioscience* 59: 237-244.

Pelletier, J.D., M. Cline, S.B. DeLong. 2007. Desert pavement dynamics: numerical modeling and field-based calibration. *Earth Surface Processes and Landforms* 32:1913-1927.

PWA, 2010. *Geomorphic Assessment of Calico Solar Project Site – Draft Appendix A (Biology Report).* Philip Williams & Associates, Ltd. San Francisco, CA. p.25.

Sharifi, M., A. Gibson, P. Rundel. 1999. Phenological and physiological responses of heavily dusted creosote bush (*Larrea tridentate*) to summer irrigation in the Mojave Desert. *Flora*, 194: 369-378.

Seager, R., M. Ting, I. Held, Y. Kushnir, J. Lu, G. Vecchi, H.P. Huang N. Harnik, A. Leetmaa, N.C. Lau, C. Li, J. Velez, N. Naik. 2007. Model Projections of an Imminent Transition to a More Arid Climate in Southwestern North America. *Sci.* 316: 1181-1184.

SES 2008 – Stirling Energy Systems/R. Liden (tn 49181). Application for Certification, dated December 1, 2008. Submitted to CEC/Docket Unit on December 1, 2008. Wells, S. G., L. D. McFadden, J. Poths, and C. T. Olinger. 1995. Cosmogenic 3He surface-exposure dating of stone pavements: implications for landscape evolution in deserts. *Geology* 23:613-616.

Wood, Y.A., R.C. Graham, & S.G. Wells. 2005. Surface control of desert pavement pedologic process and landscape function, Cima Volcanic field, Mojave Desert, California. Catena 59:205-230.

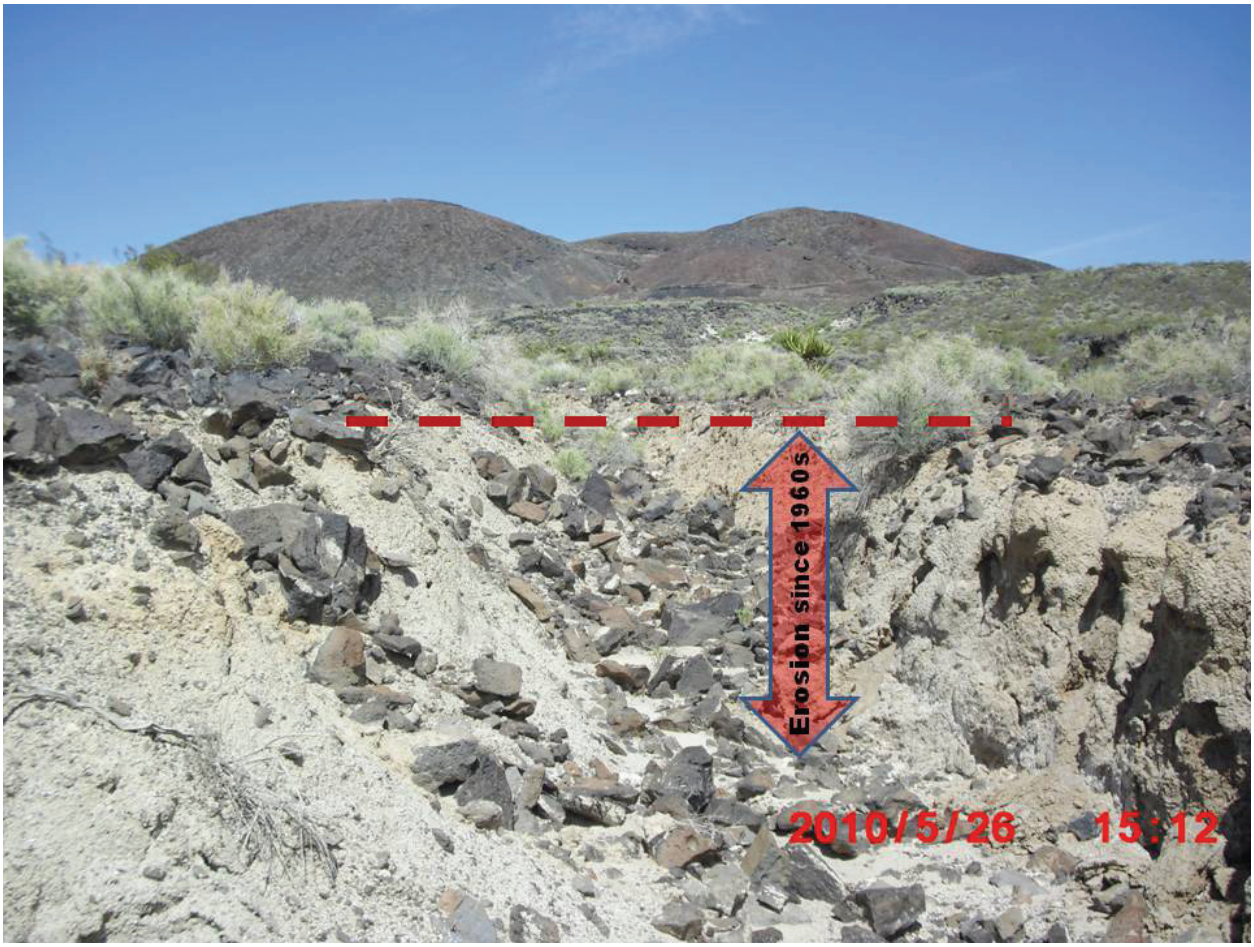

Figure 1: Erosion caused by run-off along a mining road where desert pavement was removed in the 1960s. Here the top layer was simply bulldozed to the side exposing the accumulated Av Horizon. This mining road is located approx. 45 miles north-east of the project area. The pre-mining road conditions of this area were flat and uninterrupted.

Figure 2: As in the proposed project area, the desert pavement itself consists of a thin layer of rocks which has captured sand and dust over the millennia. Once the top layer is removed the accumulated sand, clay and silt below the desert pavement is easily eroded away as shown in this photo.

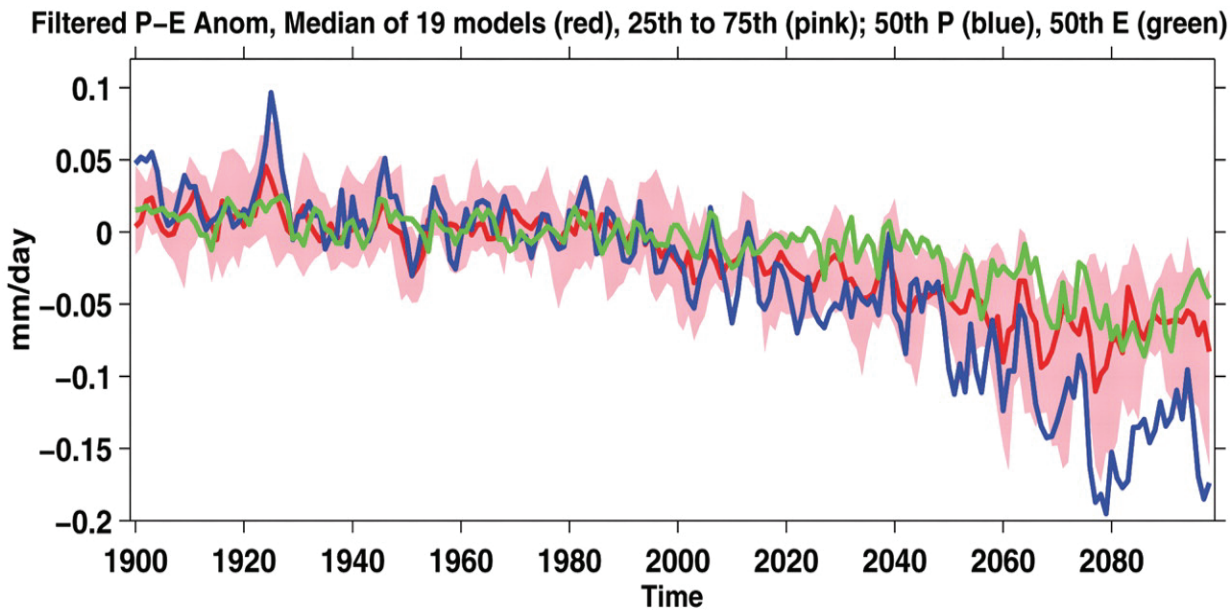

Figure 3: Modelled changes in annual mean precipitation minus evaporation over the American Southwest (125{degrees}W to 95{degrees}W and 25{degrees}N to 40{degrees}N, land areas only), averaged over ensemble members for each of the 19 models, from Seager et al., Science 316, 1181 - 1184 (2007).

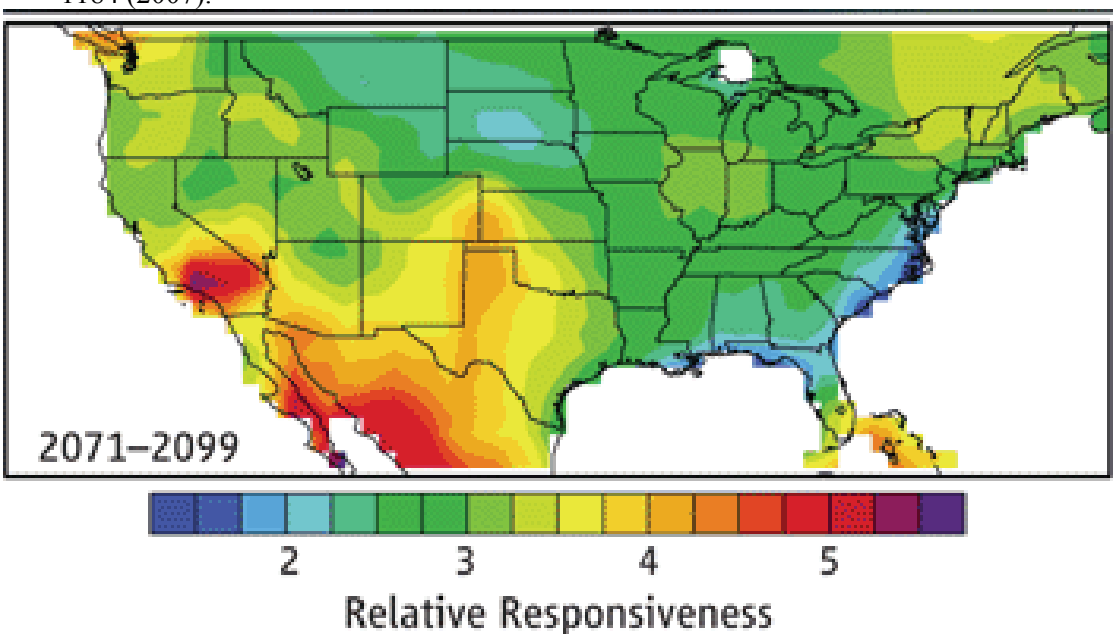

Figure 4: Results of 15 GCMs from the IPCC Fourth Assessment Report show areas of the southwestern United States and northern Mexico as the most persistent hotspots for climate change. Responsiveness of the southwestern hotspot comes from increased variability in precipitation from one year to the next (not from progressive warming or a long-term rise or fall in precipitation) (Diffenbaugh et al. 2008, Kerr 2008).

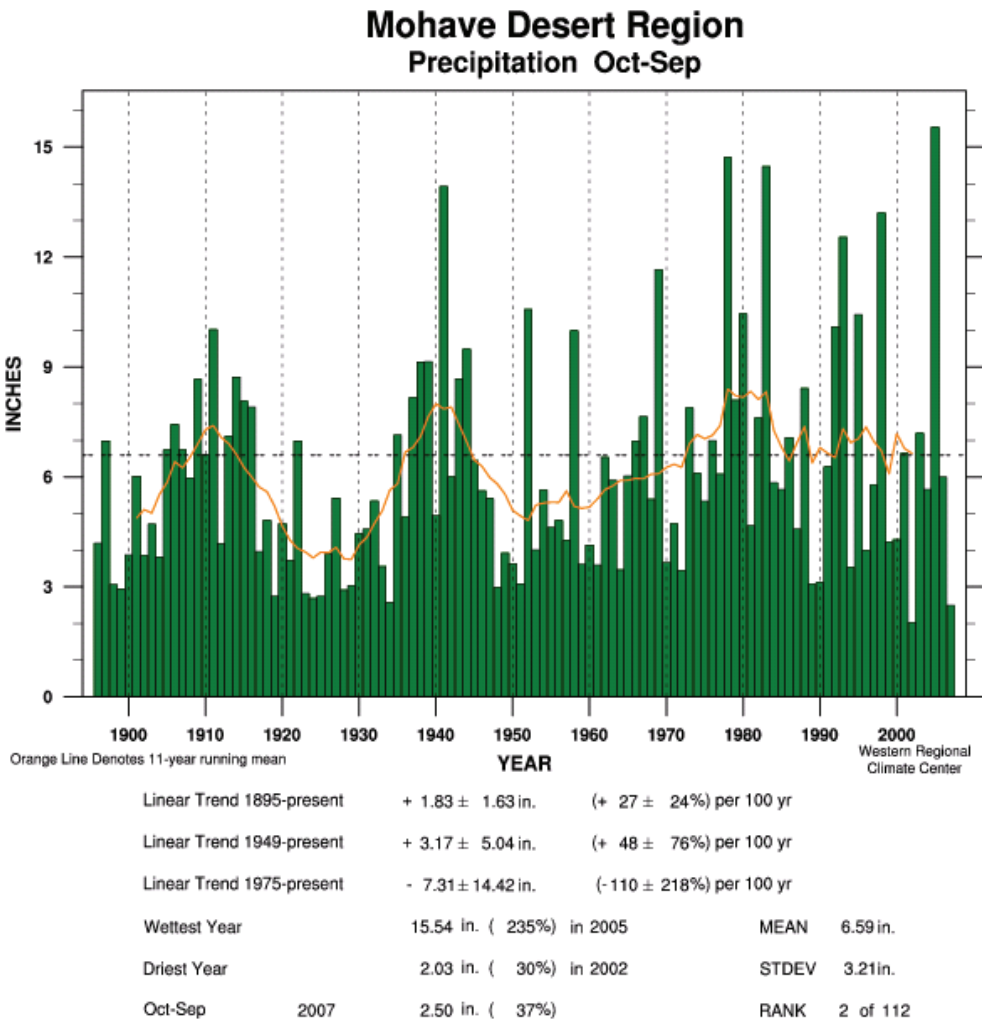

Figure 5: Precipitation for the Mojave Desert Region for water years (Oct. – Sept.) starting in 1895. Note that the wettest and driest years on record all have happened in this century, indicating that the hotspot in the desert southwest suggested in Figure 5 is already occurring.

DECLARATION OF BORIS POFF
CALICO SOLAR PROJECT
08-AFC-13

I, Boris Poff, declare as follows:

1. I prepared the testimony attached hereto and incorporated herein by reference as it relates to the Supplemental Staff Assessment prepared for the project known as the Calico Solar Project.
2. It is my professional opinion that the attached testimony is true and accurate.
3. I am personally familiar with the facts and conclusions described within the attached testimony and if called as a witness, I could testify competently thereto.

I declare under penalty of perjury that the foregoing is true and correct to the best of my knowledge and belief.

Dated: July 29, 2010.

Signed _____

At: Las Vegas, Nevada

Calico Solar – 08-AFC-13
DECLARATION OF SERVICE

I, Bonnie Heeley, declare that on July 29, 2010, I served and filed copies of the attached Rebuttal Testimony of Boris Poff on Behalf of California Unions for Reliable Energy on Soil and Water Resources for the Calico Solar Project dated July 29, 2010. The original document, filed with the Docket Unit, is accompanied by a copy of the most recent Proof of Service list, located on the web page for this project at www.energy.ca.gov/sitingcases/calicosolar/CalicoSolar_POS.pdf. The document has been sent to both the other parties in this proceeding as shown on the Proof of Service list and to the Commission's Docket Unit electronically to all email addresses on the Proof of Service list; and by depositing in the U.S. mail at South San Francisco, CA, with first-class postage thereon fully prepaid and addressed as provided on the Proof of Service list to those addresses NOT marked "email preferred."

AND

By sending an original paper copy and one electronic copy, mailed and emailed respectively to:

CALIFORNIA ENERGY COMMISSION
Attn: Docket No. 08-AFC-13
1516 Ninth Street, MS 4
Sacramento, CA 95814-5512
docket@energy.state.us.ca.

I declare under penalty of perjury that the foregoing is true and correct. Executed at South San Francisco, CA, on July 29, 2010

_____/s/_____
Bonnie Heeley

CALIFORNIA ENERGY COMMISSION
Attn: Docket No. 08AFC13
1516 Ninth Street, MS-4
Sacramento, CA 95184
docket@energy.state.ca.us

Felicia Bellows
Vice President, Development
Tessera Solar
4800 North Scottsdale Road
Suite 5500
Scottsdale, AZ 85251
Felicia.bellows@tesserasolar.com

Gloria D. Smith, Sr. Atty.
Sierra Club
85 Second Street, 2nd Flr.
San Francisco, CA 94105
Gloria.smith@sierraclub.org

Angela Leiba
AFC Project Manager
URS Corporation
1615 Murray Canyon Rd., #1000
San Diego, CA 92108
Angela_Leiba@URSCorp.com

Allan J. Thompson
Attorney at Law
21 C Orinda Way #314
Orinda, CA 94563
allanori@comcast.net

Jim Stobaugh
BLM-Nevada State Office
PO Box 12000
Reno, NV 89520
Jim_stobaugh@blm.gov

Rich Rotte, Project Mgr.
Bureau of Land Management
Barstow Field Office
2601 Barstow Road
Barstow, CA 92311
Richard_Rotte@blm.gov

Anthony Eggert
Commissioner & Presiding Member
California Energy Commission
1516 Ninth Street
Sacramento, CA 95814
aeggert@energy.state.ca.us

Jeffrey D. Byron
Commissioner & Associate Member
California Energy Commission
1516 Ninth Street
Sacramento, CA 95814
jbyron@energy.state.ca.us

Paul Kramer
Hearing Officer
California Energy Commission
1516 Ninth Street
Sacramento, CA 95814
pkramer@energy.state.ca.us

Caryn Holmes
Staff Counsel
California Energy Commission
1516 Ninth Street MS-14
Sacramento, CA 95814
cholmes@energy.state.ca.us

Christopher Meyer
Project Manager
California Energy Commission
1516 Ninth Street
Sacramento, CA 95814
cmeyer@energy.state.ca.us

Ella Foley Gannon, Partner
Bingham McCutchen, LLP
Three Embarcadero Center
San Francisco, CA 94111
Ella.gannon@bingham.com

Loulena Miles
Adams Broadwell Joseph & Cardozo
601 Gateway Boulevard, Suite 1000
South San Francisco, CA 94080
lmiles@adamsbroadwell.com

Becky Jones
California Department of Fish & Game
36431 41st Street East
Palmdale, CA 93552
dfgpalm@adelphia.net

Basin & Range Watch
Laura Cunningham
Kevin Emmerich
PO Box 70
Beatty, NV 89003
atmoictoadranch@netzero.net

Patrick C. Jackson
E-MAIL PREFERRED
ochsjack@earthlink.net

California ISO
e-recipient@caiso.com

Defenders of Wildlife
Joshua Basofin
EMAIL PREFERRED
jbasonfin@defenders.org

Kristy Chew, Adviser to
Commissioner Byron
EMAIL PREFERRED
kchew@energy.state.ca.us

Society for the Conservation of Bighorn Sheep
Bob Burke & Gary Thomas
PO Box 1407
Yermo, CA 92398
Cameracoordinator@
sheepsociety.com

Steve Adams, Co-Staff Counsel
California Energy Commission
1516 Ninth Street
Sacramento, CA 95814
sadams@energy.state.ca.us

Jennifer Jennings
California Energy Commission
1516 Ninth Street
Sacramento, CA 95814
publicadviser@energy.state.ca.us

County of San Bernardino
Ruth E. Stringer, Co. Counsel
Bart W. Brizzee, Dpty. Co.Co.
385 N. Arrowhead Ave., 4th Flr.
San Bernardino, CA 92415-0140
bbrizzee@cc.sbcounty.gov

Newberry Community Service District
Wayne W. Weierbach
PO box 206
Newberry Springs, CA 92365
newberryCSD@gmail.com

Lorraine White, Adviser to
Commissioner Eggert
EMAIL PREFERRED
lwhite@energy.state.ca.us

EXHIBIT 406

Curriculum Vita: Boris Poff, Ph.D.

Education:	Ph.D. 2007 Northern Arizona University - Flagstaff, AZ. (Forest Science) M.S. 2002 Northern Arizona University - Flagstaff, AZ. (Forestry) B.A. 1993 San Jose State University - San Jose, CA. (Journalism) A.A. 1989 Sacramento City College, Sacramento, CA. (Communications)
Related Work Experience:	June 2008 – Present Department of the Interior, National Park Service, Mojave National Preserve Barstow, California Title: Hydrologist, Resources Specialist May 2006 – January 2008 (and as volunteer until May 2008) Department of the Agriculture, United States Forest Service, Rocky Mountain Research Station Flagstaff, Arizona Title: Hydrologist August 2003 – May 2006 Department of the Agriculture, United States Forest Service, Rocky Mountain Research Station Flagstaff, Arizona Title: Hydrologic Technician January 2000 –June 2003 Northern Arizona University School of Forestry Hydrology Lab Flagstaff, Arizona Title: Research Assistant
Affiliations:	• Northern Arizona Type 2 Incident Management Team – MEDL(t) • Society of American Foresters – Member • American Water Resources Association – Member • George Wright Society – Member • Arizona Nevada Academy of Science – Board of Governors
Other Experience	• Technical Writer/Product Safety Engineer: Rockford Engineering Services, Sunol, CA/Dreieich Germany 1991-1993 • Vice-Director: Class 22 Ltd., London, UK 1994-1998 • EMT: Guardian Medical Transport, Flagstaff, AZ 2004-2005 • Ski Patrol: Arizona Snowbowl, Flagstaff, AZ 2004-2008

EXHIBIT 407

Influences of eolian and pedogenic processes on the origin and evolution of desert pavements

Leslie D. McFadden, Stephen G. Wells, Michael J. Jercinovich
Department of Geology, University of New Mexico, Albuquerque, New Mexico 87131

ABSTRACT

Well-developed desert pavements are present above eolian deposits that mantle flows of the Cima volcanic field, located in the Mojave Desert, California. Soil-stratigraphic data and geochemical data demonstrate that eolian and pedogenic processes play major roles in the evolution of these pavements. Eolian dust (1) accelerates mechanical fragmentation of flow rock, providing the source material for pavements, and (2) accumulates slowly below basaltic colluvium in flow depressions, eventually promoting development of cumulate soils below the evolving stone pavement. An increase in dust flux during the Holocene has raised ancient Pleistocene pavements as much as 20 cm above the former land surface. The results of our studies demonstrate for the first time that most desert pavements do not form by deflation, by overland flow, or by upward migration of stones through a slowly formed, clayey argillic horizon. Desert pavements are born and maintained at the surface.

INTRODUCTION

Desert pavements, consisting of a one- to two-particle-thick layer of closely packed, angular to subrounded gravel, are one of the more prominent landforms of hot and arid regions (Cooke and Warren, 1973; Mabbutt, 1977; Ritter, 1986). Desert pavements on surfaces of alluvial fans usually exhibit very little relief, are darkly varnished, and occur above a relatively gravel-free layer in which a moderately to strongly developed soil has formed. Characteristics of desert pavements have been used to map Quaternary surficial deposits (Denny, 1965; Bull, 1974; Shlemon, 1978; Christenson and Purcell, 1985), and changes in the chemical composition of varnish and the presence of organic carbon in varnish coating gravel of pavements have proved to be useful for estimating the age of the underlying materials on which the pavement formed (Dorn and Oberlander, 1981; Dorn et al., 1986; Harrington, 1986; Dethier and Harrington, 1986).

Development of desert pavements is usually attributed to deflation, erosion of fine-grained material (Cooke and Warren, 1973; Ritter, 1986), or upward migration of gravel through an increasingly clay-rich, gravel-depleted B horizon via alternating shrinking and swelling (Springer, 1958; Jessup, 1960; Cooke, 1970; Mabbutt, 1977; Dan et al., 1982). On the basis of recent studies of pavement, soil, and landscape development in the Cima volcanic field, we conclude, instead, that pavements are born at the land surface and that pavement clasts are never deeply buried in the underlying soil. Stone pavements on eolian-mantled lava flows in this area form at the surface by two major processes: (1) colluviation of basaltic clasts from topographic highs into topographic depressions filled with eolian silt and (2) detachment and uplifting of clasts from bedrock surfaces as eolian fines accumulate in fractures and along flow surfaces. The pavements are maintained at the surface as cumulate soils develop beneath the pavements in response to the incorporation of eolian silts and clays deposited on the land surface.

PAVEMENT EVOLUTION

The origin and evolution of stone pavements on the basalt flows are directly linked to two fundamental processes: (1) deposition and pedogenic alteration of the eolian mantle and (2) mechanical weathering to form the rubble zone. The source of the clasts in the pavements is mechanically weathered basaltic bedrock derived from topographic highs. Salt-rich eolian fines accumulate in fractures of the basalt (McFadden et al., 1986), and wetting and drying of the fines result in volumetric changes related to crystal growth or shrinking and swelling of clay (Cooke and Warren, 1973). This volumetric change enhances fracturing and displaces the basaltic clasts vertically and laterally (Fig. 1). As displacement occurs, additional eolian fines and salts are deposited between the clasts, further enhancing separation of clasts from the underlying bedrock. Mechanical weathering of

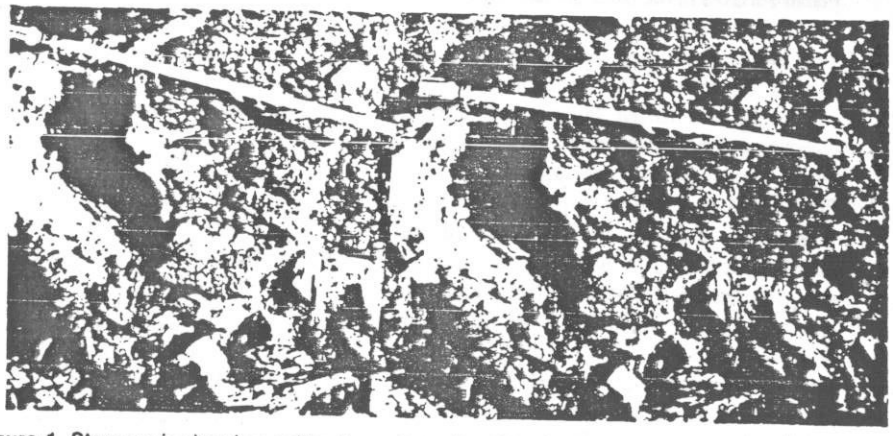

Figure 1. Stereopair showing eolian fines deposited in late Pleistocene fractured basaltic flow rock with pahoehoe texture. Fragments have been displaced as much as 4 cm laterally and 2 cm vertically from subjacent flow.

GEOLOGY, v. 15, p. 504–508, June 1987

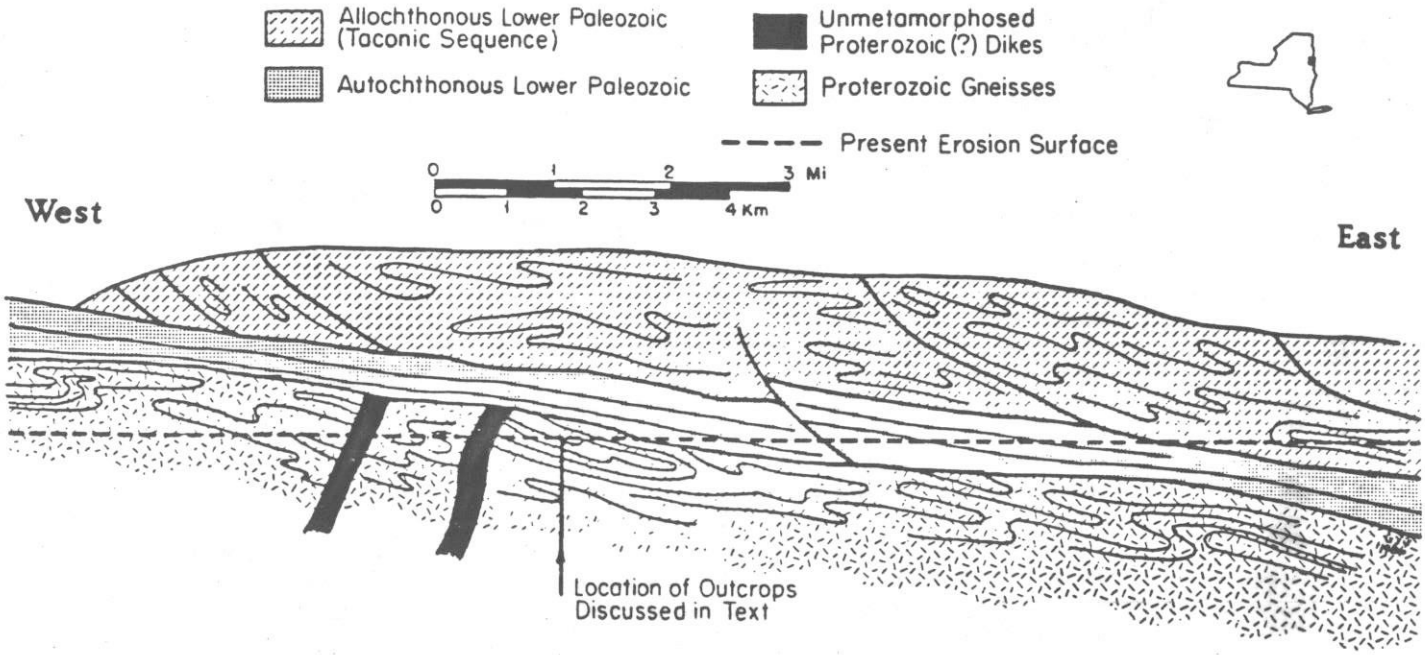

Figure 4. Schematic cross section of Fort Ann–Whitehall area during Taconic orogeny. Arrow shows location of outcrops discussed in text.

beyond the contact now exposed, as illustrated schematically in Figure 4. During thrusting, stresses transmitted through the autochthonous lower Paleozoic rocks caused minor east-over-west displacement along favorably oriented foliation planes in the underlying Proterozoic gneiss. The preponderance of north-northeast–striking planes that dip gently to moderately east-southeast would be nearly optimum for such movement. This displacement produced the observed foliation-parallel slickensides and minor offset of vertical dikes. In addition, minor cataclasis occurred along contacts between rocks of contrasting mechanical properties, such as gneiss and marble, and thus provided access for fluids. Similar features have not been reported in the overlying Paleozoic rocks, possibly because planar surfaces in the latter are less well defined.

Simultaneously, tectonic overpressures created by the overriding thrust slice(s) expelled connate brines from the autochthonous Paleozoic rocks and forced these brines into the underlying crystalline rocks along foliation planes, lithologic contacts, and faults. These fluids are likely to have been enriched in Mg, in view of the evidence for hypersaline depositional environments in the Paleozoic rocks. The overpressures were sufficient to create and maintain open spaces, which then were filled by K-feldspar, dolomite, and celadonite. The brines also caused dolomitization of the marbles, serpentinization of calc-silicate minerals, and precipitation of cherty silica. The mineral assemblages are consistent with an origin at temperatures not over 420 °C in the presence of an aqueous fluid; the actual temperatures may have been much lower in view of the presence and purity of the K-feldspar.

Potential large-scale effects of pressurized fluids expelled from sedimentary rocks as a result of overthrust tectonics have been described recently by Hearn and Sutter (1985) and Oliver (1986). We believe that these rocks display evidence of the same phenomenon on a more local scale.

REFERENCES CITED

Bohlen, S.R., Valley, J.W., and Essene, E.J., 1985, Metamorphism in the Adirondacks. I: Pressure and temperature: Journal of Petrology, v. 26, p. 971–992.

Eggert, R.G., and Kerrich, D.M., 1981, Metamorphic equilibria in the siliceous dolomite system: 6 kbar experimental data and geologic implications: Geochimica et Cosmochimica Acta, v. 45, p. 1039–1050.

Fisher, D.W., 1985, Bedrock geology of the Glens Falls–Whitehall region, New York: New York State Museum Map and Chart Series no. 35, 58 p.

Hearn, P.P., and Sutter, J.F., 1985, Authigenic potassium feldspar in Cambrian carbonates: Evidence of Alleghenian brine migration: Science, v. 228, p. 1529–1531.

Johannes, W., 1969, An experimental investigation of the system MgO-SiO_2-H_2O-CO_2: American Journal of Science, v. 267, p. 1083–1104.

Kastner, M., and Siever, R., 1979, Low temperature feldspars in sedimentary rocks: American Journal of Science, v. 279, p. 435–479.

McLelland, J.M., 1986, Geology of the Lake George region: Geological Society of America Abstracts with Programs, v. 18, p. 53–54.

Oliver, J., 1986, Fluids expelled tectonically from orogenic belts: Their role in hydrocarbon migration and other geologic phenomena: Geology, v. 14, p. 99–102.

Puhan, D., 1978, Experimental study of the reaction dolomite + K-feldspar + water = phlogopite + calcite + CO_2 at total gas pressures of 4000 and 6000 bars: Neues Jahrbuch für Mineralogie Monatshefte, v. 3, p. 110–127.

Rodgers, J., and Fisher, D.W., 1969, Paleozoic rocks in Washington County, New York west of the Taconic klippe, *in* Bird, J.M., ed., New England Intercollegiate Geological Conference Guidebook, 61st Annual Meeting: Albany, State University of New York, p. 6.1–6.12

Rubin, D., and Friedman, G.M., 1977, Intermittently emergent shelf carbonates: An example from the Cambro-Ordovician of eastern New York State: Sedimentary Geology, v. 19, p. 81–106.

Velde, B., 1972, Celadonite mica: Solid solution and stability: Contributions to Mineralogy and Petrology, v. 37, p. 235–247.

Whitney, P.R., 1983, A three-stage model for the tectonic history of the Adirondack region, New York: Northeastern Geology, v. 5, p. 61–72.

——1985, Rocks and problems of the southeastern Adirondacks, *in* Lindemann, R.H., ed., New York State Geological Association Guidebook, 57th Annual Meeting: Saratoga Springs, New York, Skidmore College, p. 47–67.

Wise, W.S., and Eugster, H.P., 1964, Celadonite: Synthesis, stability and occurrence: American Mineralogist, v. 49, p. 1031–1083.

ACKNOWLEDGMENTS

We thank Y. W. Isachsen, L. V. Rickard, and R. H. Fakundiny for helpful discussions and assistance in preparing the manuscript, and M. L. Crawford and P. Olilla for constructive reviews. New York State Museum Journal Series, Paper no. 506.

Manuscript received October 20, 1986
Revised manuscript received February 6, 1987
Manuscript accepted February 24, 1987

topographic highs also results in the development of colluvial wedges of rubble and the concomitant infilling of topographic depressions with the colluvial material. These clasts move laterally by colluvial and alluvial processes into the topographic lows in which abundant silt has accumulated, and they form a surface layer or armor of stones (Fig. 2; Wells et al., 1985). On progressively older flows, the extent of bedrock highs decreases as the eolian mantle and stone pavement fill in the lows and coalesce; thus, the source area for basalt clasts is significantly reduced on flows older than 0.4 Ma (Wells et al., 1985). Pavements on flows younger than 0.4 Ma have mixtures of clasts that were derived episodically from topographic highs, presumably due to a decrease in the rate of supply from increasingly subdued topographic highs. In contrast, relative-age data for clasts in pavements on flows older than 0.4 Ma indicate fewer differences in the residence time of clasts in the pavement. This is supported by the data on the reddening (iron oxidation) clast undersides: only 10%–20% of clast undersides in pavements on flows younger than 0.4 Ma have weakly reddened, oxidized coatings, whereas clast undersides on flows older than 0.4 Ma are all reddened to 5YR and 2.5YR hues. This suggests that no new clasts are added to pavements once the bedrock topographic highs are reduced by erosion and buried by eolian sediments, and once stones are added to the pavements, they are typically maintained at the surface by processes that inhibit burial.

SOILS DEVELOPED IN THE EOLIAN MANTLE BENEATH THE PAVEMENT

Soils exhibiting a wide variation in the degree of development occur in deposits underlying the pavement. These deposits are quartz-rich, well-sorted sandy silts that have been transported to the flow surfaces largely as windblown suspended load (Wells et al., 1985) where they are trapped by the rough surfaces of the flow (Greeley and Iversen, 1981). Between major periods of eolian deposition, a lower eolian flux rate permits development of soils in the eolian deposits. Moderate eolian depositional rates are apparently critical for maintaining clasts at the land surface. In the Cima volcanic field, three distinct phases of soil development are recognized on flows younger than 1.1 Ma: weakly developed soils on flows younger than 0.18 Ma (Fig. 2); strongly developed soils containing thick argillic horizons on flows that are 0.18 to 0.7 Ma (Fig. 2); and strongly developed soils containing truncated argillic horizons that are massively impregnated by pedogenic $CaCO_3$ on flows that are 0.7 to 1.1 Ma (Dohrenwend et al., 1984).

A critical aspect of soil and pavement development on flow surfaces is the formation of the vesicular A (Av) horizon. Such horizons, observed in many desert soils, are typically more clay- and silt-rich than the underlying soil parent materials. The spherical vesicles are probably due to entrapped soil air that expands as soil temperature rapidly increases after summer rainfall events (Evenari et al., 1974). Some of the sand and silt fractions of the Av horizons of desert soils may be attributed to comminution of gravel lithologies susceptible to mechanical weathering (Mabbutt, 1977; Ritter, 1986); however, the paucity of basaltic material in the Av horizon emphasizes the largely eolian origin of material that composes this horizon. Vesicular horizons in the study area have a pronounced columnar structure (Fig. 2) that is attributed to alternating shrinking and swelling of the clays in the increasingly clay-enriched Av horizon (McFadden et al., 1986). Significant amounts of trapped eolian silt and fine sand and solutes are more readily transported below the surface through these cracks. The walls of the Av peds are typically coated with loose silt and are almost noncalcareous due to this process. In contrast to rapid infiltration through the cracks, infiltration through peds is very slow and eventually causes alteration of the interior, reflected by the reddened and carbonate-enriched nature of the ped interior. Moderate accretion of eolian fines into Av peds and drying of peds during the summer result in doming of the ped tops and vertical displacement of overlying clasts (Fig. 3). During the winter, soil moisture is retained and the domes collapse, causing fresh eolian fines on ped walls and in cracks between peds to be incorporated in the Av horizon. With continued Av-horizon development, the interiors of Av eventually coalesce and form a continuous B horizon.

Mabbutt (1977) suggested that some pavements might somehow be maintained at the surface as eolian material is slowly incorporated beneath the pavement. The results of our studies

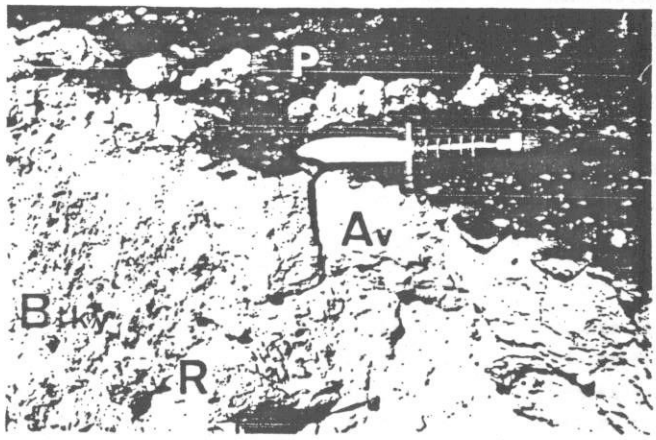

Figure 2. Stone pavement (P) formed over accretionary mantle in topographic depression on late Pleistocene flow in Cima volcanic field. Development of vesicular A (Av) horizons of phase 1 soils, carbonate- and gypsum-bearing argillic horizons (Btky) of phase 2 soils, and origin of basalt rubble (R) are discussed in text.

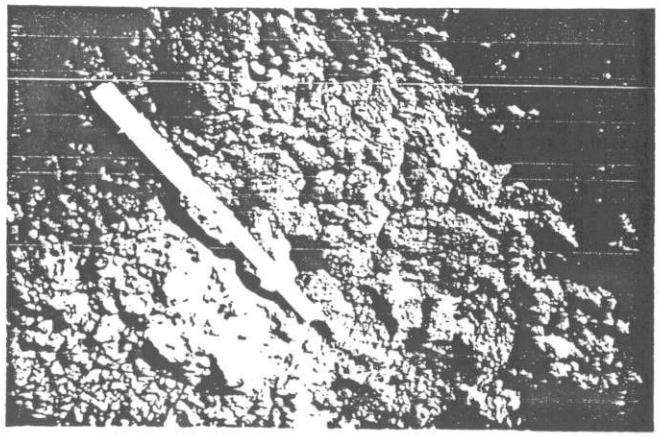

Figure 3. Domed surface of vesicular A horizon exposed after careful removal of stone pavement. Note strongly developed, nonorthogonal crack system.

show that the development of an Av horizon and ultimately a cumulate soil are critical aspects of pavement formation. Moreover, these results demonstrate that the presence of clay-enriched and virtually gravel-free B horizons that often occur below desert pavements does not require the often-invoked process of upward migration of gravel through the B horizon.

Age data for the flows and soil-stratigraphic data support the hypothesized mechanism of pavement evolution. The presence of similarly developed soils in loess beneath pavements on flows younger than 0.18 Ma and as young as 16 ka indicates that the most recent period of relatively high eolian influx rates occurred during the latest Pleistocene to early Holocene (Wells et al., 1985; McFadden et al., 1986). The apparent timing of the most recent eolian event and the accumulation of large quantities of carbonates and soluble salts in these soils strongly suggest that alkaline playas, formed after the disappearance of late Pleistocene pluvial lakes in the Mojave Desert, are a major source of these eolian materials (McFadden et al., 1986). Smoother surfaces of older volcanic flows where bedrock crops out are rare and trap loess less efficiently. The most recent loess is typically present as a thin veneer that buries an older loess deposit in which a very strongly developed soil is present (Fig. 2). The source of clasts in the desert pavement on such surfaces can only have been derived from a preexisting pavement formed on a now buried soil. On flows with rough surfaces, however, high rates of loess deposition precluded development of a soil, and the preexisting pavement was buried (Wells et al., 1985). Remaining topographic highs on these flows provided materials for development of the present desert pavement.

CHEMICAL ALTERATION OF THE STONE PAVEMENT

X-ray fluorescence analysis of volcanic rocks of a variety of ages in the Cima field shows that their composition is quite similar (Turrin et al., 1986). We hypothesize, therefore, that chemical weathering of basalt in the pavement and in the rubble produces authigenic minerals whose chemical compositions reflect contrasting weathering environments rather than compositional differences. To test this hypothesis, sample clasts were collected from the pavement and underlying soil on selected flow surfaces of various ages and were examined by using optical petrographic techniques, scanning electron microscopy, and electron microprobe analysis (Fig. 4; Table 1).

Decomposition of the basalt has occurred mainly by alteration of the glass–iron ox mesostasis. Olivine is the primary sili mineral that is chemically altered in both pa ment and rubble. Olivine alteration is character ized by uptake of H_2O, TiO_2, Al_2O_3, C Na_2O, K_2O, and P_2O_5. SiO_2, MgO, and M however, are generally depleted relative to fresl olivine. The primary products of alteration i pavement and rubble samples include authig clay (Fig. 4) and ferric oxyhydroxides that f layers 10 to 50 μm thick on fracture and vesicl walls. Microprobe analyses indicate that the au thigenic clay is a mixed-layer clay, prob consisting of illite and smectite or illite and miculite (Table 1; Fig. 4).

Alteration of the rocks in the pavement di from alteration of rubble in several major spects. Authigenic clay in pavement samples ap pears to be significantly enriched in Al_2O_3 an depleted in CaO relative to authigenic cla rubble. Also, structural formula calculation dicate that there is a greater percentage of F and Mg relative to Al in octahedral sites in au thigenic clay of rubble than in octahedral sit authigenic clay of pavement clasts (Table Additionally, rubble clays are more Na and K rich (i.e., higher illite component) than sur pavement clays. In general, porosity due to p ence of fractures and vesicles is greater in roc of the rubble compared to rocks in th pavement.

TABLE 1. MICROPROBE ANALYSES OF AUTHIGENIC CLAY MINERALS IN BASALT CLASTS FROM LATE PLEISTOCENE AND MIDDLE PLEISTOCENE PAVEMENTS AND RUBBLE

	Late Pleistocene flow pavement*(wt %)	Rubble† (wt %)	Middle Pleistocene flow pavement§(wt %)	Rubble# (wt %)
SiO_2	43.65 ±3.45	44.14 ±2.32	46.02 ±1.57	36.71 ±3.09
TiO_2	0.75 ±0.47	0.73 ±0.19	0.37 ±0.15	7.72 ±0.91
Al_2O_3	24.20 ±3.32	14.82 ±1.28	23.44 ±0.95	13.52 ±1.27
Fe_2O_3**	8.14 ±1.92	7.05 ±0.95	5.37 ±0.59	15.27 ±3.86
MnO	0.43 ±0.47	0.11 ±0.06	0.05 ±0.03††	0.23 ±0.15
MgO	3.18 ±0.60	4.31 ±0.66	4.26 ±0.57	3.59 ±1.71
CaO	1.76 ±1.32	2.04 ±0.57	1.39 ±0.55	6.27 ±2.17
Na_2O	0.19 ±0.31	0.63 ±0.22	0.14 ±0.07	1.14 ±0.35
K_2O	2.06 ±0.32	2.61 ±0.35	2.22 ±0.34	1.19 ±0.32
P_2O_5	0.80 ±0.93	0.53 ±0.48	0.35 ±0.33	1.10 ±1.10
Total	84.31	76.26	83.07	82.21

Note: Flow ages: late Pleistocene—0.13 ±0.06 Ma; middle Pleistocene—0.56 ±0.16 Ma (Turrin et al., 1986). Structural formula on basis of 20 (O) and (OH).

* $(Si_{6.38}Al_{1.62})(Al_{2.55}Ti_{.08}Fe_{.90}Mn_{.05}Mg_{.69})Ca_{.28}Na_{.05}K_{.38}P_{.10}$

† $(Si_{7.16}Al_{.84})(Al_{1.99}Ti_{.09}Fe_{.86}Mn_{.02}Mg_{1.04})Ca_{.35}Na_{.20}K_{.54}P_{.07}$

§ $(Si_{6.74}Al_{1.26})(Al_{2.78}Ti_{.04}Fe_{.59}Mn_{.01}Mg_{.93})Ca_{.22}Na_{.04}K_{.41}P_{.04}$

\# $(Si_{5.85}Al_{2.15})(Al_{.39}Ti_{.57}Fe_{1.83}Mn_{.03}Mg_{.85})Ca_{1.07}Na_{.35}K_{.24}P_{.15}$

** All Fe calculated as Fe_2O_3.

†† Below detection limit.

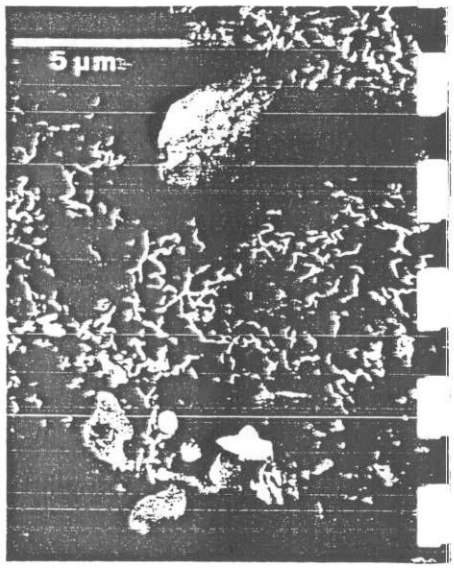

Figure 4. Scanning electron microscope ph tomicrograph showing crenulate, interloc authigenic clay crystals formed during ch cal alteration of latest Pleistocene basalti flow rubble in Cima volcanic field. Electro microprobe analysis and structural for calculations of authigenic clay indicate mixed-layer clay consists of illite and smec

These differences in character of chemical weathering of pavement and rubble samples imply that alteration has taken place in contrasting geochemical environments. Precipitation of alkaline clays in rubble samples may be favored by alteration of basalt under alkaline soil conditions, whereas alteration under less alkaline to neutral conditions in a largely subaerial pavement environment may favor development of more Al-rich clay. However, a more severe alteration of rubble should occur in the relatively well insulated subsoil environment; thus, the magnitude of chemical weathering is ultimately greater in rubble samples than in pavement samples. Accordingly, a rubble sample from an early Pleistocene flow displays the greatest magnitude of chemical and physical weathering. This sample also contains abundant zeolite and rare celestite, authigenic minerals that have precipitated in fractures (Fig. 5, A and B). Chemical alteration of the rubble parallels the significant chemical alteration of the loess parent materials of well-developed soils underlying pavements on surfaces older than 0.2 Ma in the Cima field (McFadden et al., 1986).

The paragenesis of authigenic minerals indicated in strongly altered rubble is clay → zeolites + calcite(?) → celestite. This sequence suggests that the most recent authigenesis occurred in a strongly alkaline environment and is consistent with the hypothesis that much of the accumulated pedogenic carbonates and sulfates are derived by deflation of Holocene alkaline playas (McFadden et al., 1986).

DISCUSSION

We hypothesize that stone pavements on alluvial fans of desert piedmonts have probably evolved in a manner similar to that proposed for the stone pavements in the Cima volcanic field. Surfaces of alluvial fans in the deserts of the southwestern United States initially have a bar-and-swale topography inherited from the braided pattern of ephemeral streams in arid environments (Bull, 1974). Fan surfaces of early Holocene age, however, exhibit partial pavement development, and stone pavements are ubiquitous on fan surfaces of late Pleistocene age. Vesicular A horizons that are nearly identical to those observed in the Cima volcanic field constitute the initially developed horizon of soils on such fan deposits. Weakly developed color B horizons are present below the vesicular A horizon of middle to early Holocene soils, but a weak to moderately strong and usually nongravelly argillic horizon is present below the vesicular A horizon of late Pleistocene and older soils on these fans (McFadden, 1982; McFadden and Bull, 1987; Wells et al., 1987).

Eolian processes have significantly influenced soil development on alluvial deposits in deserts. Much of the silt, clay, carbonates, and soluble salts that have accumulated in soils formed in arid environments are attributable to incorporation of eolian materials rather than to chemical weathering of soil parent materials (Brown, 1956; Gile et al., 1966, 1981; Lattman, 1973; Machette, 1985; McFadden and Tinsley, 1985). As discussed previously, however, eolian activity during the Quaternary has been strongly episodic in the Mojave Desert, the most recent period of relatively high eolian influx rates having occurred during the latest Pleistocene to early Holocene. A major increase in eolian activity during the Holocene has also been documented in the desert of southern Nevada. Whitney et al. (1986) reported that eolian silt overlying a sequence of early through late Pleistocene alluvial units was deposited between 6.5 and 3 ka, on the basis of thermoluminescence age determinations of the silt.

We propose that the vesicular A horizon and potentially much of the uppermost B horizon of Pleistocene soils on fan surfaces of the Mojave Desert record the significant increase in eolian activity that began as early as the latest Pleistocene and has continued into the Holocene. The rate of incorporation of eolian material has been slow enough to permit development of cumulate soils and concomitant uplift of preexisting stone pavements. Thus, although in some cases accumulation of a surficial gravel lag may be attributed to eolian or fluvial removal of fines, we believe that such processes can contribute very little to the evolution of pavements formed on piedmonts.

The results of analysis of the chemical composition of the varnish on clasts of desert pavements also strongly support the proposed process of pavement development. Dorn and Oberlander (1981) showed that varnish-forming, mixotrophic microorganisms require the near neutral pH conditions that are present only in a subaerial environment. Cation ratios of varnish from pavements on late Pleistocene fan surfaces are significantly lower than the cation ratios of varnish from clasts of early or middle Holocene pavements (Dorn, 1983, 1984; Dorn et al., 1986). If well-developed pavements can form only after a clay-rich B horizon develops and causes upward migration of gravel, a significant number of clasts in late Pleistocene pavements should have relatively high cation-ratio values that would reflect the emergence of these clasts sometime during the Holocene. Cation-ratio and varnish micromorphologic data from a variety of study areas (Dorn, 1983, 1984; Dorn et al., 1986) imply, instead, that varnish development has occurred on stones exposed continuously since abandonment of the fan surface. Pavements in the Mojave Desert that are probably as old as middle Pleistocene (Bull, 1974; Wells et al., 1985; McFadden et al., 1986) must therefore coexist with soils that have formed largely in eolian deposits of Holocene age. Thus, on the basis of our studies in the Cima volcanic field, we conclude that desert pavements (1) are born at the land surface and (2) remain at the land surface via eolian deposition and simultaneous development of cumulate soils beneath the pavements.

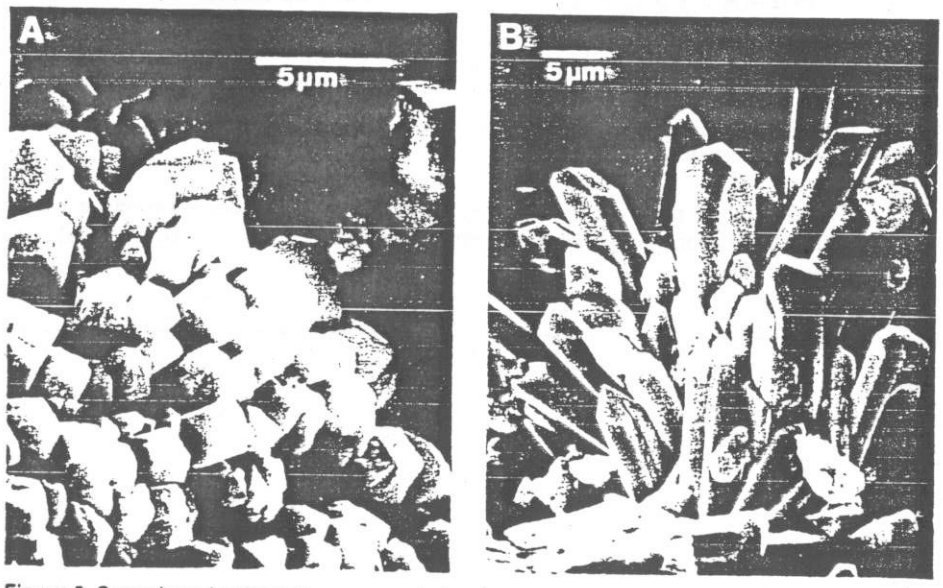

Figure 5. Scanning electron microscope photomicrographs showing authigenic minerals present in basaltic rubble in well-developed, phase 3 soil on early Pleistocene flow in Cima volcanic field. A: Spherulitic zeolite crystals. Electron microprobe data indicate that zeolite is probably phillipsite. B. Spherulitic celestite ($SrSO_4$) crystals.

REFERENCES CITED

Brown, C.N., 1956, The origin of caliche on the northeast Llano Estacado, Texas: Journal of Geology, v. 64, p. 1–15.

Bull, W.B., 1974, Geomorphic tectonic analysis of the Vidal region, *in* Information concerning site characteristics, Vidal Nuclear Generating Station [California]: Los Angeles, Southern California Edison Company, Appendix 2.5B, amendment 1, 66 p.

Christenson, G.E., and Purcell, C., 1985, Correlation and age of Quaternary alluvial-fan sequences, Basin and Range province, southwestern United States, *in* Weide, D.E., ed., Soils and Quaternary geology of the southwestern United States: Geological Society of America Special Paper 203, p. 115–122.

Cooke, R.U., 1970, Stone pavements in deserts: Association of American Geographers Annals, v. 60, p. 560–577.

Cooke, R.U., and Warren, A., 1973, Geomorphology in deserts: London, Batsford Ltd., 394 p.

Dan, J., Yaalon, D.H., Moshe, R., and Nissum, S., 1982, Evolution of Reg soils in southern Israel and Sinai: Geoderma, v. 28, p. 173–202.

Denny, C.S., 1965, Alluvial fans in the Death Valley region, California and Nevada: U.S. Geological Survey Professional Paper 466, 66 p.

Dethier, D.P., and Harrington, C.D., 1986, Late Quaternary erosion history of the western Española Basin, New Mexico: Geological Society of America Abstracts with Programs, v. 18, p. 351.

Dohrenwend, J.C., McFadden, L.D., Turrin, B.D., and Wells, S.G., 1984, K-Ar dating of the Cima volcanic field, eastern Mojave Desert, California: Late Cenozoic volcanic history and landscape evolution: Geology, v. 12, p. 163–167.

Dorn, R.I., 1983, Cation-ratio dating: A new rock varnish age-determination technique: Quaternary Research, v. 20, p. 49–73.

—— 1984, Geomorphological interpretation of rock varnish in the Mojave Desert, *in* Dohrenwend, J.C., ed., Surficial geology of the eastern Mojave Desert, California (Geological Society of America annual meeting guidebook): Reno, Nevada, Mackay School of Mines, p. 150–161.

Dorn, R.I., and Oberlander, T.M., 1981, Microbial origin of desert varnish: Science, v. 213, p. 1245–1247.

Dorn, R.I., Banforth, D.B., Cahill, T.A., Dohrenwend, J.C., Turrin, B.D., Donahue, D.J., Jull, A.J.T., Long, A., Macku, M.E., Weil, E.B., Whitley, D.S., and Zabel, T.H., 1986, Cation-ratio and accelerator-radiocarbon dating of rock varnish on Mojave artifacts and landforms: Science, v. 231, p. 830–833.

Evenari, J., Yaalon, D.H., and Gutterman, Y., 1974, Note on soils with vesicular structures in deserts: Zeitschrift für Geomorphologie, v. 18, p. 162–172.

Gile, L.H., Peterson, F.F., and Grossman, R.B., 1966, Morphological and genetic sequences of carbonate accumulation in desert soils: Soil Science, v. 101, p. 347–360.

Gile, L.H., Hawley, J.W., and Grossman, R.B., 1981, Soils and geomorphology in the Basin and Range area of southern New Mexico—Guidebook to the Desert Project: New Mexico Bureau of Mines and Mineral Resources Memoir 39, 222 p.

Greeley, R., and Iversen, J.D., 1981, Eolian processes and features at Amboy Lava field, California: UNESCO Workshop on Physics of Desertification, Proceedings, 23 p.

Harrington, C.D., 1986, The use of rock varnish as a Quaternary dating method within the central Rio Grande rift, New Mexico, and the Nevada Test Site: Geological Society of America Abstracts with Programs, v. 18, p. 360.

Jessup, R.W., 1960, The Stony Tableland soils of the southeastern portion of the Australian arid zone and their evolutionary history: Journal of Soil Science, v. 11, p. 188–196.

Lattman, L.H., 1973, Calcium carbonate cementation of alluvial fans in southern Nevada: Geological Society of America Bulletin, v. 84, p. 3013–3028.

Mabbutt, J.A., 1977, Desert landforms: Cambridge, Massachusetts, MIT Press, 340 p.

Machette, M.N., 1985, Calcic soils of the southwestern United States, *in* Weide, D.L., ed., Soils and Quaternary geology of the southwestern United States: Geological Society of America Special Paper 203, p. 1–22.

McFadden, L.D., 1982, The impact of temporal and spatial climatic change on alluvial-soils genesis in southern California [Ph.D. thesis]: Tucson, University of Arizona, 430 p.

McFadden, L.D., and Bull, W.B., 1987, Quaternary soil development in the Mojave Desert, California, *in* Whitley, D.S., ed., Late Pleistocene archeology and environment in California: Salt Lake City, University of Utah Press (in press).

McFadden, L.D., and Tinsley, J.C., 1985, The rate and depth of accumulation of pedogenic carbonate accumulation in soils: Formulation and testing of a compartment model, *in* Weide, D.L., ed., Soils and Quaternary geology of the southwestern United States: Geological Society of America Special Paper 203, p. 23–42.

McFadden, L.D., Wells, S.G., and Dohrenwend, J.C., 1986, Influences of Quaternary climatic changes on processes of soil development on desert loess deposits of the Cima volcanic field, California: Catena, v. 13, p. 361–389.

Ritter, D.F., 1986, Process geomorphology: Dubuque, Iowa, Wm. C. Brown, 603 p.

Shlemon, R.J., 1978, Quaternary soil-geomorphic relationships, southeastern Mojave Desert, Cali nia and Arizona, *in* Mahaney, W.C., Quaternary soils: Norwich, England, Unive of East Anglia, Geo Abstracts, Ltd., p. 187–207

Springer, M.E., 1958, Desert pavement and vesicula layer of some desert soils in the desert of Lahontan Basin, Nevada: Soil Science Societ America Proceedings, v. 22, p. 63–66.

Turrin, B.D., Dohrenwend, J.C., Drake, R.E., an Curtis, G.H., 1986, Potassium-argon ages f the Cima volcanic field, eastern Mojave De California: Isochron/West, v. 44, p. 9–16.

Wells, S.G., Dohrenwend, J.C., McFadden, L.D Turrin, B.D., and Mahrer, K.D., 1985, Late Cen ozoic landscape evolution on lava flow surf of the Cima volcanic field, Mojave De California: Geological Society of America Bu letin, v. 96, p. 1518–1529.

Wells, S.G., McFadden, L.D., and Dohrenwend, 1987, Influence of late Quaternary clin changes on geomorphic and pedogenic proc on a desert piedmont, eastern Mojave Deser California: Quaternary Research (in press).

Whitney, J.W., Shroba, R.R., Simonds, F.W., Harding, S.T., 1986, Recurrent Quater movement on the Windy Wash fault, Ny County, Nevada: Geological Society of Americ Abstracts with Programs, v. 18, p. 787.

ACKNOWLEDGMENTS

The U.S. Geological Survey (Project 9320-03359 provided financial support for the field studies an much of the laboratory analysis of the soils. The I tute of Meteoritics of the University of New Me generously provided support for use of the Microbean Analysis Laboratory.

We thank John Dohrenwend for useful discu and comments regarding the geologic history o Cima volcanic field; Brent Turrin for his effor K-Ar dating of flows in the Cima volcanic field, a well as his contributions to the understanding o geologic history of this area; and D. Weide D. Ritter for constructive criticism.

Manuscript received December 12, 1986
Revised manuscript received February 9, 1987
Manuscript accepted February 23, 1987

Reviewer's comment

The ideas in this paper are *great!* I grew up BELIEVING that desert pavements were forme either (a) deflation or (b) upward movement of rocks. This paper has the potential to dispel all those old ideas.

David W

EXHIBIT 408

Sciencexpress Report

Model Projections of an Imminent Transition to a More Arid Climate in Southwestern North America

Richard Seager,[1] Mingfang Ting,[1] Isaac Held,[2,3] Yochanan Kushnir,[1] Jian Lu,[4] Gabriel Vecchi,[2] Huei-Ping Huang,[1] Nili Harnik,[5] Ants Leetmaa,[2] Ngar-Cheung Lau,[2,3] Cuihua Li,[1] Jennifer Velez,[1] Naomi Naik[1]

[1]Lamont Doherty Earth Observatory of Columbia University, Palisades, NY, USA. [2]NOAA Geophysical Fluid Dynamics Laboratory, Princeton, NJ, USA. [3]Program in Atmospheric and Oceanic Sciences, Department of Geosciences, Princeton University, Princeton, NJ, USA. [4]National Center for Atmospheric Research, Boulder, CO, USA. [5]Tel Aviv University, Tel Aviv, Israel.

How anthropogenic climate change will impact hydroclimate in the arid regions of Southwestern North America has implications for the allocation of water resources and the course of regional development. Here we show that there is a broad consensus amongst climate models that this region will dry significantly in the 21st century and that the transition to a more arid climate should already be underway. If these models are correct, the levels of aridity of the recent multiyear drought, or the Dust Bowl and 1950s droughts, will, within the coming years to decades, become the new climatology of the American Southwest.

The Third Assessment Report of the Intergovernmental Panel on Climate Change (IPCC) reported that the average of all the participating models showed a general decrease in rainfall in the subtropics during the 21st century although there was also considerable disagreement amongst the models (*1*). Subtropical drying accompanying rising CO_2 is also found in the models participating in the second Coupled Model Intercomparison Project (*2*). Here we examine future subtropical drying by analyzing the time history of precipitation in 19 climate models participating in the Fourth Assessment Report (AR4) of the IPCC (*3*). The future climate projections followed the A1B emissions scenario (*4*) in which CO_2 emissions increase until about 2050 and decrease modestly thereafter leading to a CO_2 concentration of 720 ppm in 2100. We also analyzed the simulations by these models of the 1860–2000 period in which the models were forced by the known history of trace gases and, with some variation amongst the models, estimated changes of solar irradiance, volcanic and anthropogenic aerosols and land use. These simulations provide initial conditions for the 21st century climate projections. For each model, climatologies were computed over the 1950–2000 period by averaging over all the simulations available for each model. All climate changes shown are departures from this climatology.

We define an area (shown as a box on Fig. 4) called `The Southwest' including all land between 125°W and 95°W and 25°N and 40°N that incorporates the southwestern United States and parts of northern Mexico . Fig. 1 shows the modeled history and future of the annual mean precipitation minus evaporation (*P*–*E*) averaged over this region for the period common to all the models, 1900–2098. The median, 25th and 75th percentiles of the model *P*–*E* distribution and the median of *P* and *E* are shown. For cases in which there were multiple simulations with a single model these were averaged together before computing the distribution. *P*–*E* equals the moisture convergence by the atmospheric flow and, over land, the amount of water that goes into runoff.

In the multi-model ensemble mean there is a transition to a sustained drier climate that begins in the late 20th and early 21st centuries. In the ensemble mean both *P* and *E* decrease but the former by a larger amount. *P*–*E* primarily reduces in winter when *P* reduces and *E* is unchanged or modestly increased while in summer both *P* and *E* decrease (not shown). The annual mean reduction in *P* for this region, calculated from rain gauge data within the Global Historical Climatology Network, was 0.09 mm/day between 1932 and 1939 (the Dust Bowl drought) and 0.13 mm/day between 1948 and 1957 (the 1950s Southwest drought). The ensemble median reduction in *P* that drives the reduction in *P*–*E* reaches 0.1 mm/day in mid-century and one quarter of the models reach this in the early part of the current century.

Figure 2 shows for the 19 models the annual mean *P*–*E* difference between 20 year periods in the 21st century and the model's 1950–2000 climatology. Almost all models have a drying trend in the American Southwest and consistently so throughout the century. Only one of the 19 models has a trend to a wetter climate. Of the total of 49 individual projections conducted with the 19 models, even as early as the 2021 to 2040 period, only 3 show a shift to a wetter climate. Examples of modeled history and future precipitation for single simulations of four individual models are shown in Fig. 3 and provide an idea of potential trajectories towards the more arid climate.

Figure 4 shows (contours, all panels) a map of the change in *P*–*E* for the decades between 2021 and 2040 minus the

1950–2000 period for one of the IPCC models: the Geophysical Fluid Dynamics Laboratory climate model CM2.1 (*5*). In general, large regions of the relatively dry subtropics dry further while wetter higher latitude regions become wetter still. In addition to the American Southwest, the Southern Europe-Mediterranean-Middle East region also experiences a severe drying. This pattern of subtropical drying and moistening at higher latitudes is a robust feature of current projections with different models of future climate (*6*).

The change (δ) in *P–E* (in m/s) is balanced by a change in atmospheric moisture convergence, viz.:

$$\rho_w g\delta(P-E) = -\delta\left(\int_0^{p_s} \nabla\cdot(\overline{\underline{u}\,\overline{q}})dp + \int_0^{p_s} \nabla\cdot(\overline{\underline{u}q'})dp\right) \quad (1)$$

Overbars indicate monthly means and primes departures from the monthly mean, ρ_w is the density of water. The change in moisture convergence can be divided into contributions from the 'mean flow' and from 'eddies'. In the former the atmospheric flow $(\overline{\underline{u}})$ and the moisture $(\overline{q})$ are averaged over a month before computing the moisture transport, while the latter is primarily associated with the highly variable wind ($\underline{u}'$) and moisture (q') fields within storm systems. The moisture convergence is integrated over pressure (p) from the top of the atmosphere ($p = 0$) to the surface (p_s). The mean wind and humidity fields in Eq. 1 can be taken to be their climatological fields. (The rectification of interannual variability in the monthly mean flow and moisture fields is found to be negligible.) Changes in the mean flow contribution can, in turn, be approximated by one part associated with the 1950–2000 climatological circulation $(\overline{\underline{u}}_P)$ operating on the increase in climatological atmospheric humidity $(\delta\overline{q}$, a consequence of atmospheric warming) and another part due to the change in circulation climatology $(\delta\overline{\underline{u}})$ operating on the 1950–2000 atmospheric humidity climatology $(\overline{q}_P)$. The nonlinear term involving changes in both the mean flow and moisture field is found to be relatively small (not shown). Hence Eq. 1 can be approximated by:

$$\rho_w g\delta(P-E) \sim -\int_0^{p_s} \nabla\cdot(\overline{q}_P\delta\overline{\underline{u}} + \overline{\underline{u}}_P\delta\overline{q})dp - \delta\int_0^{p_s} \nabla\cdot(\overline{\underline{u}'q'})dp \quad (2)$$

We therefore think in terms of a three-fold decomposition of *P–E*, as displayed in Fig. 4 (colors) for the GFDL CM2.1 model: a contribution from the change in mean circulation, a contribution from the change in mean humidity, and a contribution from eddies.

The mean flow convergence term involving only changes in humidity (Fig. 4B) causes increasing *P–E* in regions of low level mean mass convergence and decreasing *P–E* in regions of low level mean mass divergence, generally intensifying the existing pattern of *P–E* (*6*). This term helps explain much of the reduction in *P–E* over the subtropical oceans where there is strong evaporation, atmospheric moisture divergence and low precipitation (*6*). Over land areas, in general, there is no infinite surface water source and *P–E* has to be positive and sustained by atmospheric moisture convergence. Over the American Southwest, in the current climate, it is the time varying flow that sustains most of the positive *P–E* while the mean flow diverges moisture away. Here, the 'humidity contribution' leads to reduced *P–E* as the moisture divergence by the mean flow increases with rising humidity. Over the Mediterranean region there is mean moisture divergence and again rising humidity leads to increased mean moisture divergence and reduced *P–E*.

Over the ocean the contribution of humidity changes to changes in *P–E* can be closely approximated by assuming that the relative humidity remains fixed at its 1950–2000 values (*6*). Over almost all land areas, and especially over those that have reduced *P–E*, the relative humidity decreases in the early 21st century. This is because, unlike over the ocean, evaporation cannot keep pace with the rising saturation humidity of the warming atmosphere. Over land the humidity contribution to the change in *P–E* is distinct from that associated with fixed relative humidity.

Decreases in *P–E* can also be sustained by changes in atmospheric circulation that alter the mean moisture convergence even in the absence of changes in humidity (Fig. 4A). This 'mean circulation contribution' leads to reduced *P–E* at the northern edge of the subtropics (e.g. the Mediterranean region, the Pacific and Atlantic around 30°N and parts of southwestern North America). The change in moisture convergence by the transient eddies (Fig. 4C) dries southern Europe and the subtropical Atlantic and moistens the higher latitude Atlantic but does not have a coherent and large impact over North America.

A significant portion of the mean circulation contribution, especially in winter, can be accounted for by the change in zonal mean flow alone (not shown), indicating that changes in the Hadley Cell and the extratropical mean meridional circulation are important. In summary, increases in humidity and mean moisture divergence, changes in atmospheric circulation and intensification of eddy moisture divergence, cause drying in the subtropics, including over western North America and the Mediterranean region. For the Southwest region, the annual mean *P–E* reduces by 0.086 mm/day which is largely accounted for by an increase in the mean flow moisture divergence. Changes in the circulation alone contribute 0.095 mm/day of drying and changes in the humidity alone contribute 0.032 mm/day. This is modestly offset by an increased transient eddy moisture convergence of 0.019 mm/day.(*7*).

Within models the poleward edge of the Hadley Cell and the mid-latitude westerlies move poleward during the 21st century (*8–10*). The descending branch of the Hadley Cell causes aridity and hence the subtropical dry zones expand poleward. In models, a poleward circulation shift can be forced by rising tropical SSTs in the Indo-Pacific region (*11*) and by uniform surface warming (*12*). The latter results are relevant because the spatial pattern of surface warming in the AR4 models is quite uniform away from the poles. One explanation (*13*, *14*) is that rising tropospheric static stability, an established consequence of moist thermodynamics, stabilizes the subtropical jet streams at the poleward flank of the Hadley Cell to baroclinic instability. Consequently the Hadley Cell extends poleward, increasing the vertical wind shear at its edge, to a new latitude where the shear successfully compensates for the suppression of baroclinic instability by rising static stability.

While increasing stability is likely to be a significant component of the final explanation, a fully satisfying theory for the poleward shift of the zonal mean atmospheric circulation in a warming world must account for the complex interplay between the mean circulation (Hadley Cell and the mid-latitude Ferrell Cell) and the transient eddies (*13*, *14*) that will determine where precipitation will increase and decrease in the future. However not all of the subtropical drying in the Southwest and Mediterranean region can be accounted for by zonally symmetric processes and a full explanation will require attention to moisture transport within localized storm tracks and stationary waves.

The six severe, multiyear, droughts that have struck western North America in the instrumental record have all been attributed, using climate models, to variations of sea surface temperatures (SSTs) in the tropics, particularly persistent La Niña-like SSTs in the tropical Pacific Ocean (*15–19*). The future climate of intensified aridity in the Southwest is caused by different processes since the models vary in their tropical SST response to anthropogenic forcing. Instead it is caused by rising humidity that causes increased moisture divergence and changes in atmospheric circulation cells that include a poleward expansion of the subtropical dry zones. The drying of subtropical land areas that, according to the models is imminent or already underway, is unlike any climate state we have seen in the instrumental record. It is also distinct from the multidecadal megadroughts that afflicted the American Southwest during Medieval times (*20-22*) which have also been attributed to changes in tropical SSTs (*18*, *23*). The most severe future droughts will still occur during persistent La Niña events but they will be worse than any since the Medieval period because the La Niña conditions will be perturbing a base state that is drier than any experienced recently (*25*).

References and Notes

1. U. Cubasch et al., in *Climate Change 2001 - The Scientific Basis: Contribution of Working Group I to the Third Assessment Report of the Intergovernmental Panel on Climate Change* (Eds. Houghton, J.T. et al.) (Cambridge University Press, 2001), pp. 525–582.
2. M. R. Allen and W. J. Ingram, *Nature* **419**, 224 (2002).
3. Details of the models analyzed can be found at http://www-pcmdi.llnl.gov/ipcc/model_documentation/ipcc_model_documentation.php and the data at https://esg.llnl.gov:8443/index.jsp .
4. N. Nakicenovic, R. Swart (Eds.), *Special Report on Emissions Scenarios* (Cambridge University Press, New York, 2000).
5. T. L. Delworth et al., *J. Climate* **19**, 643 (2006).
6. I. M. Held, B. J. Soden, *J. Climate* **19**, 5686 (2006).
7. The model P–E is not fully accounted for by the computed moisture flow convergence by the sum of the components of the mean flow and transient eddies (the imbalance is 0.022 mm/day). Calculations were performed with daily data on the model grid using closely matching numerics but errors can be introduced by not using sub-daily data and by neglect of moisture diffusion, potentially large over mountains) which was not archived. The data is available at http:/kage.ldeo.columbia.edu/SOURCES/.LDEO/.ClimateGroup/.GFDL .
8. J. H. Yin, *Geophys. Res. Lett.* doi:10.1029/2005GL023684 (2005).
9. P. J. Kushner, I. M. Held and T. L. Delworth, *J. Climate* **14**, 2238 (2001).
10. L. Bengtsson, K. I. Hodges and E. Roeckner, *J. Climate* **19**, 3518-3543.
11. N.-C. Lau. A. Leetmaa and M. J. Nath, *J. Climate* **19**, 3607 (2006).
12. S. Lee, *J. Atmos. Sci.* **56**, 1353 (1999).
13. T. Schneider, *Ann. Rev. Earth Plan. Sci.* **34**, 655 (2006).
14. C. C. Walker and T. Schneider, *J. Atmos. Sci.* **63**, 3333.
15. 13. S. D. Schubert, M. J. Suarez, P. J. Region, R. D. Koster, J. T. Bacmeister, *Science* **303**, 1855 (204).
16. S. D. Schubert, M. J. Suarez, P. J. Region, R. D. Koster, J. T. Bacmeister, *J. Climate* **17**, 485 (2004).
17. R. Seager, Y. Kushnir, C. Herweijer, N. Naik, J. Velez. *J. Climate* **18**, 4068 (2005).
18. C. Herweijer, R. Seager and E. R. Cook, *The Holocene* **16**, 159 (2006)
19. H.-P. Huang, R. Seager and Y. Kushnir, *Clim. Dyn.* **24**, 721 (2005).
20. S. Stine, *Nature* **369**, 546 (1994).
21. E. R. Cook, C. A. Woodhouse, M. Eakin, D. M. Meko and D. W. Stahle, *Science* **306**, 1015(2004).
22. C. Herweijer, R. Seager, E. R. Cook and J. Emile-Geay, *J. Climate* **20**, 1353.

23. E. R. Cook, R. Seager, M. A. Cane, D. W. Stahle, *Earth Sci. Rev.* **81**, 93 (2007).
24. This work was supported at LDEO by NOAA grants NA03OAR4320179, NA06OAR4310151, NA03OAR4320179 and NA03OAR4320179, and NSF grants ATM05-01878 and ATM03-47009. We thank R. Dole, W. Robinson, and M. Wallace for useful conversations

.

5 January 2007; accepted 26 March 2007
Published online 5 April 2007; 10.1126/science.1139601
Include this information when citing this paper.

Fig. 1: Modeled changes in annual mean precipitation minus evaporation over the American Southwest (125°W–95°W, 25°N–40°N, land areas only) averaged over ensemble members for each of the 19 models. The historical period used known and estimated climate forcings and the projections used the SResA1B emissions scenario. Shown are the median (red line) and 25th and 75th percentiles (pink shading) of the *P–E* distribution amongst the 19 models, and the ensemble medians of *P* (blue line) and *E* (green line) for the period common to all models (1900 to 2098). Anomalies for each model are relative to that model's climatology for 1950–2000. Results have been six year low pass Butterworth filtered to emphasize low frequency variability that is of most consequence for water resources. Units are in mm/day. The model ensemble mean *P–E* in this region is around 0.3 mm/day.

Fig. 2: The change in annual mean *P–E* over the American Southwest (125°W–95°W, 25°N–40°N, land areas only) for 19 models relative to model climatologies for 1950-2000. Results are averaged over twenty year segments of the current century. The number of ensemble members for the projections are listed by the model name at left. Black dots represent ensemble members, where available, and red dots represent the ensemble mean for each model. Units are in mm/day.

Fig. 3: The change in annual mean *P–E* over the American Southwest (125°W–95°W, 25°N–40°N, land areas only) for four coupled models relative to model ensemble mean climatologies for 1950–2000. The results are from individual simulations of the 1860 to 2000 period forced by known and estimated climate forcings and individual projections of future climate using the SResA1B scenarios of climate forcings. Since the modeled anomalies have not been averaged together here these time series provide an idea of plausible evolutions of Southwest climate towards a more arid state. The models are the National Center for Atmospheric Research Community Climate System Model, Geophysical Fluid Dynamics Laboratory model CM2.1, Max Planck Institut Für Meteorologie model ECHAM5 and Hadley Centre for Climate Change model HadCM3. All time series are for annual mean data and a six year low pass Butterworth filter has been applied. Units are in mm/day.

Fig. 4: The change in annual means of *P–E* for 2021–2040 minus 1950–2000 (all panels, contours) and contributions to the change in vertically integrated moisture convergence (colors, negative values imply increased moisture divergence) by the mean flow due to changes in the flow (top), the specific humidity (middle) and the transient eddy moisture convergence (bottom), all for the GFDL CM2.1 model. The box shows the area we define as the "Southwest."

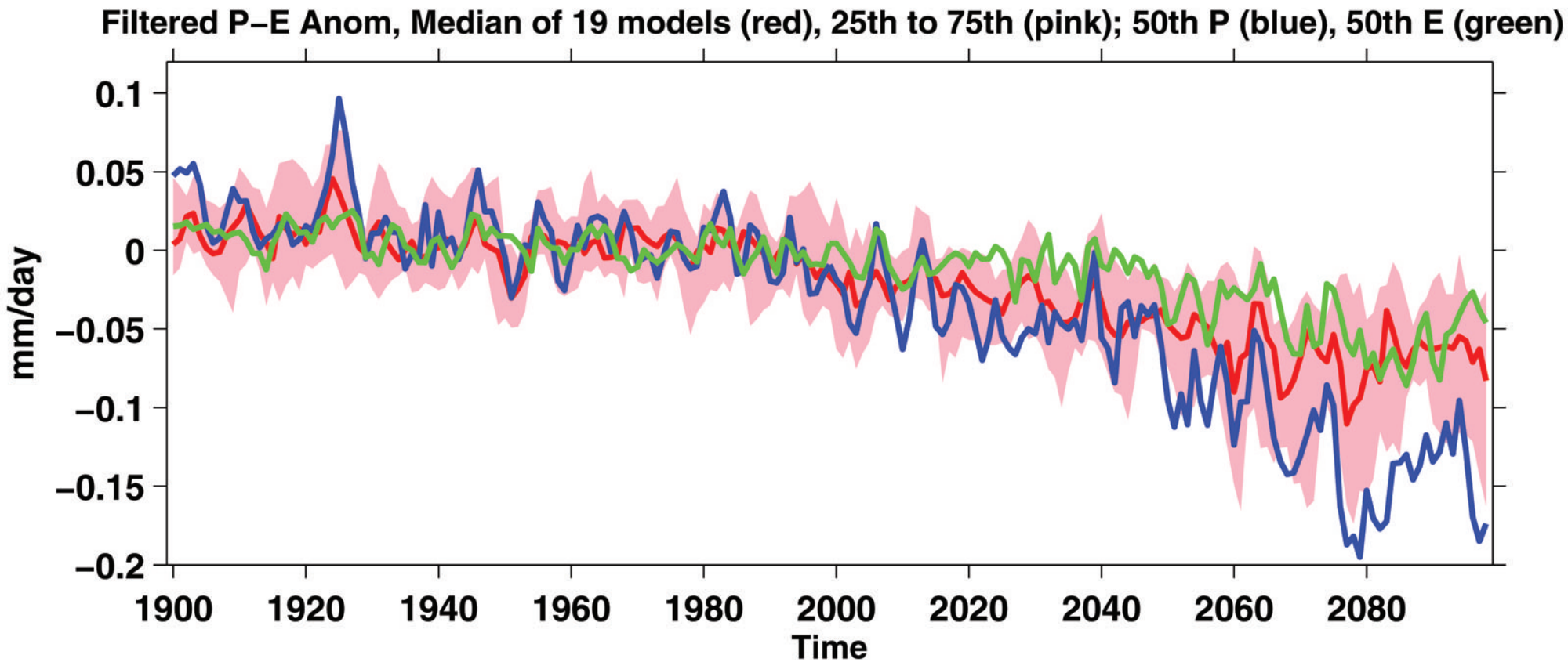
Filtered P−E Anom, Median of 19 models (red), 25th to 75th (pink); 50th P (blue), 50th E (green)
0.1
0.05
0
−0.05
−0.1
−0.15
−0.2
mm/day
1900
1920
1940
1960
1980
2000
2020
2040
2060
2080
Time

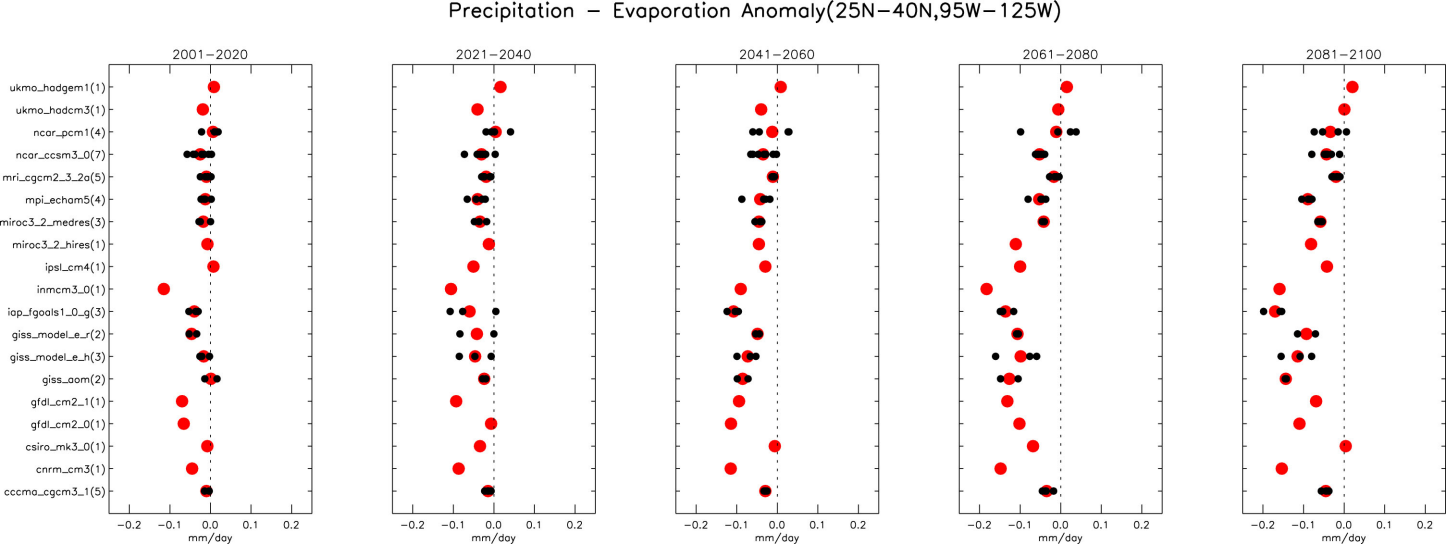
Precipitation − Evaporation Anomaly(25N−40N,95W−125W)
2001−2020
2021−2040
2041−2060
2061−2080
2081−2100
ukmo_hadgem1(1)
ukmo_hadcm3(1)
ncar_pcm1(4)
ncar_ccsm3_0(7)
mri_cgcm2_3_2a(5)
mpi_echam5(4)
miroc3_2_medres(3)
miroc3_2_hires(1)
ipsl_cm4(1)
inmcm3_0(1)
iap_fgoals1_0_g(3)
giss_model_e_r(2)
giss_model_e_h(3)
giss_aom(2)
gfdl_cm2_1(1)
gfdl_cm2_0(1)
csiro_mk3_0(1)
cnrm_cm3(1)
cccma_cgcm3_1(5)
−0.2
−0.1
0.0
0.1
0.2
mm/day

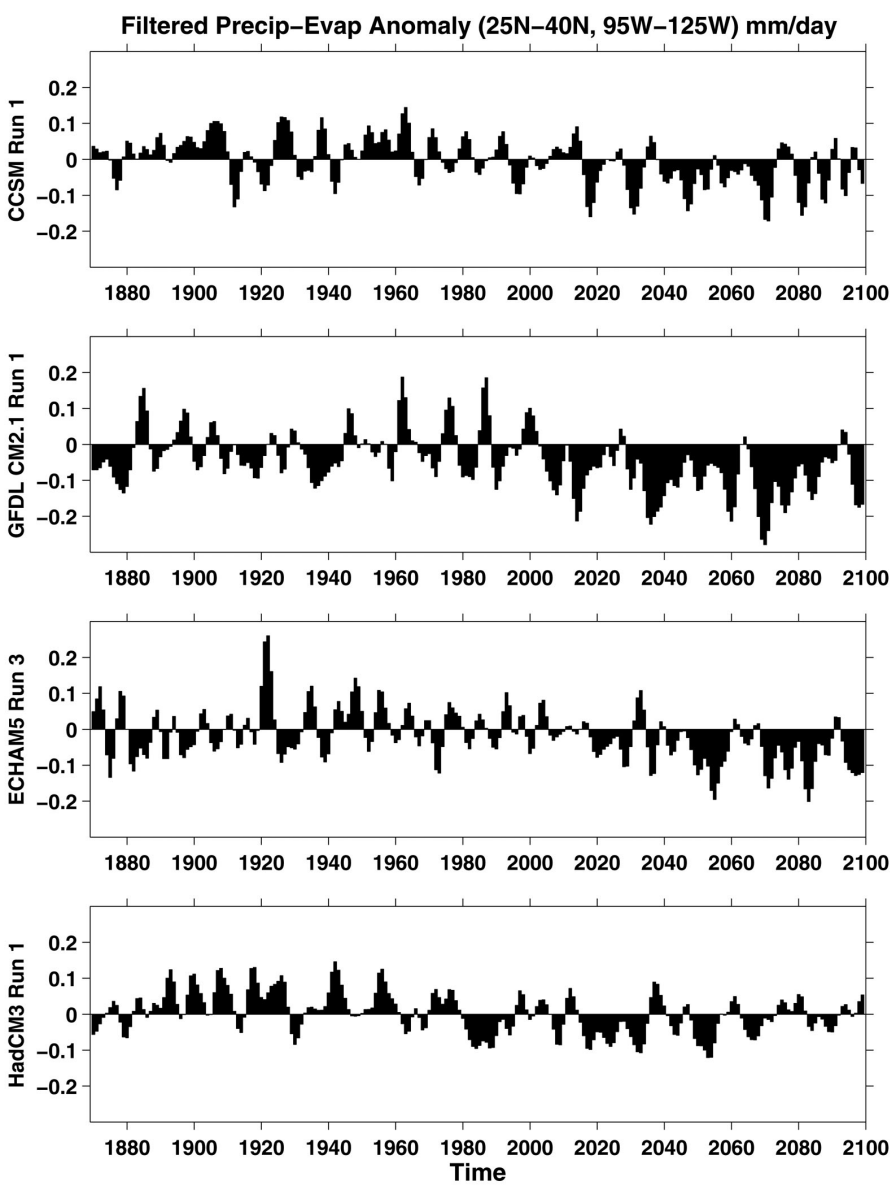
Filtered Precip−Evap Anomaly (25N−40N, 95W−125W) mm/day
CCSM Run 1
GFDL CM2.1 Run 1
ECHAM5 Run 3
HadCM3 Run 1
0.2
0.1
0
−0.1
−0.2
1880
1900
1920
1940
1960
1980
2000
2020
2040
2060
2080
2100
Time

Contributions to Change in Moisture Convergence (2021-2040) - (1950-2000)

a) Mean Circulation Contribution

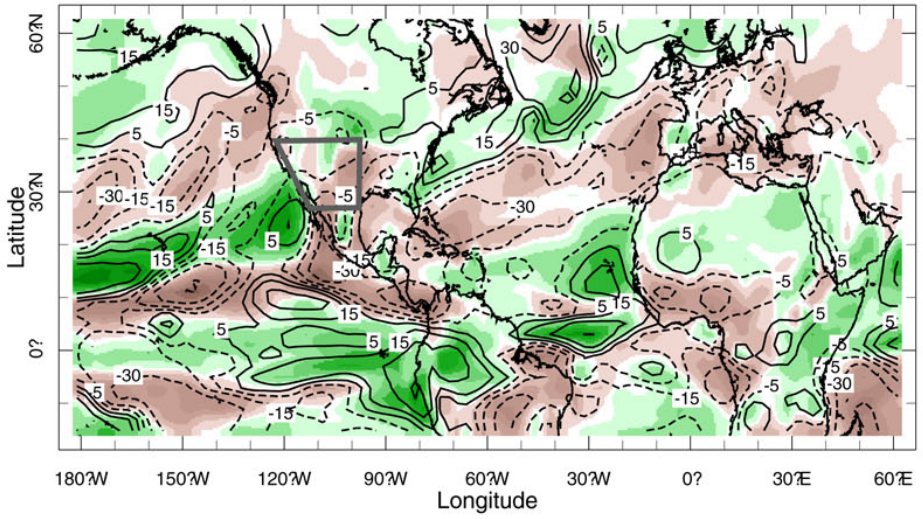

b) Q Contribution to Mean

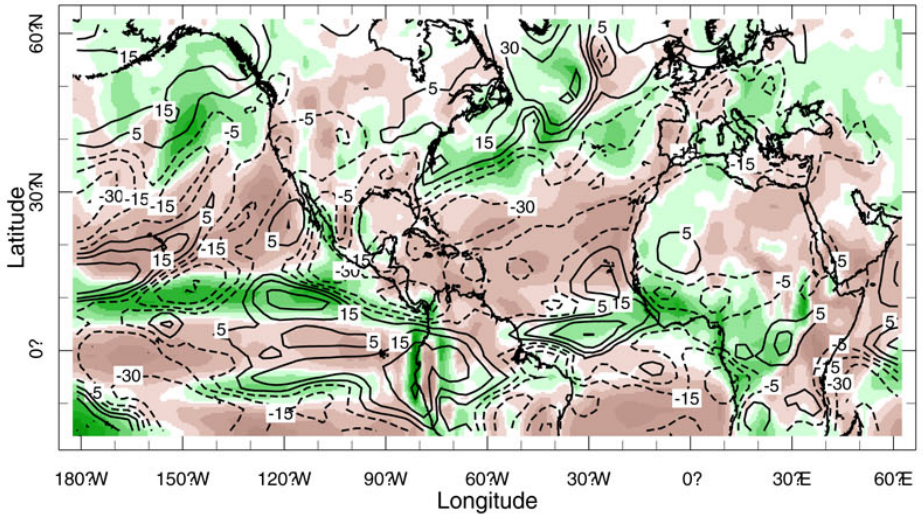

c) Transient Contribution

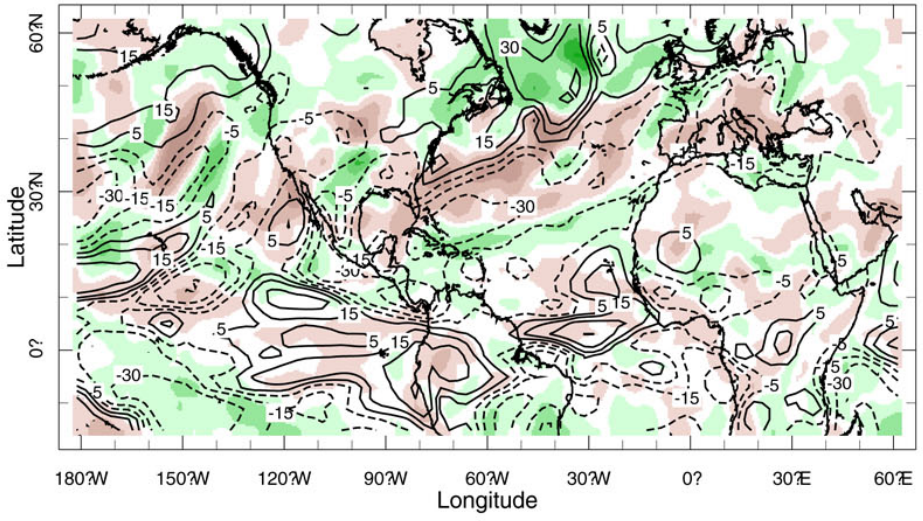

EXHIBIT 409

Journal of Arid Environments (2000) **46:** 000–000
doi:10.1006/jare.2000.0711, available online at http://www.idealibrary.com on IDEAL®

Degradation of sandy arid shrubland environments: observations, process modelling, and management implications

Gregory S. Okin‡, Bruce Murray* & William H. Schlesinger†

**Division of Geological and Planetary Sciences 100-23, California Institute of Technology, Pasadena, CA, 91125, U.S.A.*
† Department of Botany, Duke University, Durham, NC, 27708-0340,U.S.A.

(Received 27 March 2000, accepted 25 August 2000)

Field remote sensing, and modelling observations from a degraded Mojave Desert shrubland were used to develop a model of the progressive degradation of areas adjacent to sites of direct anthropogenic disturbance. Aeolian removal and transport and dust, sand, and litter are the primary mechanisms of degradation, killing plants by burial and abrasion, interrupting natural processes of nutrient accumulation, and allowing the loss of soil resources by abiotic transport. It is concluded that any arid shrubland with wind-erodible soils is susceptible to degradation, and where possible development of these lands should be avoided.

© 2000 Academic Press

Keywords: desertification; wind erosion; Mojave Desert; shrublands; paleolakes; agriculture

Introduction

The Manix Basin in the Mojave Desert of south-eastern California is the site of ancient Lake Manix (Buwalda, 1914; Meek, 1989, 1990; Dohrenwend *et al.*, 1991). Far from being a unique geological setting, the fine-grained lacustrine sediments in the basin are part of the Pleistocene legacy shared by depressions throughout the entire basin and Range and Mojave provinces (Smith & Street-Perrott, 1983). Morrison (1991*b*, 1991*a*) has reported that 'nearly all closed or formerly closed basins in the Great Basin have ancient strandlines marked by lacustrine bars, spits, embankments, terraces, deltas, and wave-cut cliffs at elevations well above the playas or permanent lakes of today'. The lacustrine sediments of Pleistocene age that form the floors of these basins share qualities that make them amenable for agriculture and other human activities: very low slopes, little or o relief, subsurface water resources, and fine-grained sediments suitable for farming or other activities. The intersection of the human uses of Pleistocene paleolakes with their geological history creates opportunities for land degradation much greater than typically recognized.

‡ Corresponding author. Tel.: (626) 395-6465, Fax: (626) 585-1917, E-mail: okin@gps.caltech.edu.

0140-1963/00/000000 + 22 $35.00/0 © 2000 Academic Press

JARE 20000711 PROD.TYPE: TYP ED: JOLLY
PAGN: NVS – SCAN: Venki\Anitha\Preethy

Wind erosion in the Mojave Desert is the principle mechanism of land degradation. Agriculture, urban development, military maneuvers, pipeline, road and powerline construction, and recreational vehicles all destroy vegetation cover and expose the soil to wind erosion (Sharifi *et al.*, 1999). These activities can result in increased dust emission, blowing sand, and damage of native vegetation.

Although the processes of arid land degradation have been well-established elsewhere in the south-western U.S. (see for example, Schlesinger *et al.*, 1990), no published process model exists for shrubland degradation in the Mojave Desert or other shrublands. In this paper, we report on the importance of human-induced wind erosion in initiating and propagating land degradation in the Manix Basin of the Mojave Desert. Based on these observations, we develop a model of wind-driven desertification in sandy arid shrublands.

Arid land degradation has received significant attention in the technical and popular media over the past several decades. Much of this interest has been practical in nature owing to the facts that: (1) desertification is widespread throughout the south-western United States and globally (Mabbutt & Floret, 1980; Walker, 1982; Warren & Hutchinson, 1984; Verstraete & Schwartz, 1991; Khalaf & Al-Ajmi, 1993; Dregne, 1995); (2) it has severe financial and societal consequences including property damage, increased health and safety hazards, and decreased agricultural productivity (Clements *et al.*, 1963; Bowden *et al.*, 1974; Fryrear, 1981; Hyers & Marcus, 1981; Leathers, 1981; Leys & McTainsh, 1994; Bach, 1998); and (3) some forms of desertification are irremediable on human timescales at reasonable cost (Whitford, 1992; Dregne, 1995). The increasing use of desert shrublands by humans for habitation, agriculture, industry, and recreation increases the amount of arid land directly impacted (Verstraete & Schwartz, 1991). Thus, it is important to understand the processes of arid land degradation in these environments. Improved process understanding will allow improved identification of areas at heightened risk of desertification before serious damage has occurred.

History and features of the Manix Basin, California

Our observations are drawn from the Manix Basin in the Mojave Desert, about 25 miles ENE of Barstow in south-eastern California (centred around 34°56·5′N·116°41·5′ W at an elevation of about 540 m). The basin has an area of 40,700 ha and was the site of ancient Lake Manix which existed during the peak pluvial episode of the last glaciation and drained through Afton Canyon to the east (Smith & Street-Perrott, 1983; Meek, 1989). Much of the basin is filled with lacustrine, fluvial, and deltaic sediments capped by weak armoring (Meek, 1990). There is clear evidence of pre-modern wind erosion, indicating that wind erosion, transport, and deposition has long been a dominant geological process in the area (Evans, 1992).

The modern climate of the Manix Basin is arid with an average annual precipitation of 100 mm, falling mostly in the winter, although there can be significant summer precipitation in some years (Table 1). The average annual temperature is 19·6°C, the average

Table 1. *Average precipitation (cm) by season at Daggett Airport*

	Jan–Mar	Apr–Jun	Jul–Sept	Oct–Dec	Annual
1944–1997	3·7	0·9	2·9	2·4	10·0
1980–1989	4·5	1·1	3·1	3·1	12·7
1990–1997	6·0	0·3	2·8	2·0	11·1

Source: National Climate Data Center, U.S. Precipitation by State, California: http://www.ncdc.noaa.gov/ol/climate/online/coop-precip.html

JARE 20000711

winter temperature of 9·1°C, and the average summer temperature is 31·4°C (Meek, 1990). The average wind speed at the airport in Daggett is 5·5 m s^{-1} at a height of 6·1 m and is typically from the west (National Climate Data Center, 1993).

The vegetation in undisturbed areas of the basin in dominated by an association of *Larrea tridentata* and *Ambrosia dumosa*, with minor occurrence of *Atriplex polycarpa, Atriplex hymenelytra, Atriplex canescens, Ephedra californica,* and *Opuntia* spp. *Prosopis glandulosa* occurs in some areas of the basin. Areas that have been disturbed directly by human activity are dominated by *A. polycarpa* with total cover often greater than that in undisturbed desert. *Schismus*, an exotic annual grass, in ubiquitous, but grass cover varies significantly with yearly precipitation.

There has been extensive human activity in the Manix Basin with several phases of agriculture utilizing ground-water recharged by the Mojave River. The basin was used for dryland farming in the 1800s (Tugel & Woodruff, 1978). Limited irrigated farming started in the basin in 1902 with the acreage of irrigated land increasing sharply after World War II (Tugel & Woodruff, 1978). Today alfalfa hay is the major agricultural product. In the Coyote Dry Lake sub-basin, square flood-irrigated fields and abandoned flood irrigation equipment are seen in early Landsat images. After the mid-1970s, central-pivot agriculture became the dominant form of land use in the area, but many fields have since been abandoned throughout the northern part of the basin due to increasing costs of ground-water pumping (Ray, 1995).

Methods

In this study a series of Landsat Multispectral Scanner (MSS) and Airborne Visible Infrared Imaging Spectrometer (AVIRIS) images from the Manix Basin from 1979, 1982, 1985, 1988, 1997, and 1998 were used in order to identify areas of blowing sand associated with central-pivot agriculture in the basin. AVIRIS measures the total upwelling spectral radiance in 224 bands from 400 to 2500 nm in 20-m ground pixels from a NASA ER-2 aircraft flying at 20-km altitude. Landsat MSS measured upwelling radiation in four visible-near infrared broad multispectral bands in 80-m ground pixels. Geographical information about the extent and locations of blowing sand were the object of the remote sensing analysis. Simple spatial information is readily available from uncalibrated remote sensing images. Therefore, no attempt was made to calibrate the images or correct for atmospheric scattering. The images were incorporated into a geographical information system.

A series of field trips between 1996 and 1999 were undertaken to the Manix Basin in order to verify remote-based observations of sand blow-outs. In 1998 and 1999, perennial vegetation cover was estimated at several sites in the Manix Basin by measuring individual plant diameters in circular plots with 5-m radii (12 replicates each) and assuming full, circular shrub canopies.

Finally, a quantitative assessment of observed wind erosion and deposition rates was undertaken in order to link observed phenomena with physical and mathematical wind erosion models.

Results and discussion

Remote observation from the Manix Basin

The Landsat MSS and AVIRIS images taken in Fig. 1 clearly indicate the growth of sand blow-outs downwind of abandoned agricultural fields in the Manix Basin. Deposition of sand downwind of the fields is a progressive process, with sand plumes lengthening in each successive image. No regrowth of perennial vegetation was observed in these

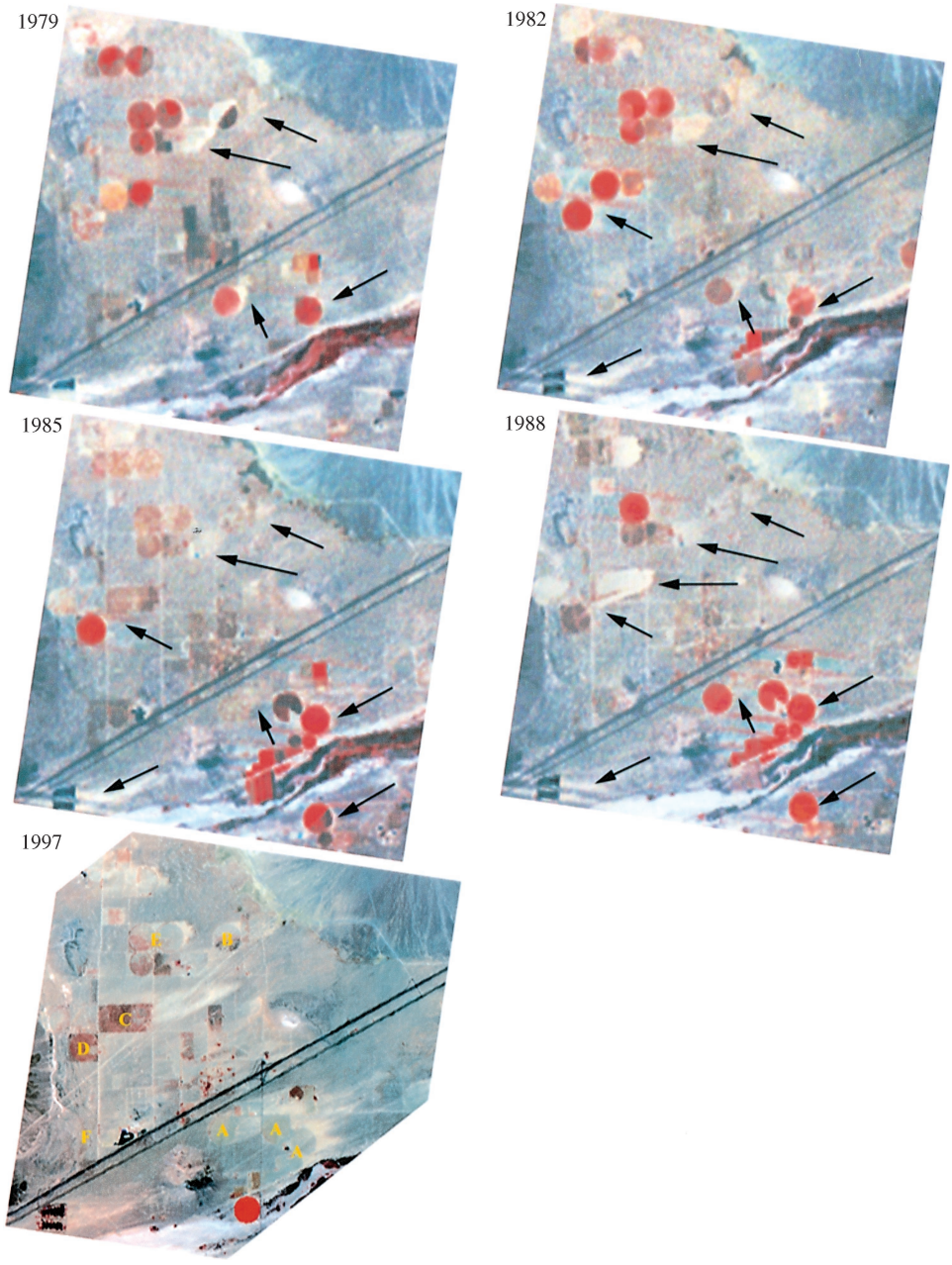

Figure 1. 1979–1988: Landsat Multispectral Scanner (MSS) images of the Manix Basin. Red is MSS band 4 (800–1100 nm), green in MSS band 2 (600–700 nm), and blue is MSS band 1 (500–600 nm). Interstate 15 goes diagonally through the centre of the images. North is up and active fields appear bright red in these images. The wind blows from west to east across the basin causing sand blowouts to appear as bright areas east of the fields. Arrows indicate the progressive appearance of sand mobilized from agricultural fields. 1997: An Airborne Visible Infrared Imaging Spectrometer (AVIRIS) image of the same area taken in 1997, and processed to display colours in the same way as in the MSS images. The relative sharpness of this image is due to the higher spatial resolution of the AVIRIS instrument. The dark-red area C consists of two fields covered with *A. polycarpa* while area A is an abandoned field with very little shrub cover. Both areas exhibit dramatic sand blowouts downwind.

Table 2. *Direct and indirect disturbance for some selected fields in the Manix Basin*

Location (see Fig. 1)	Total time cultivated (years)	Time since abandonment (years)	Soil Texture	Area subject to direct disturbance (ha)	Area subject to indirect disturbance (ha)	Indirect/direct (area ratio)
A	> 7	< 10	Sand/loamy sand	185	518	2·8
B	1	26	Sand/loamy sand	62	109	1·8
C	5	15, 17	Sand	182	241	1·3
D	6	11	Loamy sand	79	91	1·2
E	6 to 8	10, 14	Loamy sand	124	33	0·3

JARE 20000711

sand plumes. Thus, the occasional darkening of the sand blow-outs is inferred to be due to annual vegetation related to winter rainfall. Annual cover can be relatively high in wet years, but seldom lasts through the spring and summer months.

Anthropogenic disturbance in the Manix Basin may be separated into two types: direct and indirect. Direct anthropogenic disturbance refers to human activities and the consequence of those activities in the area in which they were performed. This includes the actual fields, roads, pastures, corrals, trails, and so on that are affected by land use practices. Indirect disturbance refers to the consequences of direct disturbance in areas not directly disturbed. Our observations demonstrate that both direct and indirect disturbance are extensive in the Manix Basin, and that they are coupled by wind erosion and redeposition of wind-blown sediment.

Ray (1995) has reported that in 1985 agriculture in the Manix Basin reached its greatest extent with 37 active central-pivot irrigated fields accounting for 3062 ha of land in cultivation. Agricultural activity in the basin has decreased in the last decade. Thus, at least 3000 ha of land have been directly disturbed in the Manix Basin. By areal analysis of 1998 AVIRIS data, the relative areas of direct and indirect disturbance were identified in the form of sand blow-outs, for some of the fields in the Manix Basin (Table 2). No clear relationship was found between time of abandonment nor of cultivation with the magnitude of indirect disturbance. All fields were located in soils with sandy or loamy sand soils, the dominant soil textures in the basin (Tugel & Woodruff, 1978).

Sand may be blown several kilometres beyond the downwind boundary of a field and therefore the area of indirect disturbance can exceed the directly disturbed area by several-fold. With 3000 ha of land directly disturbed in the basin, 3000 to 9000 ha of land may be expected to be indirectly disturbed by agriculture. This sums to 6000–12,000 ha total disturbance or 15–30% of the total basin floor area, and approximately 23–45% of the non-playa area of the basin. Other disturbances, such as housing developments and roads are also present in the basin, while large areas of the basin are taken up by the Coyote and Troy playas. Anthropogenic degradation appears to have a major impact on land quality and status in the Manix Basin.

Field observations in the Manis Basin

Direct disturbance

Before the fields of the Manix Basin could be cultivated they were cleared of vegetation. Vegetation cover shelters the soil from the erosive force of the wind by: (1) reducing the force of the wind near the ground; (2) extracting momentum above the surface (Wolfe & Nickling, 1993); and (3) trapping soil particles in transport (Lancaster & Baas, 1998). Tillage destroys fragile surface armours, thereby reducing the threshold shear velocity (Gillette *et al.*, 1980; Gillette, 1988; Tegen & Fung, 1955; López, 1998). Vegetation removal and soil cultivation, therefore, have the combined effect of dramatically increasing soil erodibility in the Manix Basin (as seen in Fig. 1). Mechanical agriculture itself visibly mobilizes dust and sand on windy days and ensures that the soil surface is exposed for at least part of the year. Active fields, therefore, become sustained sources of material for aeolian transport immediately upon clearing.

The magnitude of deflation associated with wind erosion of agricultural fields in the Manix Basin is difficult to quantify. However, in one agricultural field in the Manix Basin abandoned about 30 years ago (Fig. 1, area F), wind erosion has led to an average deflation rate of more than 1·5 cm per year, as evidence by wind excavation of buried irrigation pipes. These pipes provide a rare field constraint on deflation, as the vertical feeder sections were once flush with the ground.

Areas that have been cleared to vegetation and then abandoned follow one of two principal trajectories with respect to their vegetative cover. Areas may be recolonized

Table 3. *Percent cover by species in undisturbed desert compared with areas on abandoned central-pivot agriculture fields*

	Undisturbed	On-field (low-cover)	On-field (high cover)
Larrea tridentata	4·8%	0·8%	0·0%
Ambrosia dumosa	1·1%	0·4%	0·0%
Atriplex polycarpa	0·8%	8·3%	32·5%
Total fractional cover	6·7%	9·5%	32·5%

Plant counts were carried out in February 1998 and April 1999 in 5-m radius circles.
The 'Undisturbed' plant cover data represent three sites with 12, 4, and 12 replicates, respectively.
The 'On-field (low cover)' data represent two sites with 12 replicates each. The 'On-field (high cover)' data represent one site with 8 replicates.

principally by *A. polycarpa*, a perennial shrub, and annual exotic grasses such as *Schismus*. Perennial vegetation cover estimates from various sites in the Manix Basin are shown in Table 3. We found 8 to 30% cover a *A. polycarpa* on abandoned fields, while undisturbed areas typically have approximately 5 to 7% cover, dominated by *L. tridentata*. In some cases, only the upwind portions of abandoned fields support a low cover of *A. polycarpa*, even after a decade or more of disuse. This may be due to the fact that fetch, and therefore, mass transport rate of the wind, is lowest here, minimizing plant abrasion and seed removal. These fields have only been abandoned for at most 30 years, and are nowhere near the 65 years Carpenter *et al.* (1986) estimate for a creosote bush scrup community to approach climax conditions nor the several hundred years estimated by Vasek *et al.* (1975). Stylinski & Allen (1999) have suggested that in arid shrublands, altered stable states can occur if a community is pushed beyond its threshold of resilience by anthropogenic disturbance. The dramatic differences between abandoned agricultural fields and undisturbed desert in the Manix Basin after several decades certainly argue for centuries for recovery, if it occurs at all.

Some of the abandoned fields in the Manix Basin do not support any native perennial vegetation, even after a decade or more of disuse. This may be explained by: (1) transport of sand by wind over the exposed soil surface killing young seedlings; and/or (2) absence of climatic or soil conditions suitable for plant germination (Lovich & Bainbridge, 1999). In an experiment aimed at restoring Mojave Desert farmland by seeding native plants in order to reduce dust emissions, Grantz *et al.* (1998) found *A. canescens* could be established in areas without deep sand. However, 'this revegetation was achieved in an anomalous year with above average and late rainfall that eliminated early competition from annual species and later fostered abundant shrub growth. This success was not reproducible in more normal years'. Thus, natural germination of native perennial vegetation on abandoned fields may be rare, explaining the lack of cover on some abandoned fields in the Manix Basin. The importance of germination conditions highlights the dramatic role of interannual climate variability and long-term regional climatic conditions on the response of these ecosystems to human disturbance. Bare fields in the Manix Basin may be expected to take much longer than the vegetated fields to approach climax conditions, if they recover at all.

Once fields are abandoned, they serve as sources of wind-borne sediment at least until a deflationary soil pavement is re-established or they are some how crusted (López, 1998). Landsat MSS and AVIRIS imaged in Fig. 1 depict the mobilization of sand from abandoned agricultural fields in the Manix Basin. Area C, which appears as dark red in the 1997 AVIRIS image, is a set of two fields abandoned in the early 1980s according to Landsat images of the basin from 1973 to 1992; area A was abandoned in 1988 (Ray,

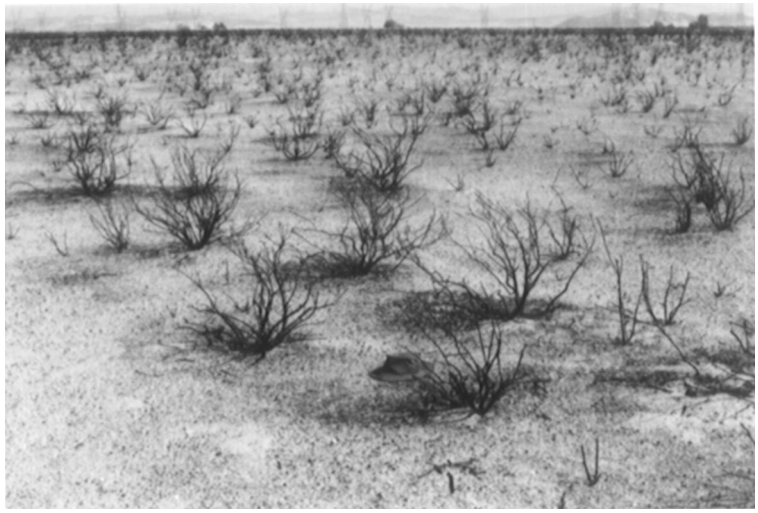

Figure 2. Photograph taken in an abandoned field in the Manix Basin after a fire in the summer of 1998 showing the response of highly disturbed areas to fire. Prior to the fire, this abandoned field had been covered with approximately 30% cover of *A. polycarpa*. Most individuals in the path of the fire in the area of high *A. polycarpa* cover were killed as shown here. Nearby, in adjacent undisturbed desert, only the annual grasses burned and perennial plant mortality was low.

1995). Areas downwind of both fields show significant sand encroachment even though area A has almost no cover and C has relatively high (~30%) *A. polycarpa* cover. Thus, even after regrowth of *A. polycarpa*, abandoned fields remain sources of aeolian sand. High *A. polycarpa* cover may increase roughness length and decrease boundary layer velocity, but once the soil crust was removed, these soils clearly remained.

A notable consequence of the trajectory that areas of direct disturbance follow is their potential response of fire. Lovich & Bainbridge (1999) have reported a 10-year average of 175 fires in the Mojave and Colorado deserts of California that affected an average of 10,927 ha annually. Besides this, there are no published definitive studies of fire return intervals or typical areas burned in individual fires in the Mojave Desert. Nonetheless, it is clear that fire has only recently become a factor in shaping the structure and dynamics of plant communities in the Mojave Desert. In prehistoric times, limited biomass, large intershrub spacing, low combustibility of some native plants and sparse ground cover to support and propagate combustion are thought to have led to very low fire frequencies. The recent proliferation of exotic annual plants has increased the fuel load and fire frequencies in many ecosystems around the world have increased in recent years (Lovich & Bainbridge, 1999).

A fire in the Manix Basin that occurred in June 1998 indicates that areas of high *A. polycarpa* cover have different fire responses than undisturbed areas or abandoned areas of direct disturbance with little or no vegetation regrowth. After the 1998 Manix Basin fire, the mortality of nearly all shrubs on the *A. polycarpa*-covered abandoned field was observed. The same fire burnt a nearby undisturbed area dominated by *L. tridentata* and *A. dumosa*. Here, the fire killed few shrubs and was only sustained in areas with a dense cover of exotic annual grasses as a type of under-storey fire. A fire in an abandoned field covered with *A. polycarpa*, therefore, re-exposed the soil surface to wind erosion while a fire in an undisturbed area has little effect on the landscape (Fig. 2). Disturbed areas that are subsequently burned therefore are likely to have much longer recovery times than their unburned neighbours, both due to fire mortality and the enhanced vulnerability of burnt landscapes to wind erosion.

Figure 3. Photograph taken downwind of an abandoned field in the Manix Basin in the spring of 1988 displaying evidence of active sand movement (sand ripples) and plant mortality. The plants in the foreground are *L. tridentata* and *A. dumosa* individuals that have been buried, abraded and ultimately killed by the encroaching sands.

Indirect disturbance

Indirect disturbance in the Manix Basin primarily takes the form of redeposition of wind-borne sediments onto previously undisturbed adjacent lands. Three types of material are removed from abandoned agricultural fields by wind erosion: saltation-sized particles, suspension-size particles, and organic litter. The removal of all three contributes to indirect disturbance. Saltation of large particles results in their redeposition wherever wind velocities drop, typically in adjacent, downwind vegetated areas or in the lee of plants growing on the field itself.

The encroachment of blowing sand into adjacent shrublands has dramatic consequences for the landscape. Field observations indicate that blowing sand abrades plants, resulting in leaf stripping and damage to the cambium and therefore to the plant's ability to distribute and use water. Young plants are especially vulnerable to the effect of blowing sand as they lack woody tissue. This results in the suppression of revegetation in bare areas and the loss of vegetation on adjacent lands. Nitrogen-fixing microbial communities and cryptobiotic crusts are buried by sand, reducing inputs of nitrogen to the soil (Belnap *et al.*, 1993; Evans & Belnap, 1999).

Blowing sand creates dunes in the wind-shadows of plants. Inspection reveals that these dunes typically have a coarser texture than the material from which they were derived, a result of the progressive removal of fines in a continual process of winnowing (Gibbens *et al.*, 1983; Hennessy *et al.*, 1986; Lyles & Tatarko, 1986). Dunes can grow and coalesce resulting in: (1) burial of large plants not able to grow fast enough to keep up with dune growth; (2) burial of all vegetation including very young shrubs in inter-shrub spaces; and (3) complete blanketing of the soil surface by sand. The persistence of branches and twigs from buried or abraded vegetation decreases the erodibility of the surface, but with time these disintegrate (Fig. 3). Since new vegetation growth is inhibited by blowing sand, the ability of vegetation in stem erosion is limited.

Anthropogenic additions

Chemical fertilizers or other soil amendments are often added to agricultural fields to increase productivity or soil workability. Inorganic salts also may be added inadvertently to the soil as irrigation water evaporates. The transportation of materials from an area of direct disturbance may be accompanied by the dispersal of these soil additives across the landscape. The dispersal of salts by wind onto adjacent undisturbed areas may contribute to the decreased plant growth on these areas by increasing osmolyte concentrations in soil solutions. Okin *et al.* (in press) have reported that Cl^-, SO_4^{-2}, and Na^+ are significantly elevated on and downwind of an abandoned field in the Manix Basin relative to the upwind areas as salts have spread with the moving sands. On the field, Cl^-, SO_4^{-2}, and Na^+ accumulated at average rates of approximately 9·9, 30, 29% per year, respectively over 7 years. This represents a dramatic addition of ions to the soil and may limit the usability of these areas for extended agriculture or influence the recovery of agricultural fields after abandonment.

Soil additives (including nitrate and phosphate) act as chemical tracers of mass flux and determine the relative effects of physical abrasion and nutrient loss in propagating desertification in arid shrublands. Okin *et al.* (in press) have reported significantly elevated concentrations of plant-available N and P on and downwind of an abandoned field in the Manix Basin. Fertilizer has been broadcast across the landscape as the soil from the field has been transported by wind. Despite elevated nutrient concentrations on the abandoned agricultural field at Manix, the absence of shrubs on this field indicates that recolonization of fields by native shrubs after their abandonment is not simply related to nutrient content of the soils, but is dependant more on germination conditions as suggested by Grantz *et al.* (1998). The area immediately downwind of the fertilized field has seen an increase in plant mortality and not a bloom in response to increased nutrient concentrations. This indicates that abrasion and burial of vegetation may dictate a landscape's response to wind erosion, especially in years without favourable germination conditions.

Quantitative assessment

Are the observed rates of deflation and burial of adjacent lands that are suggested quantitatively plausible in the Manix Basin? Using published threshold shear velocities and equations for the flux of wind-borne sediments, we conclude that observed deflation rates at the Manix basin are reasonable in light of literature values and theoretical considerations. Our quantitative assessment thus provides insight into the magnitude of deflation, redeposition of saltation-sized particles, and emission of nutrient-laden dust.

With erosion and transport processes have been reviewed many times in the literature (see for example Greeley & Iversen, 1985; Table 3·5). Here, the analysis of Bagnold (1941) will be followed because it is still prevalent in the modern literature of aeolian transport and because it provides a simple method for determining the magnitude of sand transport. From momentum considerations and simplifying assumptions about the path of saltating grains, Bagnold derived a relationship for the horizontal mass flux of saltating grains integrated over all heights:

$$q = C\sqrt{\frac{d}{D}}\,\frac{\rho_a}{g}\,U_*^3, \tag{1}$$

where q is the horizontal mass flux in g cm^{-1} s^{-1}, U_* is the shear velocity, d is the grain diameter of the sand in question, D is the grain diameter of a standard 0·25-mm sand,

ρ_a is density of air, g is the acceleration due to gravity, and C is 1·8 for a naturally graded sand. Assuming that $d = D$, Bagnold's equation simplifies to

$$q = 1{\cdot}5 \times 10^{-9}\,(U - U_t)^3, \tag{2}$$

where U is the wind velocity and U_t is the threshold wind velocity measured at 1 m height. U and U_t are related to shear velocity, U_*, and threshold shear velocity, U_{*t}, respectively, by Bagnold's formula:

$$U_z = \frac{U_*}{k} \ln\left(\frac{z}{z_0}\right), \tag{3}$$

where U_z is wind speed at height z, k is von Karmann's constant taken to be 0·4, and z_0 is the roughness length (Bagnold, 1941).

Shao & Raupach (1993) have shown from energetic considerations that vertical dust flux due to suspension, F, in mass per area per unit time is linearly related to q. Based on this, Gillette *et al.* (1997) have obtained a value for F/q of $5{\cdot}4 \times 10^{-4}\,\mathrm{m}^{-1}$ from wind tunnel experiments, which is of the order of that for sandier soils (Gillette, 1977; Shao & Raupach, 1993; Gillette *et al.*, 1997) and is therefore applicable here.

For a field with cross-wind diameter, x, and area, A:

$$\Delta\tau_{saltation} = \frac{q}{\rho_B}\frac{x}{A}, \tag{4}$$

where ρ_B is the bulk density of the soil and rate of deflation due to saltation, $\Delta\tau_{saltation}$, is expressed as cm year^{-1}. ρ_B is taken to be $1{\cdot}25\,\mathrm{Mg\,m}^{-3}$ for a dry, medium-texture mineral soil (Brady & Weil, 1999), x is taken to be 750 m, and $A = \frac{\pi}{4}x^2$ for a circular field. A/x is a equivalent to erosive fetch. The total average mass rate of erosion is:

$$F_{Total} = q\left(\frac{x}{A}\right) + F \approx q\left(\frac{x}{A}\right), \tag{5}$$

and the total deflation rate (in cm year^{-1}) is given approximately by:

$$\Delta\tau_{total} = \Delta\tau_{saltation} + \Delta\tau_{suspension} = \frac{q}{\rho_B}\left(\frac{x}{A} + \frac{F}{q}\right), \tag{6}$$

where the mass flux due to saltation, q, depends on a detailed wind record, z_0, and U_{*t} by equations (2) and (3).

The threshold shear velocity required to account theoretically for $\Delta\tau_{Total} = 1{\cdot}5$ cm year^{-1} in the Manix Basin was found iteratively using equation (6), Gillette *et al.*'s (1997) value for $F/q = 5{\cdot}4 \times 10^{-4}\,\mathrm{m}^{-1}$, $z_0 = 0{\cdot}04$ cm (an average of values reported by Gillette *et al.* (1980) for non-playa, uncrusted soil), and the wind conditions at Daggett Airport in the Manix Basin where wind speed has been collected hourly since 1961. U_{*t} was found to be 103 cm s^{-1}, well within the bounds of reported values for arid agricultural soils of 20–132 cm s^{-1} (Gillette, 1988). These results indicate that empirically-understood processes can account for observations in the Manix Basin and, therefore, that it is reasonable to invoke these processes to drive indirect disturbance in the conceptual model developed here.

The value $q = 8{\cdot}56$ Mg m^{-1} year^{-1} calculated from $U_{*t} = 103$ cm s^{-1} by equation (2) implies that the equivalent of 10^8–10^9 sand grains saltate through each metre of width per year. In fact, considering that the majority of wind erosion occurs during storms of a few days in duration, this constitutes an extremely concentrated attack on vegetation and is capable of overwhelming plants' self-healing capabilities.

The effect of abrasion acts in tandem with redeposition and dune formation to compromise vegetation in adjacent downwind areas. The total volume, V in m^3 $year^{-1}$, of soil moved by saltation from an abandoned agricultural field is given by:

$$V = \frac{qx}{\rho_B} T, \tag{7}$$

where T is the time in years before the re-establishment of an armoured surface. If the density of the soil is approximately the same after redeposition downwind, volume is conserved and the average depth of burial is given by V/A_b, where A_b is the area buried by the mobilized sand, which can be estimated from remote sensing imagery. Area C in the Manix Basin (Fig. 1, Table 2) has been abandoned for 16 years and has a sand plume downwind with an area of 241 ha. Using the value of q calculated above, we estimate that the average depth of this sand plume is 6·8 cm. However, mobilized sand usually accumulates in the wake of plants, leading to dunes larger than the average depth of burial. In the Manix Basins we have observed dunes greater than 1 m in height. There is currently no theory for determining dune height based on flux measurements or calculations.

Using Gillette *et al.*'s (1997) value for F/q, and reasonable values for x/A, $q(x/A)$ should always be greater than F, indicating that sand mobilization is more important as a wind erosion process than dust emission is terms of mass loss. However, dust emission represents the permanent removal of material from the regional ecosystem due to its potential for long-range transport. Nutrients, especially P, are often concentrated on small particles in soils (Avnimelech & McHenry, 1984; Leys & McTainsh, 1994). Assuming constant suspension flux, the removal of nutrient i from the bulk soil at time t may be written as:

$$F_i^d(t) = C_i^d(t) F, \tag{8}$$

where $C_i^d(t)$ is the concentration of soil nutrient i on the emitted dust and has units of mass of nutrient per mass dust. $F_i^d(t)$, therefore, is in units of mass of nutrient i lost per unit area per unit time. The mass per unit area of soil in a layer of depth, D, is:

$$M^D = \rho_B D, \tag{9}$$

and therefore, the reservoir of nutrients in this layer is $C_i^s(t) M^D$, where $C_i^s(t)$ is the concentration of nutrient i in the soil.

Conservation of mass gives:

$$M_i^{s,D}(t + \mathrm{d}t) - M_i^{s,D}(t) = C_i^d(t) F \mathrm{d}t, \tag{10}$$

where $M_i^{s,D}(t)$ is the mass of nutrient i at time t in a layer of soil of depth, D. Under the approximation that M^D is constant with time, we can divide equation (9) by M^D yielding:

$$C_i^{s,D}(t + \mathrm{d}t) - C_i^{s,D}(t) \approx C_i^d(t) \frac{F}{M^D} \mathrm{d}t, \tag{11}$$

where $C_i^{s,D}(t)$ is the concentration of nutrient i at time t in a layer of soil of depth, D. The ratio of $C_i^d(t)$ to $C_i^{s,D}(t)$ is assumed to be a constant, k_i, that is analogous to a chemical fractionation factor for nutrient i between dust and the bulk soil.

Rearranging equation (10) yields:

$$\frac{\mathrm{d}C_i^s}{\mathrm{d}t} \approx -k_i \frac{F}{\rho_B D} C_i^s. \tag{12}$$

Therefore, the time for the concentration of nutrient i in a layer of soil of depth D to drop by $1/e$ times its original value is given by t_i^D:

$$t_i^D = \frac{\rho_B D}{k_i F} = \frac{t^D}{k_i}, \tag{13}$$

where t^D is the time it takes to completely excavate a layer of depth D with a mass flux rate equal to F. For $D = 0{\cdot}05$ m (a typical sampling depth), $F = 4{\cdot}62$ kg m^{-2} year^{-1} (at $U_{*_t} = 103$ cm s^{-1}) and with a bulk density of 1·25 Mg m^{-3}, t^D is approximately 14 years. Reported values of nitrogen enrichment in Australian arid zone soils are in the order of 10 (Leys & McTainsh, 1994; Carter *et al.*, 1999), although Larney *et al.* (1998) have reported values as low as 1·1.

Talbot *et al.* (1986) have reported concentrations of water-soluble N and P in Saharan dust of 2·58 mg g^{-1} and 123 μg g^{-1} respectively. Using the inferred threshold shear velocity of 103 cm s^{-1} and equation (7), we calculate N and P losses of 1200 μg cm^{-2} year^{-1} (120 kg N ha^{-1} year^{-1}) and 57 μg cm^{-2} year^{-1} (5·7 kg P ha^{-1} year^{-1}), respectively. Typical concentration of N and P reported by Schlesinger *et al.* (1996) in undisturbed Mojave Desert soils are approximately 2 μg N g^{-1} and 0·66 μg P g^{-1}, respectively. Comparing these values with those of Talbot *et al.* (1986) implies that k_N and k_P may be as high as 10^1–10^3 and therefore that t_i^D may be as small as a few years.

Available N and P concentrations at a site in the Jornada Basin measured by Okin *et al.* (in press) indicate approximately a 5-fold net loss of available N and a 3-fold net loss of plant-available P in the 8 years since the establishment of the site. Thus, the e-folding times of N and P, t_N^D and t_P^D, in this surface soil undergoing active deflation and aerosol emission are inferred to be approximately 5–10 years. Wind erosion, therefore, impacts soil fertility in areas of both direct and indirect disturbance on short timescales. This has dramatic implications for nutrient availability in disturbed areas, especially for seed germination in surface soils where the degree of nutrient depletion will be greatest.

Conclusions

Anthropogenic desertification of arid shrublands

Extensive remote sensing, field, and quantitative assessment of arid land degradation in the Manix Basin leads us to conclude that in arid shrublands direct anthropogenic disturbance resulting in the destruction of soil crusts and vegetation cover can cause indirect disturbance of adjacent areas by initiating the disintegration of islands of fertility. Figure 4 illustrates a proposed model for the degradation of arid shrublands based on these observations. The inferred sequence can be visualized as:

(1) Transport of sand from disturbances resulting in deflation of the disturbed surface.
(2) Mobilization of dust and plant litter by wind, depleting the soils of nutrients in areas of direct disturbance.
(3) Damage to and burial of plants by saltating sand in adjacent downwind areas.
(4) Reduction of vegetation cover downwind, leading to an expanding area in which wind removes dust and litter material, depleting the soils of nutrients.

A feedback threshold may be reached when these mechanisms act to dramatically reduce shrub cover in previously undisturbed areas. The accessibility of this threshold is related to allogenic changes in regional climate and interannual variability. Reduced precipitation or increased temperature may exacerbate landscape vulnerability and cooler, wetter conditions may aid amelioration.

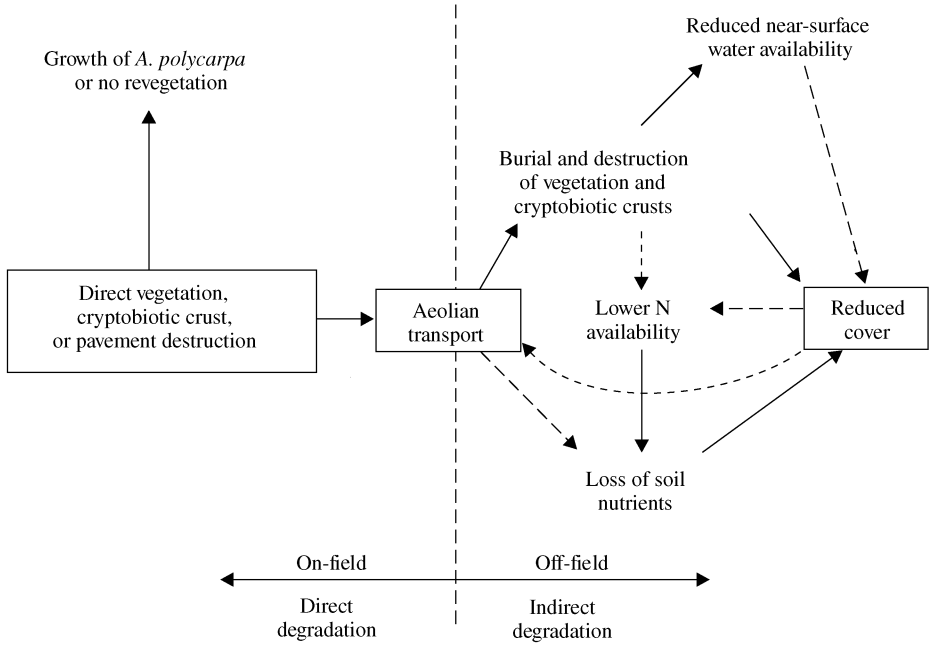

Figure 4. Process model for shrubland degradation developed from observations at the Manix Basin, California. Direct disturbance through vegetation, crust, or pavement destruction drives aeolian transport which leads to indirect degradation in the form of reduced cover in adjacent areas.

Nutrient relations and soil resources

Shrubs are the loci of nutrient accumulation and represent islands of fertility in shrubland ecosystems (Schlesinger *et al.,* 1990). How then does wind erosion affect soil resources in degraded shrublands?

Nutrient removal from islands of fertility has three main mechanisms: (a) physical removal of litter and organic matter by the wind; (2) wind suspension of dust particles with a high concentrations of plant nutrients (Leys & McTainsh, 1994); and (3) retarded accumulation of organic N due to increased surface and air temperatures (Post *et al.*, 1985). In areas of indirect disturbance, the mantle of winnowed dune sand may lead to decreased fertility of the surface soil, which is vital for seedling establishment. Areas of direct disturbance which are the sources for dune sand will also become less fertile through preferential removal of fines by wind. Removal of litter beneath shrubs limits the future availability of organic N and C to plants (Lyles & Tatarko, 1986; Schlesinger & Pilmanis, 1998).

Islands of fertility associated with shrubs are normally sites for recolonization by seedlings (Schlesinger & Pilmanis, 1998). These young plants are more vulnerable to sand abrasion and burial than their mature predecessors and their establishment may be limited. In many areas adjacent to abandoned agricultural fields in the Manix Basin, shrub sites are generally not recolonized and become areas of soil nutrient removal, effectively dismantling the islands of fertility. Schlesinger & Pilmanis (1998) have reviewed field experiments in which shrubs have been removed by cutting, herbicides, or fire. These studies show variable rates of soil degradation, but in each case, 'a loss of the local biogeochemical cycle associated with shrubs has allowed physical processes to

disperse soil nutrients across the landscape'. Thus, the progressive reduction in fertility acts in tandem with the mechanical action of sand to further decrease shrub cover which, in turn, increases the susceptibility of the land of wind erosion. The permanent removal of suspension-sized particles from the soil by wind erosion results in a change of the soil texture, which may also reduce soil binding properties, resulting in increased wind erodibility.

In a study aimed at determining the effect of wind erosion on nutrient availability, Okin *et al.* (in press) have measured available N and P at a disturbed site in the Jornada LTER site in south-central New Mexico. Their results indicated that surface soils upwind of the disturbance are richer in available N and P than those from downwind, if the soils from the upwind transect are considered representative of the original conditions throughout the study site. This indicates approximately a 5-fold net loss of available N and a 3-fold net loss of plant-available P from the soils blown off of the disturbed area. In addition, the site itself lost nearly 94% of its available N and nearly 79% of its plant-available P. Similar results have been reported by Leys & McTainsh (1994) in Australia.

The nutrient cycle may be further disrupted when soil microbial communities are buried or destroyed by blown sand, minimizing their ability to fix atmospheric nitrogen and add it to the nutrient reservoir of the soil. The burial of cryptobiotic crusts also reduces their ability to enhance infiltration of water leading to decreased near-surface soil moisture (Belnap *et al.*, 1993; Belnap, 1995).

It has been suggested by Gibbens *et al.* (1983), Lyles & Tatarko (1986), Hennessy *et al.* (1986), and Leys & McTainsh (1994) that permanent removal of suspension-size particles from the soil by wind erosion may reduce water-holding and cation-exchange capacities. This may result in less water in the surface soil, marginalizing the water balance of desert shrubs and increasing their susceptibility to drought and climate change. On short timescales, this may be particularly important for the establishment of annual grasses. In wet years, these grasses form a carpet that reduces the susceptibility of soils to wind erosion (Lancaster & Baas, 1998). In dry years, decreased near-surface soil moisture makes the landscape more vulnerable to wind erosion. Dust storm frequency has been correlated with reduced soil moisture, indicating that soil erosion and nutrient removal are accelerated by decreased soil moisture (Brazel & Nickling, 1987).

Lessons for land managers

Several aspects of the arid shrubland degradation observed at the Manix Basin can provide lessons for land management in these environments. Wind erosion is the principle mechanism of degradation in arid shrublands on basin floors. The principle consequences of land degradation are therefore:

(1) sand blasting of vegetation and equipment;
(2) burial of vegetation and equipment;
(3) dust emissions leading to decreased nutrient availability, cation-exchange capacity, water-holding capacity, and atmospheric pollution.

For virgin lands, not already converted to human uses, we stress that if possible, arid shrublands with sandy wind erodible soils should not be used for many activities. These are extremely fragile lands, the degradation of which could easily upset marginal economic gains from their cultivation or make recreation and habitation impossible. Furthermore, disturbance of arid shrubland landscapes may disturb successional processes, resulting in permanent landscape change. Where development is deemed necessary, planning must precede plowing. The principle consideration must be the wind erodibility of soils. In the United States, county-wide soil surveys typically provide information on soil texture. Soils of sandy or loamy sand textures, even when covered by

a thin layer of protective crust (deflationary crust, desert pavement, or cryptobiotic crusts), are very vulnerable to wind erosion. Activities which break up soil crusts and destroy vegetation are best avoided. High-risk activities include agriculture, grazing, ORV recreation, and military training. Roads, when necessary, should be situated to minimize the area of wind-erodible soils affected. The location of natural wind breaks such as trees, hills, and mountains should also be used to determine the location of planned developments.

For land already under cultivation or used for recreational purposes, we suggest technological and logistical methods for minimizing the effects of wind erosion in local vegetation, crops, and infrastructure. Equipment, sheds, and other buildings should be situated upwind of fields so that they are not sandblasted or buried. Fields, likewise, should not be situated such that one is close to and downwind of another, or else sand eroded from one will be deposited on another. Talbot (1947) has observed that uncultivated areas between fields in the extremely sandy western lowlands of the Cape Province, South Africa, may stem wind erosion and keep redeposition of sand from occurring in undesirable places. Other wind breaks, preferably indigenous plants which do not need to be watered after establishment, will also help stem erosion. Attempts must be made to keep vegetation on fields as much as possible. In light of this, nitrogen-fixing cover crops may be planted which would minimize erosion and add nitrogen when tilled back into the soil. Fallow periods, especially in the windiest time of the year should be avoided, and cover crops planted instead. Fertilizers may need to be added every few years, when significant nutrient loss is detected and when nitrogen-fixing cover crops are not sufficient to renew the soil resources. When abandoned, fields should be planted with a final, long-lived perennial indigenous cover that will help minimize wind erosion for years to come, and will allow natural succession processes to take place.

Novel management techniques may provide the best opportunities for sustainable management of arid shrublands. We suggest yearly monitoring of soil nitrogen and phosphorous in order to identify times or places where dust emission has significantly depleted the soil of nutrients. Where possible, use should be made of remote sensing and precision farming technologies to ascertain soil condition and to respond appropriately. Carter *et al.* (1999) have reported success in stemming erosion and improving soil conditions by adding clays of sub-soil origin to sandy soils in Western Australia. These and other techniques could be used to dramatically improve the sustainability of agriculture in arid lands.

Agriculture in the Manix Basin is a good example of unregulated and unmanaged human activities for short-term gain leading to long-term loss of value. As farming in the basin has became less profitable, farmers, simply abandoned the land to natural degradation processes without implementing long-term remediation strategies. A principal lesson from this area, therefore, is that policy mandates and financial incentives need to be put in place which promote soil conservation initiatives during land-use and require restoration of the landscape after cultivation stops. Efforts at remediation do not need to focus on restoring the environment to its pristine condition, although this is preferable. Instead, they can focus on halting or slowing soil erosion of planting long-lived, native, and perennial shrubs that will partially protect the surface. Funds for post-agriculture remediation should be earmarked before cultivation begins, and must be considered a part of the cost of business in vulnerable lands. In this way, remediation becomes the responsibility of the short-term land-user and not someone else's long-term problem.

Regional drivers and effects

In addition to the increasing intensity of human disturbance, arid lands are affected by changes in regional climate. How might climate change affect arid shrubland degradation?

The 1980s and 1990s—the decades in which large areas of the Manix Basin were abandoned from agriculture and in which the greatest land degradation has been seen—were neither unusually windy nor dry. The annual average wind speed for the period 1961 to 1990 was 5·5 m s^{-1}, identical to the period of 1980–1989 (National Climate Data Center, 1993). Annual precipitation was only slightly higher between 1970 and 1990 than for the period 1941 to 1997 (Table 1). When the decadal-scale regional climate in the Manix Basin shifts to a windier or drier period, the area affected by nutrient loss and aeolian sand mobilization may be expected to increase dramatically.

There has been much discussion about the relative importance of human *vs*. indirect climate drivers of desertification. Both can have a dramatic impact on the landscape (Schlesinger *et al*., 1990; Brown *et al*., 1997). Climate change may either increase or decrease anthropogenic effects on a landscape. For example, during wetter than average years, the presence of annual grass cover greater than about 15% halts wind erosion, and increased soil moisture leads to higher threshold shear velocities (Brazel & Nickling, 1987; Lancaster & Baas, 1998). In drier than average years, threshold shear velocity may be lower due to decreased soil moisture, and annual cover is greatly reduced leading to accelerated degradation. In the northern Mojave Desert, Schultz & Ostler (1993) have reported a dramatic decrease in total plant cover after only 4 years of drought. Clearly, resistance to climate-induced changes is dependent on the degree of anthropogenic disturbance and *vice versa*. Thus, regional decadal-scale climate conditions may be expected to dramatically influence the rate of arid shrubland degradation.

Extrapolation to other areas

The primary driving mechanism in the process model developed from observations in the Pleistocene paleolake Manix is the aeolian mobilization of sand, dust, and litter material as initiated by anthropogenic disturbance of the surface crust and vegetation cover. Any process that destroys the surface crust in an arid or semi-arid shrubland and increases the boundary layer velocity over a soil with saltation- and suspension-size particles will result in the progressive devegetation of the downwind area. Thus, our model can be extended to incorporate any arid or semi-arid shrubland with a source of wind-erodable material.

Other land forms in the arid south-west

Any arid shrubland with a source of wind-erodable, fine-grained material at the surface may be susceptible to anthropogenic degradation. Our study of the Manix Basin indicates that arid shrublands on Pleistocene paleolake beds are especially susceptible to anthropogenic degradation. Pleistocene lacustrine deposits are common in basin floors throughout the arid south-western United States, where large, shallow pluvia l lakes existed during the Last Glacial Maximum (Smith & Street-Perrott, 1983; Morrison, 1991*a*, *b*). Closed basins that were once Pleistocene lakes exist in many now-arid areas throughout the globe. The degradation observed in the Manix Basin is simply an example which can be applied to similar geological environments globally. They exhibit qualities that make them amenable for many human uses, such as very low slopes, little or no relief, subsurface water resources, and fine-grained sediments suitable for farming or other activities. Thus, the areas of greatest potential usefulness are also susceptible to serious degradation.

The armoured soils of desert bajadas—defined as broad, gently inclined alluvial surfaces extending from the base of mountain ranges to inland basins—may also be susceptible to a similar process of human-induced degradation. Although these soils are typically too gravelly or steep to be used for agriculture, these landforms may be wind

erodible when disturbed by human activities. When present, the soil armour has been argued to develop through the 'born at the top' model of McFadden *et al.* (1987), wherein fine, wind-mobilized particles are trapped by surface cobbles that float atop the accumulation of fine-grained material. Removal of the very stable desert pavement therefore exposes a layer of extremely wind-erodable wind-derived material, sometimes metres thick. Anthropogenic disturbance in these areas is likely to have profound consequences. Certainly, 'born at the top' pavements downwind of areas of active dunes will be at high risk of degradation should be cover of protective pebbles be disturbed. Other soils of aeolian origin, including stabilized dunelands, will similarly be susceptible to anthropogenic degradation of the type discussed here.

Cryptobiotic soil crusts—communities of cyanobacteria, lichens, and mosses—are found throughout the world's deserts. These crusts bind fine soil particles by linked cyanobacterial fibres which protect the soil from wind erosion. Belnap (1995), Williams *et al.* (1995), and Marticorena *et al.* (1997) have suggested that the presence of cryptobiotic crusts dramatically decreases wind and water erosion. When disturbed, cryptobiotic crusts lose most of their protective qualities allowing mobilization of the underlying mineral soils. Shrubland areas with widespread cryptobiotic crusts are thus also vulnerable to progressive degradation should human activities disturb these fragile soil crusts.

Global implications

The problem of wind-induced land degradation is not limited to the south-western United States. Greater use of mechanized agriculture in arid regions throughout the world, as well as other land-use demands, is increasing the amount of arid and semi-arid shrublands brought into cultivation or under human influence (see, for example, Luk, 1983; Kealah, 1989; Khalaf & Al-Ajmi, 1993; Zha & Gao, 1997; Kasusya, 1998; Khresat *et al.*, 1998; Koch & El Baz, 1998; Mitchell *et al.*, 1998). This trend, linked with political/economic instability or the marginal and water-limited nature of arid land agriculture, makes sustainable arid region agriculture especially challenging.

Nations with a large proportion of their territory situated in arid environments with wind-erodible soils are particularly vulnerable to the consequences of land degradation. Great care needs to be employed in the responsible stewardship of these lands to promote sustainable agricultural, and economic and social development.

Summary

Aeolian mobilization of dust, sand, and litter triggered by anthropogenic disturbance contributes to the destruction of islands of fertility by killing shrubs through burial and abrasion. This interrupts nutrient-accumulation processes and allows the loss of soil resources by abiotic transport processes. The resulting reduction of vegetation cover, in turn, increases susceptibility to wind erosion.

Land degradation processes necessarily exist in the context of regional climate and can either be bolstered or hindered by climatic conditions and changes, a fact that makes the rate of degradation ultimately climate-related. The process model developed here suggests various remediation techniques to halt shrubland degradation, but ultimately indicates that development of landscapes susceptible to wind erosion should be avoided where possible.

In the face of largely unsustainable socioeconomic factors, the vulnerability of arid lands to degradation argues for the development of linked degradation process models and monitoring strategies in order to minimize environmental damage and to promote sustainable management of human activities in arid lands. The dramatic landscape

changes that accompany arid shrubland degradation can be monitored using present and future remote sensing techniques and technologies. When informed by process models, such as the one presented here, remote monitoring tools may be used in the future to identify areas at risk of runaway degradation before large areas are adversely affected.

Globally, degradation of already-marginal arid lands represents a dramatic threat to local populations, food resources, and regional stability. Presently, the United Nations Convention to Combat Desertification is before the United States Senate for ratification. This treaty provides for scientific and technical exchange to combat desertification. The processes of arid land degradation must be understood, effective monitoring techniques developed, and effective remediation and management techniques implemented to avoid costly and prolonged environmental crises. The model presented here represents a small step in attaining these goals.

The authors wish to thank Drs Lancaster, Gillette, Monger, and Meek for their useful comments on the manuscript.

References

Avnimelech, Y. & McHenry, J.R. (1984). Enrichment of transported sediments with organic carbon, nutrients, and clay. *Soil Science Society of America Journal*, **48**: 259–266.

Bach, A.J. (1998). Assessing conditions leading to severe wind erosion in the Antelope Valley, California, 1990–1991. *Professional Geographer*, **50**: 87–97.

Bagnold, R.A. (1941). *The Physics of Blown Sand and Desert Dunes*. New York: Methuen, 265 pp.

Belnap, J. (1995). Surface disturbances: their role in accelerating desertification. *Environmental Monitoring and Assessment*, **37**: 39–57.

Belnap, J., Harper, K.T. & Warren, S.D. (1993). Surface disturbance of cryptobiotic soil crusts: Nitrogenase activity, chlorophyll content, and chlorophyll degradation. *Arid Soil Research and Rehabilitation*, **8**: 1–8.

Bowden, L.W., Huning, L.R., Hutchinson, C.F. & Johnson, C.W. (1974). Satellite photograph presents first comprehensive view of local wind: the Santa Ana. *Science*, **184**: 1077–1078.

Brady, N.C. & Weil, R.R. (1999). *The Nature and Properties of Soils*. (12th Edn). Upper Saddle Ridge, New Jersey: Prentice-Hall.

Brazel, A.J. & Nickling, W.G. (1987). Dust storms and their relations to moisture in the Sonoran-Mojave Desert region of the south-western United States. *Journal of Environmental Management*, **24**: 279–291.

Brown, J.H., Valone, T.J. & Curtin, C.G. (1997). Reorganization of an arid ecosystem in response to recent climate change. *Proceedings of the National Academy of Science*, **94**: 9729–9733.

Buwalda, J.P. (1914). Pleistocene beds at Manix in the eastern Mohave Desert region. *University of California Bulletin of the Department of Geology*, **7**: 443–464.

Carpenter, D.E., Barbour, M.G. & Bahre, C.J. (1986). Old field succession in Mojave Desert scrub. *Madroño*, **33**: 111–122.

Carter, D.J., Findlater, P.J. & McTainsh, G.H. (1999). *An economic solution to water repellency and wind erosion on light textured soils*. Commission of Land Degradation and Desertification, Perth, Australia.

Clements, T., Mann, J.F., Stone, R.O. & Eymann, J.L. (1963). *A study of windborne sand and dust in desert areas*. ES-8. Natick, Massachusetts: United States Army Natick Laboratories, Earth Sciences Division.

Dohrenwend, J.C., Bull, W.B., McFadden, L.D., Smith, G.I., Smithe, R.S.U. & Wells, S.G. (1991). Quaternary geology of the Basin and Range province in California. In: Morrison, R.B. (Ed.), *Quaternary Nonglacial Geology: Coterminous U.S.* Vol. K-2, pp. 321–352. Geological Society of America: Boulder, Colorado.

Dregne, H.E. (1995). Desertification control: A framework for action. *Environmental Monitoring and Assessment*, **37**: 111–122.

Evans, J.R. (1992). Falling and climbing sand dunes in the Cronese ("Cat") Mountain Area, San Bernardino County, California, *California Division of Mines, Geological Notes*, 107–113.

Evans, R.D. & Belnap, J. (1999). Long-term consequences of disturbance on nitrogen dynamics in an arid ecosystem. *Ecology*, **80**: 150–160.

Fryrear, D.W. (1981). Long-term effect of erosion and cropping on soil productivity. In: Péwé, T.L. (Ed.), *Desert Dust: Origin, Characteristics, and Effect on Man*. Special Paper 186, pp. 253–259. Geological Society of America: Boulder, Colorado.

Gibbens, R.P., Tromble, J.M., Hennessy, J.T. & Cardenas, M. (1983). Soil movement in mesquite dunelands and former grasslands of southern New Mexico from 1933 to 1980. *Journal of Range Management*, **36**: 145–148.

Gillette, D.A. (1977). Fine particulate emissions due to wind erosion. *Transactions of the American Society of Agricultural Engineers*, **29**: 890–897.

Gillette, D.A. (1988). Threshold friction velocities for dust production for agricultural soils. *Journal of Geophysical Research*, **93**: 12645–12662.

Gillette, D.A., Adams, J., Endo, A., Smith, D. & Kihl, R. (1980). Threshold velocities for input of soil particles into the air by desert soils. *Journal of Geographical Research*, **85**: 5621–5630.

Gillette, D.A., Fryrear, D.W., Gill, T.E., Ley, T., Cahill, T.A. & Gearhart, E.A. (1997). Relation of vertical flux of particles smaller than 10 μm to aeolian horizontal mass flux at Owens Lake. *Journal of Geophysical Research*, **102**: 26009–26015.

Grantz, D.A., Vaughn, D.L., Farber, R., Kim, B., Zeldin, M., VanCuren, T. & Campbell, R. (1998). Seeding native plants to restore desert farmland and mitigate fugitive dust and PM_{10}. *Journal of Environmental Quality*, **27**: 1209–1218.

Greeley, R. & Iversen, J.D. (1985). *Wind as a Geological Process on Earth, Mars, Venus and Titan*. Cambridge: Cambridge University Press. 333 pp.

Hennessy, J.T., Kies, B., Gibbens, R.P. & Tromble, J.M. (1986). Soil sorting by forty-five years of wind erosin on a southern New Mexico Range. *Soil Science Society of America Journal*, **50**: 391–394.

Hyers, A.D. & Marcus, M.G. (1981). Land use and desert dust hazards in central Arizona. In: Péwé, T.L. (Ed.), *Desert Dust: Origin, Characteristics, and Effect on Man*. Special Paper 186, Geological Society of America: Boulder, Colorado.

Kasusya, P. (1998). Combating desertification in northern Kenya (Samburu) through community action: a community case experience. *Journal of Arid Environments*, **39**: 325–329.

Kealah, F.I. (1989). Desertification and aeolian processes in the Kuwait Desert. *Journal of Arid Environments*, **16**: 125–145.

Khalaf, F.I. & Al-Ajmi, D. (1993). Aeolian processes and sand encroachment problems in Kuwait. *Geomorphology*, **9**: 111–134.

Khresat, S.A., Rawajfih, Z. & Mohammad, M. (1998). Land degradation in north-western Jordan: causes and processes. *Journal of Arid Environments*, **39**: 623–629.

Koch, M. &. El Baz, F. (1998). Identifying the effects of the Gulf War on the geomorphic features of Kuwait by remote sensing and GIS. *Photogrammetric Engineering and Remote Sensing*, **64**: 739–747.

Lancaster, N. & Baas, A. (1998). Influence on vegetation cover on sand transportation by wind: Field studies at Owens Lake, California. *Earth Surface Processes and Landforms*, **23**: 69–82.

Larney, F., Bullock, M., Janzen, H., Ellert, B. & Olson, E. (1998). Wind erosion effects on nutrient redistribution and soil productivity. *Journal of Soil and Water Conservation*, **53**: 133–140.

Leathers, C.R. (1981). Plant components of desert dust in Arizona and their significance for man. In: Péwé, T.L. (Ed.), *Desert Dust: Origin, Characteristics, and Effect on Man*. Special Paper 186, Geological Society of America: Boulder, Colorado.

Leys, J. & McTainsh, G. (1994). Soil loss and nutrient decline by wind erosion-cause for concern. *Australian Journal of Soil and Water Conservation*, **7**: 30–35.

López, M.V. (1998). Wind erosion in agricultural soils: An example of limited supply of particles available for erosion. *Catena*, **33**: 17–28.

Lovich, J. & Bainbridge, D. (1999). Anthropogenic degradation of the southern California desert ecosystem and prospects for natural recovery and restoration. *Environmental Management*, **24:** 309–326.

Luk, S.-H. (1983). Recent trends in desertification in the Maowusu Desert, China. *Environmental Conservation*, **10**: 213–224.

Lyles, L. & Tatarko, J. (1986). Wind erosion effects on soil texture and organic matter. *Journal of Soil and Water Conservation*, **46**: 191–193.

Mabbutt, J.A. & Floret, C. (Eds) (1980). *Case Studies on Desertification*. United Kingdom: United Nations, Scientific and Cultural Organization.

Marticorena, B., Bergametti, G., Gillette, D.A. & Belnap, J. (1997). Factors controlling threshold friction velocity in semiarid and arid areas of the United States. *Journal of Geophysical Research*, **102**: 23277–23287.

McFadden, L.D., Wells, S.G. & Jercinovich, M.J. (1987). Influence of eolian and pedogenic processes on the origin and evolution of desert pavements. *Geology*, **15**: 504–508.

Meek, N. (1989). Geomorphic and hydrologic implications of the rapid incision of Afton Canyon, Mojave Desert, California. *Geology*, **17**: 7–10.

Meek, N. (1990). Late Quaternary Geochronology and Geomorphology of the Manix Basin, San Bernardino County, California Ph.D. Thesis, University of California at Los Angeles, Los Angeles, California.

Mitchell, D.J., Fullen, M.A., Trueman, I.C. & Fearnehough, W. (1998). Sustainability of reclaimed desertified land in Ningxia, China. *Journal of Arid Environments*, **39**: 239–251.

Morrison, R.B. (1991*a*). Quaternary geology of the southern Basin and Range Province. In: Morrison, R.B. (Ed.), *Quaternary Nonglacial Geology: Coterminous U.S.* Vol. K-2, pp. 353–371. Geological Society of America: Boulder, Colorado.

Morrison, R.B. (1991*b*). Quaternary stratigraphic, hydrologic, and climatic history of the Great Basin, with emphasis on Lakes Lahonton, Bonneville, and Tecopa. In: Morrison, R.B. (Ed.), *Quaternary Nonglacial Geology: Coterminous U.S.* Vol. K-2, pp. 283–320. Geological Society of America: Boulder, Colorado.

National Climate Data Center. (1993). *Solar and Meteorological Surface Observation Network: 1961–1990, Volume III: Western United States,* [CD-ROM]. National Climate Data Center: Asheville, North Carolina.

National Climate Data Center. (1997). *U.S. Precipitation by State, California* [HTML Document]. National Climate Data Center: Asheville, North Carolina, Available: http://www.ncdc.noaa.dov/ol/climate/online/coop-precip.html [1999, January 1].

Okin, G.S., Murray, B. & Schlesinger, W.H. (in press). Desertification in an arid shrubland in the southwestern United States: Process modeling and validation. In: Conacher, A. (Ed.), *Land Degradation*. Kluwer Academic Publishers: Boston, Massachusetts.

Post, W.M., Pastor, J., Zinke, P.J. & Stangenberger, A.G. (1985). Global patterns of soil nitrogen storage. *Nature*, **317**: 613–616.

Ray, T.W. (1995). *Remote Monitoring of Land Degradation in Arid/Semiarid Regions*. Ph.D. Thesis, California Institute of Technology, Pasadena, CA.

Schlesinger, W.H. & Pilmanis, A.M. (1998). Plant-soil interactions in deserts. *Biogeochemistry*, **42**: 169–187.

Schlesinger, W.H., Raikes, J.A., Hartley, A.E. & Cross, A.F. (1996). On the spatial pattern of soil nutrients in desert ecosystems. *Ecology*, **77**: 364–374.

Schlesinger, W.H., Reynolds, J.F., Cunningham, G.L., Huenneke, L.F., Jarrell, W.M., Virginia, R.A. & Whitford, W.G. (1990). Biological feedbacks is global desertification. *Science*, **247**: 1043–1048.

Schultz, B.W. & Ostler, W.K. (1993). Effects of prolonged drought on vegetation association in the Northern Mojave Desert. *Wildland shrubs and arid land restoration symposium*, Las Vegas, Nevada.

Shao, Y. & Raupach, M.R. (1993). Effect of saltation bomardment on the entrainment of dust by wind. *Journal of Geophysical Research*, **98**: 12719–12726.

Sharifi, M., Gibson, A. & Rundel, P. (1999). Phenological and physiological responses of heavily dusted creosote bush (*Larrea tridentata*) to summer irrigation in the Mojave Desert. *Flora*, **194**: 369–378.

Smith, G.I. & Street-Perrott, F.A. (1983). Pluvial Lakes of the Western United States. In: Wright, H.E., Jr. (Ed.), *Late Quaternary Environments of the United States* (1st Edn). Vol. 1, pp. 190–212. University of Minnesota Press: Minneapolis, Minnesota.

Stylinski, C. & Allen, E. (1999). Lack of native species recovery following severe exotic disturbance in southern California shrublands. *Journal of Applied Ecology*, **36**: 544–554.

Talbot, R.W., Harriss, R.C., Browell, E.V., Gregory, G.L., Sebacher, D.I. & Beck, S.M. (1986). Distribution and geochemistry of aerosols in the tropical North Atlantic troposphere: Relationship to Saharan dust. *Journal of Geophysical Research*, **91**: 5173–5182.

Talbot, W.J. (1947). *Swartland and Sandveld. A survey of the land utilization and soils erosion in the Western Lowland of the Cape Province*. Cape Town, South Africa: Oxford University Press. 79 pp.

Tegen, I. & Fung, I. (1995). Contribution to the atmospheric mineral aerosol load from land surface modification. *Journal of Geophysical Research*, **100**: 18707–18726.

Tugel, A.J. & Woodruff, G.A. (1978). *Soil Survey of San Bernardino County, California: Mojave River Area*. Washington, D.C.: Soil Conservation Service, United States Department of Agriculture.

Vasek, F.C., Johnson, H.B. & Eslinger, D.H. (1975). Effects of pipeline construction on Creosote bush scrub vegetation of the Mojave Desert. *Modroño*, **23**: 1–64.

Verstraete, M.M. & Schwartz, S.A. (1991). Desertification and globla change. *Vegetatio*, **91**: 3–13.

Walker, A.S. (1982). Deserts of China. *American Scientist*, **70**: 366–376.

Warren P.L. & Hutchinson, C.F. (1984). Indicators of rangeland change and their potential for remote sensing. *Journal of Arid Environments*, **7**: 107–126.

Whitford, W.G. (1992). Biogeochemical consequences of desertification. *American Chemical Society Symposium Series*, **483**: 352–259.

Williams, J.D., Dobrowolski, J.P., West, N.E. & Gillette, D.A. (1995). Microphytic crust influence on wind erosion. *Transactions of the American Society of Agricultural Engineers*, **38**: 131–137.

Wolfe, S.A. & Nickling, W.G. (1993). The protective role of sparse vegetation in wind erosion. *Progress in Physical Geography*, **17**: 50–68.

Zha, Y. & Gao, J. (1997). Characteristics of desertification and its rehabilitation in China. *Journal of Arid Environments*, **37**: 419–432.

JARE 20000711

HARCOURT PUBLISHERS

JOURNAL TITLE: JARE DATE: 6/11/2000
ARTICLE NO. : 20000711

Queries and/or remarks

Manuscript Page/line	Details required	Author's response
Page 16/line 8	Okin *et al.* (in press) — pl. update.	
Page 46/line 20	Ref. 50 — National Climate Data Center. (1997). — not in text.	
Page 50	Is figure. 1 to be colour? If not, change caption.	

EXHIBIT 410

ELSEVIER

Journal of Arid Environments 65 (2006) 253–275

Journal of Arid Environments

www.elsevier.com/locate/jnlabr/yjare

Multi-scale controls on and consequences of aeolian processes in landscape change in arid and semi-arid environments

G.S. Okin[a,*], D.A. Gillette[b], J.E. Herrick[c]

[a]*Department of Environmental Sciences, University of Virginia, Charlottesville, VA 22904-4123, USA*
[b]*NOAA, EPA-82, Research Triangle Park, NC 27711, USA*
[c]*USDA ARS, Jornada Experimental Range, Las Cruces, NM 88003-8003, USA*[1]

Received 18 February 2005; received in revised form 21 April 2005; accepted 22 June 2005
Available online 1 September 2005

Abstract

Aeolian processes are tightly linked to soil and vegetation change in arid and semi-arid systems at multiple spatial and temporal scales. Wind influences patterns of vegetation and soil within the landscape, and these patterns control wind erosion at patch to landscape scales. Aggregated at larger scales, patterns in soil and vegetation distributions influence global distributions of dust and its biogeochemical impacts. Understanding the controls on aeolian processes is therefore important not only in understanding the biogeochemistry and land cover patterns in dryland environments, but also in understanding global land cover, climate, and biogeochemistry. Although the microscopic physics that control aeolian processes are well understood, the controls on these processes in real landscapes are poorly constrained, particularly for structurally complex plant communities such as shrub-invaded grasslands. This paper reviews the controls on aeolian processes and their consequences at plant-interspace, patch-landscape, and regional–global scales. Based on this review, we define the requirements for a cross-scale model of wind erosion in structurally complex arid and semi-arid ecosystems.
© 2005 Elsevier Ltd. All rights reserved.

Keywords: Aeolian processes; Desertification; Dust emission; Landscape change; Wind erosion

*Corresponding author. Tel: +1 434 924 3324; fax: +1 434 982 2137.
E-mail address: okin@virginia.edu (G.S. Okin).

[1]Mention of trade names or commercial products in this publication is solely for the purpose of providing specific information and does not imply recommendation or endorsement by the US Department of Agriculture.

0140-1963/$ - see front matter © 2005 Elsevier Ltd. All rights reserved.
doi:10.1016/j.jaridenv.2005.06.029

Nomenclature

a	ground area where wake flow intersects surface (cm^2)
A	supply limitation coefficient, $0 \leqslant A \leqslant 1$ (dimensionless)
A_B	average basal area of plants in an area, s (cm^2)
A_P	average profile area of plants in an area, s (cm^2)
b	average plant diameter (cm)
β	ratio of drag coefficient of vegetated surface to drag coefficient of unvegetated surface, $\beta \equiv C_R/C_S$ (dimensionless)
c	empirical constant with value ~0.37 (dimensionless)
C	total fractional cover (dimensionless)
C_d	drag coefficient (general notation) (dimensionless)
C_R	drag coefficient for plant (dimensionless)
C_S	drag coefficient for unvegetated soil (dimensionless)
δ	Kronecker Delta, $\delta = 1$ when $u_{*t} > u_{*tv}$ and $\delta = 0$ otherwise (dimensionless)
D	displacement height (cm)
F_a	vertical sediment (dust) flux for specified set of conditions ($g\,cm^{-2}\,s^{-1}$)
g	acceleration due to gravity (981) ($cm\,s^{-2}$)
h	average plant height (cm)
k	Von Karmann's constant (~0.4) (dimensionless)
K	the ratio of vertical flux, F, to horizontal flux, q (cm^{-1})
L	intershrub distance (cm)
L_{min}	the maximum distance that wake flow extends past the downwind edge of a plant (cm)
λ	lateral cover, $\lambda \equiv nbh/s$ (Raupach et al., 1993) (dimensionless)
n	the number of plants in an area, s (dimensionless)
N	plant number density, $N \equiv n/s$ (cm^{-2})
q_{eq}	equilibrium horizontal sediment flux for specified set of conditions ($g\,cm^{-1}\,s^{-1}$)
ρ	density of air ($g\,cm^{-3}$)
s	area on the ground with n plants (cm^2)
σ	ratio of the average plant basal area to average profile area, $\sigma \equiv A_B/A_P$ (dimensionless)
τ	surface shear stress ($g\,cm^{-1}\,s^{-2}$)
u_*	wind shear velocity ($cm\,s^{-1}$)
u_{*ts}	threshold shear velocity for an unvegetated surface ($cm\,s^{-1}$)
u_{*tv}	threshold shear velocity for an vegetated surface ($cm\,s^{-1}$)
$U(z)$	wind speed at height, z ($cm\,s^{-1}$)
z	height above the surface (cm)
z_0	roughness length (cm)

1. Introduction

The world's arid and semi-arid regions cover more than 30% of the Earth's land surface. Conversion of grasslands to shrublands is occurring at an alarming rate in these regions. Due to low and variable vegetation cover, aeolian processes (i.e. erosion and transport of particles by wind and subsequent downwind deposition of these particles) are prevalent in desert environments and wind is an important factor in redistributing sediments and dust-borne nutrients. Redistribution of material by wind occurs at multiple scales. At the plant-interspace scale, material can be scoured from interspaces and deposited underneath nearby plants (Gibbens et al., 1983). At the patch scale, wind can remove sediment from one area, deposit the coarse material in an adjacent area, and remove the fine material (dust) for long-range transport (Okin et al., 2001a, b). At the landscape scale, wind is an important geomorphic process (Greeley and Iversen, 1985). At global scales, dust emitted in one region of the globe can be important in the biogeochemistry of downwind ecosystems (Chadwick et al., 1999; Okin et al., 2004).

The two principal mechanisms for the transport of sediment by wind are saltation and suspension. In saltation, particles are removed from the surface by aerodynamic lift and travel in short, arcuate hops through the air (Bagnold, 1941). Dust particles, fine particles with Stokes' settling velocity less than the vertical component of the wind velocity during turbulent flow, are transported by suspension. The primary ecological consequence of saltation is the physical effect of saltation-sized particles on soils and vegetation.

Unlike saltating silt and sand grains, dust particles are not removed from the surface by aerodynamic forces, but instead are emitted when saltating particles sandblast the soil surface (Gillette, 1977). Horizontal mass flux (expressed in units of mass per unit distance perpendicular to the wind per unit time) is comprised mostly of saltating particles greater than 50 mm in diameter. Vertical flux (expressed in units of mass per unit area per unit time) consists of the flux of dust from the surface and available for long-range transport by wind. Because of the relative differences in transport distance for suspended and saltating particles, the saltated sediment typically has a very local influence on vegetation and soils, whereas the influence of suspended sediment can extend thousands of kilometers. The primary ecological consequences of dust emission and subsequent downwind deposition of suspended particles arise from the fact that small, saltation-sized particles are largely responsible for soil quality, generally defined. In particular, because soil nutrients are concentrated on dust particles, dust emission and redeposition have significant impacts on local and downwind soil nutrient status.

Our objective is to review the influence of aeolian processes on landscape processes and to examine the feedbacks and cross-scale interactions between vegetation cover and aeolian processes in arid lands. Emphasis is given to research and results from the Jornada Experimental Range (JER) located in the Chihuahuan Desert in southern New Mexico, USA. Special consideration is given to the controls on and consequences of aeolian processes at three scales: (1) the plant-interspace scale (cm—a few meters), (2) the patch-landscape scale (10s of m—10s of km), and (3) the regional–global scale (greater than 100s of km).

2. Plant-interspace scale

2.1. Controls on aeolian processes at the plant-interspace scale

In general, aeolian processes are initiated when the *erosivity* of the wind exceeds the *erodibility* of the surface. Wind erosivity is typically quantified as the *shear velocity* of the wind. Shear velocity is directly proportional to the rate of increase of velocity with log-height for a neutral atmosphere and is defined as $u_* \equiv \sqrt{\tau/\rho}$, where τ is the surface shear stress and ρ is the density of air. The amount of drag exerted by the surface on the wind is related to the shear velocity and the wind speed by:

$$C_{\mathrm{d}}(z) = (u_*/U(z))^2, \tag{1}$$

where C_{d} is the drag coefficient and $U(z)$ is the wind speed at height, z.

The erodibility of the surface is typically related to the *threshold shear velocity*, the shear velocity below which saltation flux will not occur. The threshold shear velocity of the surface depends on the both the soil and the vegetation. Threshold shear velocity for soils is largely determined by the texture of the soil, the amount of protective coverage provided by nonerodible clasts or crusts, and soil moisture (Ravi et al., 2004). Marticorena and Bergametti (1995) provided a parameterization for the threshold shear velocity on soils based on mean particle diameter showing that particles from approximately 80–120 μm are efficient saltators with low threshold shear velocity. Gillette et al. (2001) suggested that some soils may be "supply limited", meaning that the population of saltation-sized particles is not large enough to sustain the maximum theoretical horizontal flux.

Vegetation modulates the erodibility of the surface primarily through three mechanisms (Fig. 1, Wolfe and Nickling, 1993): (1) vegetation can directly shelter the soil from the force of wind by covering a fraction of the surface and providing a lee-side wake in which average wind speed is dramatically reduced, (2) vegetation can extract momentum from the wind, thus reducing the wind erodibility, and (3) vegetation can trap windborne particles reducing total horizontal and vertical flux and providing loci for sediment deposition.

2.1.1. Sheltering by vegetation

The wind can only act on the fraction of the soil surface that is not directly sheltered by vegetation. Vegetation provides sheltering either by covering the soil surface or by creating lee-side wakes in which turbulent flow dominates and the mean velocity is either zero or, in some cases, opposite the direction of the free-stream wind direction (Wolfe and Nickling, 1993). The degree of sheltering by the wind is therefore related to both the fractional cover and the sheltering provided by wake flow. Lee and Soliman (1977) have defined three flow regimes depending on the size of the wake behind vegetation and the vegetation spacing (see Fig. 2): (1) isolated roughness flow, where there is no interaction between wakes and adjacent downwind vegetation, (2) wake interference flow, where wakes from upwind plants intercept downwind vegetation, and (3) skimming flow, where wakes completely overlap and the entire soil surface is within the protected wake region.

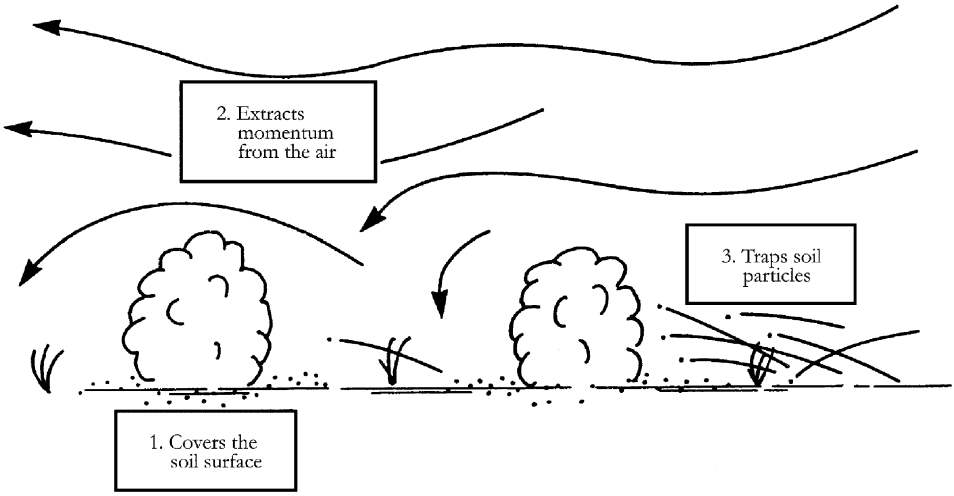

Fig. 1. The three mechanisms by which vegetation protects the soil surface from wind erosion; from Wolfe and Nickling, 1993.

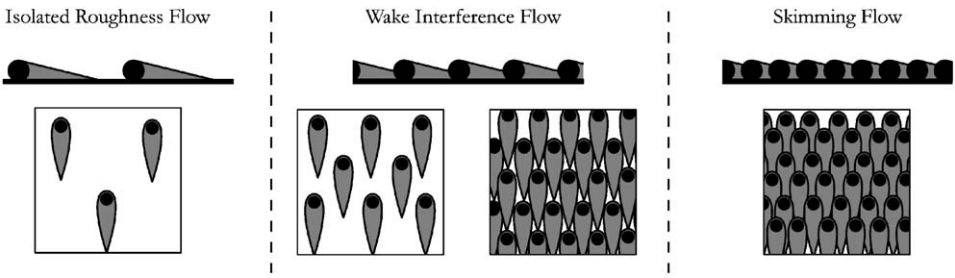

Fig. 2. Flow regimes and associated theoretical wake development. Shaded areas are wake regions; adapted from Wolfe and Nickling (1993) after Lee and Soliman (1977).

In his treatment of drag partitioning in vegetated landscapes, Raupach (1992) derived a formula to describe the area downwind of a plant (approximated to have cylindrical shape) protected from the erosive force of the wind in the wake:

$$a = cbh\frac{U(h)}{u_*}, \tag{2}$$

where a is the area where wake flow intersects with the surface, c the constant with a value of approximately 0.37, b the diameter of the plant, h the height of the plant, and $U(h)$ the wind speed at the top of the canopy (Fig. 3). If the wake is considered to be a tapering prism (Fig. 3) for plants with $b \geqslant h$, the maximum distance that the

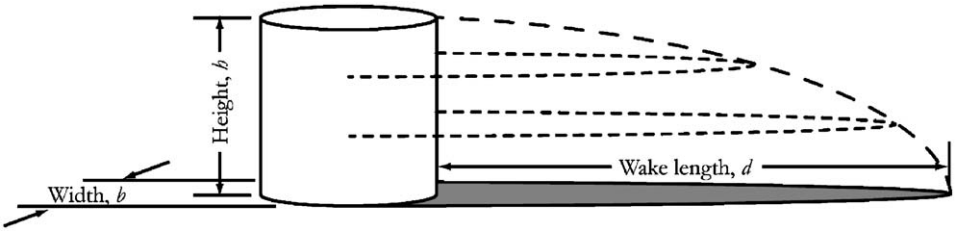

Fig. 3. Sheltering provided by a cylinder. Shaded area is the intersection of wake with ground; after Raupach (1992).

wake extends past the downwind edge of the plant, $L_{\min}$, is:

$$L_{\min} = h\frac{U(h)}{u_*} - \frac{b}{2}. \tag{3}$$

For cases in which vegetation cover is low, such that wakes from one plant do not interact with the sheltered area of other plants (e.g. isolated roughness flow),

$$\frac{U(h)}{u_*} \approx \frac{1}{\sqrt{C_S + \lambda C_R}}, \tag{4}$$

where C_S is the drag coefficient for the soil and C_R the drag coefficient for the plant. Drag coefficients quantify how the drag force on the surface varies with wind speed. The parameter λ is *lateral cover*, the total frontal silhouette area of vegetation intercepted by wind per unit ground area (Musick and Gillette, 1990; Musick et al., 1996; Shao and Lu, 2000). Values for C_R are approximately 0.25 for cylinders (Taylor, 1988) and values for C_S have been reported to be approximately 0.0025 (Crawley and Nickling, 2003). Thus, for values of λ near 0.01, the wake region should extend downwind approximately 10 times the height of the plant. Thus, Eqs. (3) and (4) are consistent with results from wind tunnel experiments by Minvielle et al. (2003) which suggested a protective wake approximately 10 times longer than vegetation height. Drag coefficients for porous objects are likely higher than those of solid objects considered in most wind tunnel and theoretical studies (Grant and Nickling, 1998; Raupach et al., 2001). For real vegetation, therefore C_R will increase (relative to values for solid cylinders) and wake area protected by vegetation ($L_{\min}$) will decrease. For porous vegetation, therefore, the area of wake protection can be expected to be less than 10 times vegetation height.

2.1.2. Momentum extraction by vegetation

Vegetation can extract momentum from the wind, reducing its erosive force on the surface. Shear velocity is related to wind speed and vegetation structural parameters by the Law of the Wall. For a neutral atmosphere:

$$U(z) = \frac{u_*}{k}\ln\left(\frac{z-D}{z_0}\right), \tag{5}$$

where k is the Von Karmann's constant, z_0 the aerodynamic roughness length, and D is the zero-plane displacement height. z_0 and D are related to surface roughness and, in vegetated areas, are mainly determined by the amount and structure of vegetation cover. When D is not equal to zero, a wake is present and wind erosion will not occur. z_0 has been related to lateral cover by Lettau (1969) and Wooding et al. (1973) using $z_0 = h\lambda/2$, where h is equal to canopy height. This relation holds for $0<\lambda<\sim 0.1$. For $\lambda>\sim 0.1$, z_0/h remains approximately constant. Marticorena et al. (1997) suggested a relation that incorporates the leveling-off of the linear relationship with increasing λ:

$$z_0 = \begin{cases} (0.479\lambda - 0.01)h & \text{for } \lambda \leqslant 0.11, \\ 0.05h & \text{for } \lambda > 0.11. \end{cases} \tag{6}$$

(*Note*: this formulation is slightly different from that found in Marticorena et al. (1997) due to a typographical error in that publication). These equations do not account for interspecific variability in the flexibility of the vegetation. These changes can be accounted for empirically by changing the coefficients.

2.1.3. Trapping of windborne sediment by vegetation

Because turbulent flow dominates in and around plant canopies, total surface shear stress within plant canopies typically approaches zero and the ability of wind to carry sediments is reduced. In addition, windborne particles can impact vegetation, losing their momentum, and be removed directly from the air stream. Thus, vegetation canopies are typically the loci of deposition in partially vegetated areas. Coarse-grained particles travel short distances and therefore are often moved from plant interspaces to adjacent regions underneath plant canopies or in plant wakes. Fine-grained particles that are suspended in the wind can also be intercepted by plant canopies and deposited within the plant canopy.

The ability of a plant canopy to trap windborne sediment depends, in part, on its porosity. Field (e.g. Grant and Nickling, 1998), wind-tunnel (e.g. Lee et al., 2002), and theoretical (e.g. Raupach et al., 2001) studies have shown that the ability of vegetation to act as a windbreak for sediment has a maximum value for an intermediate value of porosity, with porosities of approximately 20–40% showing the maximum effect.

2.2. Consequences of aeolian processes at the plant-interspace scale

The consequences of wind erosion at the plant-interspace scale are directly linked to the two main processes of aeolian transport: saltation and suspension (Fig. 4). Saltation flux dominates the horizontal mass flux during aeolian transport. Saltating particles are therefore responsible for the majority of deflation and subsequent downwind deposition of windborne sediments (Gibbens et al., 1983). Hennessy et al. (1986) determined that in mesquite duneland areas on the JER, saltation-sized particles are eroded from plant interspaces and redistributed to areas under plants, with little or no net loss of sand but a net loss of fine particles. On the

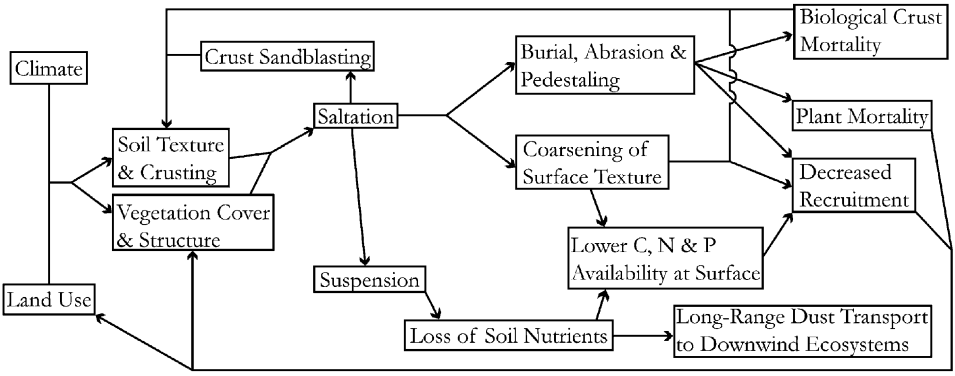

Fig. 4. Selected causes and consequences of aeolian processes.

plant-interspace scale, therefore, a landscape undergoing wind erosion exists as a fine-scale mosaic of deflational and depositional areas.

Deflation can cause "pedestaling" of plants in areas actively experiencing wind erosion. Pedestaling is a process whereby the soil surface is lowered by deflation, which exposes plant roots and can result in plant mortality. Deposition occurs when the mean wind velocity decreases, usually due to the presence of vegetation, and windborne sediments are deposited. Deposition can result in burial of vegetation, and if it occurs at a rate greater than the rate of vertical growth of a plant, can result in mortality (Okin et al., 2001a).

If the horizontal velocity of windborne particles in the saltation layer is equal to the average windspeed in the saltating layer, then the kinetic energy flux ($J\,m^{-1}\,s^{-1}$) increases as a linear function of mass and a cubic function of particle diameter. Under these assumptions, a horizontal mass flux consisting solely of 100 μm particles has approximately 1000 times greater kinetic energy flux than the same flux consisting solely of 10 μm dust particles. When saltating sand grains strike a plant, this excess energy causes physical damage, mainly in the form of destruction of the cambium and leaf stripping (Okin et al., 2001a). If this physical damage does not directly result in plant mortality, it almost certainly results in slowed growth, which may compromise a plant's ability to overcome burial or pedestaling. Abrasion and burial by saltation-sized particles therefore act in tandem to stress vegetation. The excess kinetic energy of saltating particles can also sandblast fragile soil crusts that form in desert regions, reducing the threshold shear velocity of the affected surface and exposing it to increased wind erosion (Gillette and Pitchford, 2004).

Suspension-sized particles are winnowed from areas undergoing erosion and can either be removed for long-range transport (Gillette, 1974) or trapped by near-field vegetation (Raupach et al., 2001). Fine-grained particles account for the majority of the soil resources important to vegetation, including nutrient exchange capacity and water-holding capacity. The contribution of fine particles to soil nutrient availability results from the fact that particles in this size fraction have a high surface area and

soil nutrients such as nitrate, ammonium, potassium, magnesium, and phosphate are adsorbed onto these particles, especially those with clay mineralogy.

Long-range transport of dust particles contributes to overall loss of soil resources for an area undergoing wind erosion (Okin et al., 2001b). At the plant-interspace scale, winnowing results in the depletion of fine particles from plant interspaces (Hennessy et al., 1986). Plant interspaces are therefore the sites of decreased soil resource availability (Wright and Honea, 1986; Schlesinger et al., 1996; Okin et al., 2001a, b). The interception and trapping of the suspended load can lead to increased soil resource availability within and around plant canopies (Raupach et al., 2001). A landscape undergoing wind erosion therefore exists as a fine-scale mosaic of areas of winnowing and trapping resulting, in part, in the well-documented resource island phenomenon in shrublands (Schlesinger et al., 1990; Schlesinger et al., 1996).

3. Patch-landscape scale

3.1. Controls on aeolian processes at the patch-landscape scale

Horizontal mass flux has been modeled by a large number of authors using different approaches. Bagnold (1941) approached the problem first and provided a physically reasonable solution that was later confirmed by the analysis of Owen (1964). Equations that predict saltation have been suggested by many authors and verified by wind tunnels, field experiments, and alternate theoretical derivations. Many good discussions exist in the literature of the physical and mathematical formulations for mass flux during wind erosion (e.g. Shao and Lu, 2000). One such formulation is by Shao and Raupach (1993):

$$q_{eq} = A\frac{\rho}{g}u_*(u_*^2 - u_{*tv}^2)\delta, \tag{7}$$

where q_{eq} is the horizontal mass flux ($\mathrm{g\,m^{-1}\,s^{-1}}$), ρ the density of air, g the acceleration due to gravity, u_* the wind shear velocity, and u_{*tv} the threshold shear velocity of a vegetated surface (m/s). δ is set equal to 0 for $u_{*tv} \geqslant u_*$ and 1 otherwise. The parameter A in Eq. (7) has been suggested by Gillette et al. (2001) and Gillette and Chen (2001) as a correction to account for the relative availability of sand particles for transport. In the absence of other information, A is typically assumed to be equal to 1.0. Vertical mass flux, F_a ($\mathrm{g\,m^{-2}\,s^{-1}}$), is linearly related to horizontal mass flux by a constant K that is typically on the order of 10^{-2}–$10^{-3}\,\mathrm{m^{-1}}$, but can vary by several orders of magnitude based on soil texture and other factors (Gillette, 1977; Alfaro and Gomes, 2001).

In an analysis of drag partitioning over a vegetated surface, Raupach et al. (1993) derived an equation to estimate the impact of vegetation on the threshold shear velocity, u_{*tv}:

$$u_{*tv} = u_{*ts}\sqrt{(1-\sigma\lambda)(1+\beta\lambda)}, \tag{8}$$

where u_{*ts} is the threshold shear velocity for an unvegetated surface, σ is equal to the ratio of the average basal area to average profile area (i.e. $\sigma \equiv A_B/A_P$) of the vegetation, and β is the ratio of the drag coefficient of an isolated plant to the drag coefficient of the ground surface in the absence of the plant (i.e. $\beta \equiv C_R/C_S$). Eq. (8) may be re-expressed (Okin, 2005) as:

$$u_{*tv} = u_{*ts}\sqrt{(1-C)\left(1+\beta C\frac{A_P}{A_B}\right)}. \tag{9}$$

The first terms under the radicals in Eqs. (8) and (9) (i.e. $[1-\lambda\sigma]$ and $[1-C]$) account for the degree to which the vegetation covers the surface (see Section 2.1.1), focusing the erosive force of the wind on the exposed portion of the surface. The second terms under the radicals (i.e. $[1+\beta\lambda]$ and $[1+\beta C A_P/A_B]$) account for drag that the vegetation exerts on the wind (see Section 2.1.2), reducing the ability of wind to detach and transport particles.

Aeolian sediment flux tends to increase with the distance over which the erosion occurs (*fetch distance*), an effect known as the *fetch effect* (Gillette et al., 1996). The fetch effect is caused by aerodynamic effects (the Owen effect), particle-to-particle interactions, reattachment of separated boundary layers, and changes in the soil in the path of wind erosion. In discontinuous canopies where isolated roughness flow dominates, the fetch length is determined by the spacing between plants. Okin and Gillette (2001) used high-resolution aerial photography to investigate plant spacing in mesquite-dominated areas of the JER (see also, Ludwig et al., 2002). They concluded that plant spacing can be anisotropic, and that areas of extremely long fetch distance, known as *streets*, existed and tended to be aligned with the direction of the prevailing wind. The observed streets were inferred to be the cause of extremely high dust emission in well-developed dunelands.

Gillette and Pitchford (2004) examined wind erosion in streets of mesquite dunes to determine if fetch effect is an important factor for determining horizontal flux in vegetated areas dominated by isolated roughness flow or wake interference flow. Their study showed that flux increases along streets in the windward direction, reaching a maximum at the end of the street.

Data from Li and Okin (2004) and Hartman (personal communication) also support the importance of fetch (Tables 1–3). A very strong positive correlation exists between the percent of the surface comprised of unvegetated gaps >200 cm and average horizontal flux (Table 2). The anticorrelation between percent of the surface comprised of gaps other than those >200 cm and flux is a result of the strong anticorrelation between gaps >200 cm and other gaps (Table 3). The regression line for the >200 cm gap percentage and total horizontal flux intercepts the gap percentage axis at approximately 22%, indicating there is a minimum percentage of an area covered by large gaps that will enable significant wind erosion to occur. We hypothesize that with vegetation distributions in which there are not large gaps, wake interference and skimming flow predominate and the soil surface is largely protected from erosion.

Table 1
Gap percent, fractional cover, and horizontal flux for five vegetation plots on the JER[a]

Treatment	Percent of 50-m transect comprised of gaps of size:					Fractional cover (%)	Horizontal flux ($g\,m^{-1}\,s^{-1}$)
	25–50 cm	51–100 cm	101–200 cm	>200 cm	>500 cm		
T4	1.58	4.35	7.19	70.71	82.25	15.3	266.1
T3	6.01	15.49	21.09	35.54	72.12	19.3	80.0
T2	4.35	9.01	29.89	40.69	79.59	14.7	52.6
T1	8.31	19.48	29.19	21.21	69.88	17.4	29.8
Control	8.56	17.37	30.23	24.85	72.45	15.6	18.9

[a]Data are from four vegetation treatment plots (plus one control) in which vegetation was selectively removed. Aeolian flux was estimated in these plots using Big Springs Number Eight (BSNE) windborne sediment samplers and the method of Gillette and Pitchford (2004) for calculating total horizontal flux from the surface to 1 m. BSNE samples were from March to July, 2003. Fractional vegetation cover was estimated from three 50-m transects in each plot, oriented parallel to the direction of the prevailing wind. Unvegetated gaps were identified from transect data and the percent of each transect covered by gaps in five size bins (25–50 cm, 51–100 cm, 101–200 cm, >200 cm, and >50 cm) was calculated (see Herrick et al., 2005). Transect data were collected in August–September, 2003. Annual plant cover was ignored in these calculations because annuals are not present during the spring dust season.

Table 2
Correlation and regression statistics between gap percent or fractional cover and horizontal flux

	Percent of 50-m transect comprised of gaps of size:					Fractional cover (%)
	25–50 cm	51–100 cm	101–200 cm	>200 cm	>500 cm	
Correlation	−0.88	−0.82	−0.97	0.96	0.75	−0.22
Slope	−30.66	−13.29	−10.02	4.97	14.21	−11.93
Intercept	266.14	264.14	325.04	−102.32	−980.28	286.06
R^2	0.77	0.68	0.95	0.92	0.56	0.05

Table 3
Correlation between percent of transect comprised of gaps >200 m and other gap sizes and fractional cover

	Percent of 50 m transect comprised of gaps of size:					Fractional cover (%)
	25–50 cm	51–100 cm	101–200 cm	>200 cm	>500 cm	
Correlation	−0.97	−0.95	−0.90	1.00	0.90	−0.37

The weak anticorrelation between sediment flux and vegetation fractional cover (Table 2) indicates that threshold shear velocity is not simply a function of cover, as suggested by Eq. (9). Instead, the manner in which this cover is distributed, and in particular the degree to which vegetation is distributed to create large gaps, is vital in controlling aeolian flux. These data therefore argue strongly for including fetch

length in assessment and monitoring of wind erosion on vegetated landscapes (Herrick et al., 2005).

3.1.1. Landscape-scale controls on aeolian processes: Land use and land management

Land use and management impact both soils and vegetation in arid regions (Fig. 4). In the short-term, soil erodibility is usually increased by any activity that disturbs the soil surface (Bach, 1998; Belnap, 1995). Soil surface disturbance destroys physical and biological crusts and exposes more highly erodible subsurface material. Non-erodible gravel and rock fragments are often incorporated into the soil, exposing fine-textured material when physical disturbance mixes the surface layers of the soil. Short-term disturbance impacts are generally higher when the soil surface is dry. On wet soils, some types of disturbance will only deform the surface and may even reduce erodibility by contributing to the development of a physical crust or compacted layer, particularly in fine-textured soils such as loams and clays. Examples of activities that disturb the soil surface and increase aeolian flux are: military activities and maneuvers (Prose, 1985; Khalaf, 1989; Koch and El Baz, 1998) grazing (Wilshire, 1980; Khalaf, 1989; Fredrickson et al., 1998) and off-road vehicle (ORV) traffic (Nakata et al., 1976; Sheridan, 1978; Hyers and Marcus, 1981; Webb, 1982; Brown and Schoknecht, 2001).

The role that vegetation plays in modulating both the erosivity of winds and erodibility of the surface is impacted by any land use or management scheme that impacts vegetation cover. For example, fire can destroy above-ground biomass, reducing fractional and lateral cover of vegetation, thus exposing the surface to wind erosion. A striking example of this phenomenon is shown in Fig. 5. In October–November, 2003, large wildfires burned in the mountains of southern California. By the end of November, these fires had been extinguished, but the burn scars can still be seen in satellite imagery. The MODIS/Terra instrument captured strong winds on November 27, 2003 carrying ash and dust westward into the Pacific Ocean.

Agricultural activities often enhance aeolian activity in arid and semi-arid environments (Fig. 4). During the peak growing season, crops protect the soil from erosion by wind, but periods of bare ground during the beginning or end of the growing season can lead to significant erosion (Hagen, 1991; Nanney et al., 1993; Retta et al., 1996). The practice of maintaining some vegetation residue on the soil surface (i.e. *stubble*) has long been advocated as a practice to minimize wind erosion. Fallowing of fields, sometimes for long periods, can also be a significant source of windborne sediment (Larney et al., 1995). For example, in the Sandveld of the Western Cape Province of South Africa, a region of strong southerly winds and sandy soils (Talbot, 1947), seed potatoes are a principal crop. To protect from blight infestations, this crop can only be planted approximately one year in seven and fields are kept fallow during the remaining six years. As a means to control wind erosion on fields during the long fallow periods, stripes of vegetation are left in fields. These stripes are predominantly oriented east-west in order to minimize north-south fetch distance in fields and reduce erosion (Fig. 6). Similar impacts occur when rangeland is cleared and reseeded. Vegetative cover removal, intense surface disturbance, and

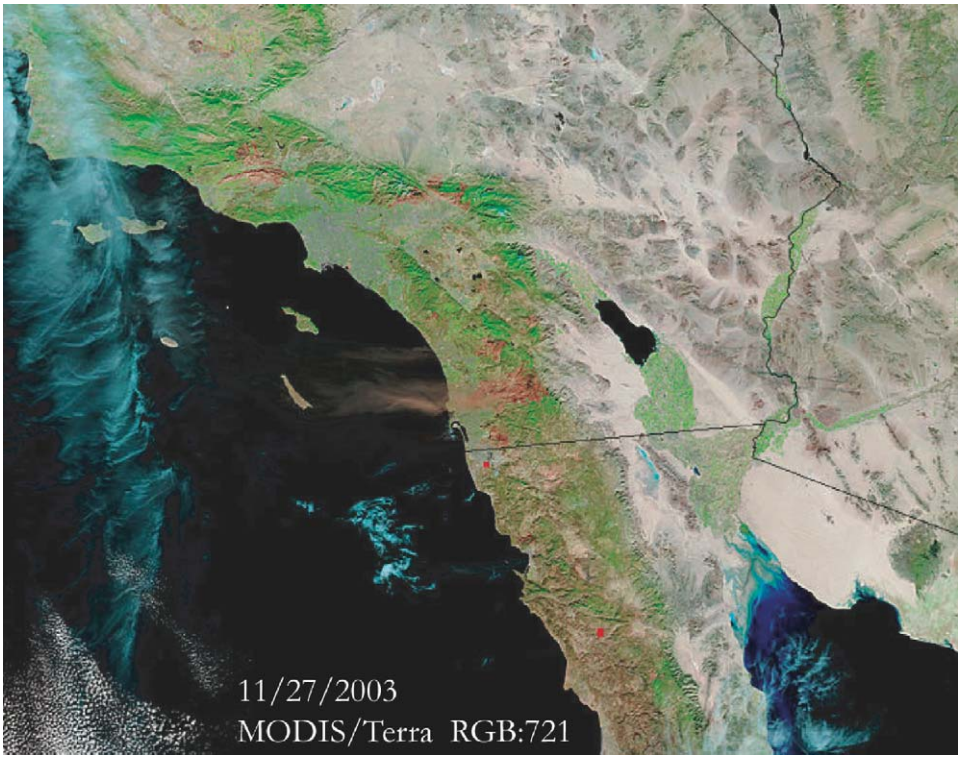

Fig. 5. False-color image of the southern California coast captured with the MODIS instrument aboard the Terra satellite on November 27, 2004. Red is MODIS band 7 (2155 nm), green is MODIS band 2 (876 nm), blue is MODIS band 1 (670 nm). Reddish areas are burn scars from fires at the end of October and beginning of November, 2003. Red dust can be seen heading westward over the Pacific from the two most southerly fire scars due to strong winds. Cyan areas over the western and southern portions of the image are clouds or sediments in the Colorado River Delta. Image courtesy of MODIS Rapid Response Project at NADA/GSFC.

typically low seedling establishment often leave soil susceptible to wind erosion for several years (Herrick et al., 1997; Breed and Reheis, 1999).

Grazing and ORV traffic tend to increase erosivity by reducing both cover and stature and by breaking physical and biological soil crusts. The effects of both types of activities tend to be highly concentrated. This leads to the creation of mosaics of areas that are relatively exposed within a pasture in which average cover is sufficient to prevent wind erosion. Off-road vehicle activity can be particularly damaging when oriented parallel to dominant winds because it has the potential to create wind erosion streets. Consequently, whereas a management activity may have a minimal effect on average cover measured within a pasture, wind erosion may increase in those small areas of the pasture in which activity is concentrated. In the long-term, both grazing and ORV activity can have persistent effects on wind erosivity by promoting changes in plant community composition, which ultimately affects both cover and structure (Fig. 4).

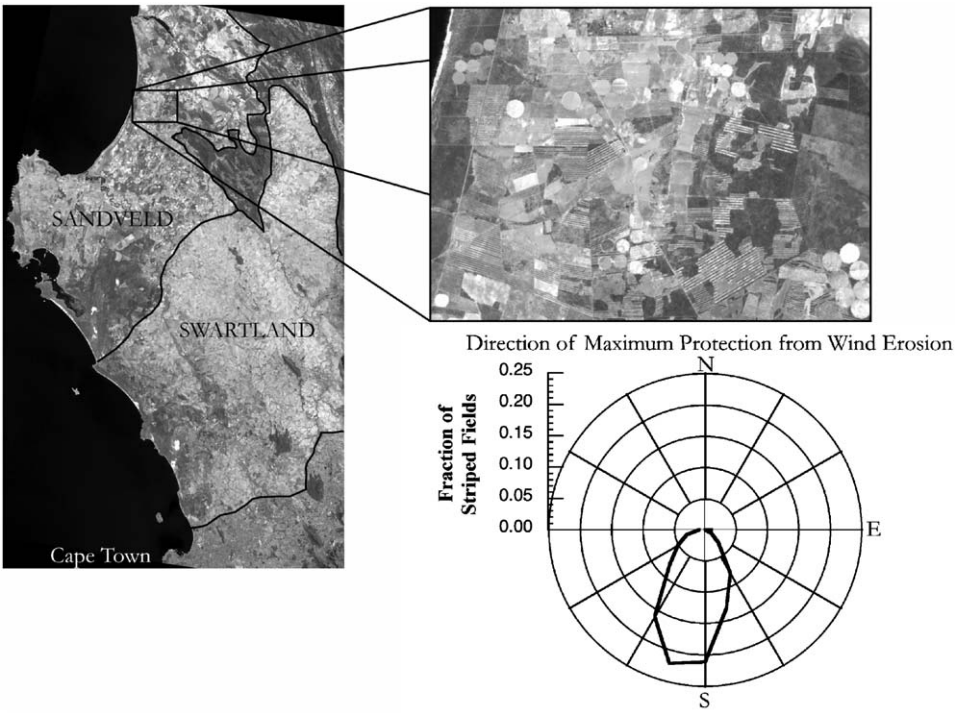

Fig. 6. Landsat ETM+ Band 8 (15-m resolution panchromatic band) images showing the southwestern coast of South Africa and a rose diagram of the directions protected from wind erosion by linear stripes of vegetation left in fields. Cape Town can be seen at the bottom of the full image. The enlarged image shows how the vegetation strips appear at full resolution in the image. The rose diagram is derived from measuring the orientation of all striped fields in the area labeled "Sandveld". Erosive winds in the region are typically from the south, the direction of maximum protection in the striped fields. Farmers in this region of South Africa are managing for wind erosion of fields during long fallow periods by maintaining short streamwise fetch lengths through the maintenance of vegetation stripes.

The timing of management activities relative to significant wind events is critical in arid and semi-arid ecosystems. While this fact is widely recognized in the case of cultivated systems, the effect of timing of grazing and ORV activity on wind erosion is rarely considered. For example, in the southwestern United States, most wind erosion occurs during the spring. Minimizing vegetation removal and soil surface disturbance during winter and spring on highly wind-erodible soils has the potential to limit long-term soil degradation. This hypothesis has not been explicitly tested at the landscape scale. Similarly, limiting road grading and maintenance activities to periods when a physical crust-producing precipitation event is likely to occur before a significant wind event should reduce sediment loss from roads and road margins.

Because of these multi-scale interactions, historic and pre-historic land uses (i.e. historic legacy, Peters and Havstad (2006)) may have long-term impacts that may or may not be readily apparent. For example, the spread of small areas of mesquite

established by Native Americans (Fredrickson et al., 2006) may have been due in part to grass abrasion, burial, and reduced soil surface stability caused by aeolian sand moving from these shrub-dominated areas.

Land managers require an ability to predict management effects on wind erosion and an understanding of the likely effects of wind erosion and deposition on susceptibility to future erosion. Whereas the effects of broadly defined land use types (e.g. cultivation vs. permanent pasture) are generally understood at the patch scale, currently available models fail to account for the cascading effects of management-mediated changes in vegetation cover and structure at multiple spatial scales. Further, these essentially agronomic models do not account for the temporally variable and interacting effects of soil surface disturbance (which increases soil erodibility) and spatially variable vegetation growth and removal (which increases wind erosivity) in perennial ecosystems. Most models also fail to address linkages among landscape units, and the direct and indirect effects of both erosion and deposition on susceptibility to future erosion.

3.2. Consequences of aeolian processes at the patch-landscape scale

The two most significant consequences of aeolian processes at the patch-landscape scale are (1) the transport of saltation-sized particles from an eroding patch to an adjacent stable patch, and (2) the large-scale reduction of surface soil resources in both erosional and depositional areas (Fig. 4). The consequences of aeolian processes at the patch-landscape scale are similar to those at the plant-interspace scale, but take place over a larger area. Thus, while saltation can lead to the movement of coarse material from plant interspaces to nearby plant canopies to create dunes at the plant-interspace scale, saltation may also lead to the growth of mesquite dunelands into former grassland areas at the patch-landscape scale.

In their studies of the impacts of saltation flux and dust emission on vegetated patches downwind of areas where vegetation had been removed, Okin et al. (2001a, b) determined that saltation flux caused physical damage to shrubs in the downwind patch. They also determined that a mantle of coarse-grained particles derived from winnowing the original soil surface and depositing the remaining particles downwind had covered the original surface. The local mantling of the original surface resulted in an effective reduction of soil nutrient resources in the surface soil (top 5 cm). This, together with increased soil instability, could result in a decrease in recruitment of new vegetation when this mantle is thicker than the depth of soil needed for seedling establishment. These results are consistent with those of Larney et al. (1998a, b) and Leys and McTainsh (1994), who showed that significant changes in soil nutrient content could result from aeolian transport of soil particles. On fine-textured soils, however, sand deposition increases plant water availability by increasing infiltration. For example, on the south end of the Jornada Basin where tarbush (*Fluourensia cernua*) dominates loamy soils with high runoff rates, black grama (*Bouteloua eriopoda*) and bunchgrasses occur in patches covered by a mantle of aeolian sand. Deposition of finer-textured material may also serve as a nutrient source, particularly for microbiotic crusts, which lack the capacity to acquire nutrients from deeper soil layers (Belnap et al., 2001).

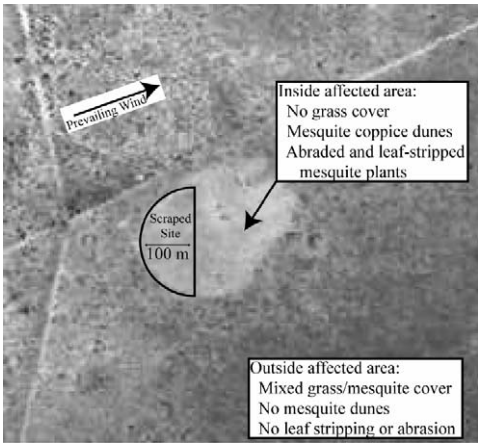

Fig. 7. The Jornada "scraped site," shown here in a 1999 low-altitude AVIRIS image with resolution of ~5 m. This site proves that wind erosion can affect ecosystem stability in this ecosystem. It has experienced an average deflation rate of 1.8 cm/yr (Gillette and Chen, 2001) and plant-available N and P have been reduced by 89% and 78%, respectively (Okin et al., 2001b). No vegetation has regrown on the scraped site itself. The vegetation community downwind of the site has changed from a grassland to a shrubland due to burial, abrasion, and leaf stripping from saltating particles off of the scraped site itself and plant-available N and P in surface soils in the downwind area have been reduced by 82% and 62%, respectively. The location of the downwind plume indicates the constancy of the wind direction at the JER.

In the decade since complete removal of vegetation at a site on the JER (the *scraped site*, Fig. 7), changes in soil texture, soil nutrients, and vegetation cover have been observed in the area downwind of the site (Okin et al., 2001b; Okin and Painter, 2004). This site has provided a dramatic example of the importance of wind erosion in understanding the relationship between adjacent vegetation patches. At a large scale on the JER, this inter-patch interaction has probably contributed to the expansion and coalescence of mesquite duneland patches. These patches, which experience the highest aeolian transport of all vegetated areas on the JER (Gillette and Pitchford, 2004), likely act as sources of coarse-grained sediment which flows into adjacent patches, burying or killing low-stature vegetation and covering the surface with a winnowed layer. This process may have also resulted in the expansion of mesquite dunes into the west side of a formerly grass-dominated playa ("Red Lake") at the north end of the JER.

4. Regional–global scale

4.1. Controls on aeolian processes at the regional–global scale

Although the controls on aeolian processes discussed in earlier sections are certainly general enough to be applied in arid and semi-arid regions around the

globe, the most important controls on aeolian processes at the global scale are not well understood. The dust observed over North Africa, for example, certainly originates in the Sahara and Sahel regions, but current technologies do not allow unique identification of the loci in these landscapes of greatest dust emission, nor what surface processes are responsible for creating the strongest sources.

Ginoux et al. (2001) and Prospero et al. (2002) argued that the dominant sources of atmospheric desert dust are topographic lows (often paleolakes or ephemeral water bodies) with little or no impact from humans. Their studies were based on satellite and modeling studies. Although this provides a significant step forward in our understanding of the spatial characteristics of dust sources, the observation that dust emission occurs primarily in topographic lows provides very little insight about the geomorphic or anthropogenic processes responsible for creating these source areas. This theory does not explain why some topographic lows are better sources than others. Furthermore, Mahowald et al. (2002) suggested that extant atmospheric remote sensing data cannot eliminate the possibility of disturbed landscapes being important sources of desert dust to the atmosphere in North Africa because topographic lows also typically coincide with areas of human activity and disturbance of vegetation and the soil surface. By comparing atmospheric loading predicted in models and observed with satellites, Tegen and Fung (1995) argued that 50% of atmospheric dust loading could be due to "disturbed" soils: soils known to have been affected by the Saharan/Sahelian boundary shift, cultivation, deforestation, and wind erosion. The importance of spatial heterogeneity in aeolian processes also provides a significant challenge to understanding the global controls on dust emission: small sources may be responsible for the bulk of dust emission in an area, but may be too small to be resolved using global observations or models (Raupach and Lu, 2004; Okin, 2005).

4.2. Consequences of aeolian processes at regional to global scales

Saltation-sized particles are important at plant and patch scales. Over millennia, saltation can also be important at landscape scales. Aeolian movement of saltation-sized particles is believed to be trivial at regional to global scales due to low rates and obstructions that ultimately stop particle movement, with the obvious exception of periglacial loess deposits. However, dust emitted from arid and semi-arid regions can be transported globally. Airborne dust, also known as mineral aerosols in the atmospheric science community, impacts global climate through its ability to scatter and absorb light (Sokolik and Toon, 1996), to affect cloud properties (Wurzler et al., 2000), and to impact atmospheric chemistry (Dentener et al., 1996). Desert dust is thought to play a major role in ocean fertilization and CO_2 uptake (Duce and Tindale, 1991), terrestrial soil formation (Chadwick et al., 1999), and nutrient cycling (Reynolds et al., 2001; Bao and Reheis, 2003; Okin et al., 2004). Dust is also an important vector for the movement of plant nutrients (Okin et al., 2004), environmental contaminants (Travis, 1975; Breshears et al., 2003), pathogens (Leathers, 1981; Plumlee and Ziegler, 2004), and allergens (Griffin et al., 2001).

5. Toward a cross-scale model of wind erosion in structurally diverse arid and semi-arid ecosystems

Many arid and semi-arid landscapes exist as a mosaic of grass and shrub cover at the patch scale, and as a mixture between two landscape endmembers at the landscape scale: sparse arid shrubland and semi-arid grassland. Transitions between grass- and shrub-dominated communities are of particular concern to land managers in many parts of the world (Schlesinger et al., 1990; Laycock, 1991; Hoffman et al., 1995; Milton and Dean, 1995). Shrub-dominated systems commonly have higher rates of runoff and wind and water erosion. Self-reinforcing feedbacks between soil erosion and plant growth can lead to relatively irreversible thresholds (Wright and Honea, 1986; Schlesinger et al., 1990). Wind erosion models that explicitly address these dynamics are required so that managers can anticipate and prevent threshold transitions from occurring. Understanding dust emission from shrub-invaded grasslands is also important to understanding dust emission on regional to global scales, and physically based improvements of modeling efforts in mixed landscapes (e.g. encompassing grasslands, shrublands, mixed shrubland-grassland, and savannas) would allow improved global dust loading predictions (Mahowald et al., 1999; Ginoux et al., 2001; Zender et al., 2003). As a first step, we suggest the construction of a model that explicitly treats landscapes as mosaics of different life forms.

The models of Raupach et al. (1993), Marticorena and Bergametti (1995), Shao and Lu (2000), Zender et al. (2003), Okin (2005) or others could be used to model wind erosion and dust emission from shrubland or grassland endmember landscapes. In regions composed of a mosaic of grass, shrub, and bare ground, constructing a model is more difficult. Individual grass plants tend to have lower stature and smaller diameters than shrubs in these environments. At the JER, Gillette and Pitchford (2004) observed that shrublands generally experience greater aeolian mass flux than grasslands on the same soils, whereas mesquite dunelands produce the most dust. It is not clear how the diversity of life forms (i.e. grasses vs. shrubs) and covers can be included in existing models cited above. Okin (2004, 2005) suggested a stochastic method similar to that of Raupach and Lu (2004) for including variable vegetation cover in models of aeolian transport, but neither of these models accounts explicitly for vegetation structural diversity. The value of these stochastic or probability-based approaches is that surface variability can be included in existing models without rewriting these models to explicitly account for interplant dynamics. Additional information is required on the variability of vegetation cover, β-parameter, shape, height, and width as well as bare soil threshold shear velocity before this approach can be fully implemented. Significant field efforts in dust-producing regions around the world will be needed to determine the magnitude of variability of these parameters. In the absence of field data for this purpose, probability distributions in the landscape features that control wind erosion and dust emission could be used as tuning parameters in local modeling studies of dust emission.

Several elements must be included in a new wind erosion model that can account for mixed life forms in desert environments and can incorporate the range of

community types observed in arid and semi-arid landscapes worldwide. Based on the considerations discussed above, we believe that such a dust emission model would have the following components:

(a) *A description of airflow between shrubs*. This component would incorporate the sheltering effect of grasses in intershrub areas but would treat grasses and shrubs separately.
(b) *An expression of the relationship between intershrub distance and sand flux*. For sites with extremely low grass cover in shrub interspaces, fetch effect can be an important determinant of the amount of wind erosion that occurs, especially in heterogeneous or anisotropic communities. This component would quantify the fetch effect in heterogeneous communities.
(c) *A threshold shear velocity for wind erosion in shrub interspaces*. We anticipate that erosion only occurs in shrub interspaces, but the threshold for particle movement can vary depending on grass cover in interspaces. Because grass cover changes seasonally and inter-annually as well as from site to site, a model which can incorporate high-frequency grass dynamics separately from low-frequency shrub change would seem to be necessary in order to incorporate differences in life forms in desert environments.
(d) *A statistical description of the dependence of intershrub distance on shrub cover and size*. Okin and Gillette (2001) found intershrub distance is dependent on both plant size and fractional cover, and that intershrub distance can be anisotropic. Thus, this component of the model would account for how shrubs are distributed on the landscape.

6. Conclusions

Aeolian processes play an important role in shaping arid and semi-arid regions worldwide. The framework proposed by Peters and Havstad (2006) to explain the heterogeneity in vegetation dynamics focuses on five key elements that connect units of variable spatial scale. Aeolian processes are related to these key elements (feedbacks, resource redistribution, transport, context, and legacy) and contribute to variable vegetation patterns and threshold behaviors at all hierarchical scales. Feedbacks exist between individual plants and wind. Saltation physically impacts downwind plants and plant cover affects transport and erosion of soil. Threshold gap sizes exist, below which erosion may not occur. Patch structure is also important given that horizontal flux increases with fetch. Mosaics of vegetation structure created by concentrated activities (e.g. grazing, ORV activity) may result in areas that are more susceptible to erosion than would be predicted based on the average cover for a pasture. Saltation processes are most important at plant and patch scales at short time-scales. At longer time-scales, saltation processes can also be important at the landscape scale. Dust emission is important at the plant and patch scales whereas dust deposition tends to be more important at the regional and global scales.

Acknowledgments

The Jornada Experimental Range is administered by the USDA Agricultural Research Service, and is a National Science Foundation supported Long Term Ecological Research site (DEB 0080412). Additional funding was provided by NSF (DEB 0316320).

References

Alfaro, S.C., Gomes, L., 2001. Modeling mineral aerosol production by wind erosion: emission intensities and aerosol size distributions in source areas. Journal of Geophysical Research-Atmospheres 106, 18075–18084.

Bach, A.J., 1998. Assessing conditions leading to severe wind erosion in the Antelope Valley, California, 1990–1991. Professional Geographer 50, 87–97.

Bagnold, R.A., 1941. The Physics of Blown Sand and Desert Dunes. Methuen, New York.

Bao, H., Reheis, M.C., 2003. Multiple oxygen and sulfur isotopic analysis on water-soluble sulfate in bulk atmospheric deposition from southwestern USA. Journal of Geophysical Research 108.

Belnap, J., 1995. Surface disturbances: their role in accelerating desertification. Environmental Monitoring and Assessment 37, 39–57.

Belnap, J., Prasse, R., Harper, K.T., 2001. Influence of biological soil crusts on soil environments and vascular plants. In: Belnap, J., Lange, O.L. (Eds.), Biological Soil Crusts: Structure, Function and Management. Springer, Berlin, pp. 281–300.

Breed, C.S., Reheis, M., (Eds.), 1999. Desert Winds: Monitoring wind-related surface processes in Arizona, New Mexico, and California, USGS Professional Paper 1598, US Government Printing Office, Washington, DC.

Breshears, D.D., Whicker, J.J., Johansen, M.P., Pinder, J.E., 2003. Field measurements of wind and water transport for contaminant mobility: comparisons and contrasts among semiarid grassland, shrubland, and forest ecosystems. Health Physics 84, S155.

Brown, G., Schoknecht, N., 2001. Off-road vehicles and vegetation patterning in a degraded desert ecosystem in Kuwait. Journal of Arid Environments 49, 413–427.

Chadwick, O.A., Derry, L.A., Vitousek, P.M., Huebert, B.J., Hedin, L.O., 1999. Changing sources of nutrients during four million years of ecosystem development. Nature 397, 491–497.

Crawley, D.M., Nickling, W.G., 2003. Drag partition for regularly arrayed rough surfaces. Boundary-Layer Meteorology 107, 445–468.

Dentener, F.J., Carmichael, G.R., Zhang, Y., Lelieveld, J., Crutzen, P.J., 1996. Role of mineral aerosol as a reactive surface in the global troposphere. Journal of Geophysical Research 101, 22869–22889.

Duce, R.A., Tindale, N.W., 1991. Atmospheric transport of iron and its deposition in the ocean. Limnology and Oceanography 36, 1715–1726.

Fredrickson, E.L., Estell, R.E., Laliberte, A., Anderson, D.M., 2006. Mesquite recruitment in the Chihuahuan Desert: historic and prehistoric patterns with long term impacts. Journal of Arid Environments 65, 285–295.

Fredrickson, E., Havstad, K.M., Estell, R., Hyder, P., 1998. Perspectives on desertification: southwestern United States. Journal of Arid Environments 39, 191–207.

Gibbens, R.P., Tromble, J.M., Hennessy, J.T., Cardenas, M., 1983. Soil movement in mesquite dunelands and former grasslands of southern New Mexico from 1933 to 1980. Journal of Range Management 36, 145–148.

Gillette, D.A., 1974. On the production of soil wind erosion aerosols having the potential for long range transport. Journal des Recherches Atmospheriques 8, 735–744.

Gillette, D.A., 1977. Fine particulate emissions due to wind erosion. Transactions of the American Society of Agricultural Engineers 29, 890–897.

Gillette, D.A., Chen, W.A., 2001. Particle production and aeolian transport from a "supply limited" source area in the Chihuahuan Desert, New Mexico, United States. Journal of Geophysical Research 106, 5267–5278.

Gillette, D.A., Pitchford, A.M., 2004. Sand flux in the northern Chihuahuan desert, New Mexico, USA, and the influence of mesquite-dominated landscapes. Journal of Geophysical Research-Earth Surface 109.

Gillette, D.A., Herbert, G., Stockton, P.H., Owen, P.R., 1996. Causes of the fetch effect in wind erosion. Earth Surface Processes and Landforms 21, 641–659.

Gillette, D.A., Niemeyer, T.C., Helm, P.J., 2001. Supply limited horizontal sand drift at an ephemerally crusted, unvegetated saline playa. Journal of Geophysical Research-Atmospheres 106, 18085–18098.

Ginoux, P., Chin, M., Tegen, I., Prospero, J.M., Holben, B., Dubovik, O., Lin, S.J., 2001. Sources and distributions of dust aerosols simulated with the GOCART model. Journal of Geophysical Research-Atmospheres 106, 20255–20273.

Grant, P.F., Nickling, W.G., 1998. Direct field measurement of wind drag on vegetation for application to windbreak design and modeling. Land Degradation and Development 9, 57–66.

Greeley, R., Iversen, J.D., 1985. Wind as a Geological Process on Earth, Mars, Venus and Titan. Cambridge University Press, Cambridge.

Griffin, D.W., Garrison, V.H., Herman, J.R., Shinn, E.A., 2001. African desert dust in the Caribbean atmosphere: Microbiology and public health. Aerobiologia 17, 203–213.

Hagen, L.J., 1991. A wind erosion prediction system to meet user needs. Journal of Soil and Water Conservation 46, 106–111.

Hennessy, J.T., Kies, B., Gibbens, R.P., Tromble, J.M., 1986. Soil sorting by forty-five years of wind erosion on a southern New Mexico Range. Soil Science Society of America Journal 50, 391–394.

Herrick, J., Havstad, K., Coffin, D., 1997. Rethinking remediation technologies for desertified landscapes. Journal of Soil and Water Conservation 52, 220–225.

Herrick, J.E., Van Zee, J.W., Havstad, K.M., Burkett, L.M., Whitford, W.G., 2005. Monitoring Manual for Grassland, Shrubland and Savanna Ecosystems. USDA-ARS Jornada Experimental Range, Las Cruces, NM, University of Arizona Press, Tucson, Arizona.

Hoffman, M.T., Bond, W.J., Stock, W.D., 1995. Desertification of the eastern Karoo, south Africa: Conflicting paleoecological, historical, and soil isotopic evidence. Environmental Monitoring and Assessment 37, 159–177.

Hyers, A.D., Marcus, M.G., 1981. Land use and desert dust hazards in central Arizona. In: Péwé, T.L. (Ed.), Desert Dust: Origin, Characteristics, and Effect on Man. Geological Society of America, Boulder, Colorado, pp. 267–280.

Khalaf, F.I., 1989. Desertification and aeolian processes in the Kuwait Desert. Journal of Arid Environments 16, 125–145.

Koch, M., El Baz, F., 1998. Identifying the effects of the Gulf War on the geomorphic features of Kuwait by remote sensing and GIS. Photogrammetric Engineering and Remote Sensing 64, 739–747.

Larney, F.J., Bullock, M.S., Mcginn, S.M., Fryrear, D.W., 1995. Quantifying wind erosion on summer fallow in southern Alberta. Journal of Soil and Water Conservation 50, 91–94.

Larney, F.J., Bullock, M.S., Janzen, H.H., Ellert, B.H., Olson, E.C.S., 1998a. Wind erosion effects on nutrient redistribution and soil productivity. Journal of Soil and Water Conservation 53, 133–140.

Larney, F.J., Bullock, M.S., Janzen, H.H., Ellert, B.H., Olson, E.C.S., 1998b. Wind erosion effects on nutrient redistribution and soil productivity. Journal of Soil and Water Conservation 53, 133–140.

Laycock, W.A., 1991. Stable states and thresholds of range condition in North American rangelands: A viewpoint. Journal of Rangeland Management 44, 427–433.

Leathers, C.R., 1981. Plant components of desert dust in Arizona and their significance for man. In: Péwé, T.L. (Ed.), Desert Dust: Origin, Characteristics, and Effect on Man. Geological Society of America, Boulder, Colorado, pp. 191–206.

Lee, B.E., Soliman, B.F., 1977. An investigation of the forces on three dimensional bluff bodies in rough wall turbulent boundary layers. Journal of Fluids Engineering 99, 503–510.

Lee, S.J., Park, K.C., Park, C.W., 2002. Wind tunnel observations about the shelter effect of porous fences on the sand particle movements. Atmospheric Environment 36, 1453–1463.

Lettau, H.H., 1969. Note on aerodynamic roughness-parameter estimation on the basis of roughness element description. Journal of Applied Meteorology 8, 828–832.

Leys, J., McTainsh, G., 1994. Soil loss and nutrient decline by wind erosion—cause for concern. Australian Journal of Soil and Water Conservation 7, 30–35.

Li, J., Okin, G.S., 2004. Soil nutrient distribution in response to wind erosion in a desert grassland, Soil Science Society of America Fall Meeting, Seattle, WA.

Ludwig, J.A., Eager, R.W., Bastin, G.N., Chewings, V.H., Liedloff, A.C., 2002. A leakiness index for assessing landscape function using remote sensing. Landscape Ecology 17, 157–171.

Mahowald, N., Kohfeld, K., Hansson, M., Balkanski, Y., Harrison, S.P., Prentice, I.C., Schulz, M., Rodhe, H., 1999. Dust sources and deposition during the last glacial maximum and current climate: a comparison of model results with paleodata from ice cores and marine sediments. Journal of Geophysical Research 104, 15895–15916.

Mahowald, N.M., Zender, C.S., Luo, C., Savoie, D., Torres, O., del Corral, J., 2002. Understanding the 30-year Barbados desert dust record. Journal of Geophysical Research-Atmospheres 107.

Marticorena, B., Bergametti, G., 1995. Modeling the atmospheric dust cycle: 1. Design of a soil-derived dust emission scheme. Journal of Geophysical Research 100, 16415–16430.

Marticorena, B., Bergametti, G., Aumont, B., Callot, Y., N'Doumé, C., Legrand, M., 1997. Modeling the atmospheric dust cycle: 2. Simulation of Saharan sources. Journal of Geophysical Research 102, 4387–4404.

Milton, S.J., Dean, W.R.J., 1995. South Africa's arid and semiarid rangelands: why are they changing and can they be restored? Environmental Monitoring and Assessment 37, 245–264.

Minvielle, F., Marticorena, B., Gillette, D.A., Lawson, R.E., Thompson, R., Bergametti, G., 2003. Relationship between the aerodynamic roughness length and the roughness density in cases of low roughness density. Environmental Fluid Mechanics 3, 249–267.

Musick, H.B., Gillette, D.A., 1990. Field evaluation of relationships between a vegetation structural parameter and sheltering against wind erosion. Land Degradation and Rehabilitation 2, 87–94.

Musick, H.B., Trujillo, S.M., Truman, C.R., 1996. Wind-tunnel modeling of the influence of vegetation structure on saltation threshold. Earth Surface Processes and Landforms 21, 589–605.

Nakata, J.K., Wilshire, H.G., Barnes, G.C., 1976. Origin of Mojave Desert dust plumes photographed from space. Geology 4, 644–648.

Nanney, R.D., Fryrear, D.W., Zobeck, T.M., 1993. Wind erosion prediction and control. Water Science and Technology 28, 519–527.

Okin, G.S., 2004. Stochastic modeling of desert dust emission: bridging the scale gap. Geological Society of America Abstracts with Programs 36, 48.

Okin, G.S., 2005. Dependence of wind erosion on surface heterogeneity: stochastic modeling. Journal of Geophysical Research 110, D11206.

Okin, G.S., Gillette, D.A., 2001. Distribution of vegetation in wind-dominated landscapes: Implications for wind erosion modeling and landscape processes. Journal of Geophysical Research 106, 9673–9683.

Okin, G.S., Painter, T.H., 2004. Effect of grain size on remotely sensed spectral reflectance of sandy desert surfaces. Remote Sensing of Environment 89, 272–280.

Okin, G.S., Murray, B., Schlesinger, W.H., 2001a. Degradation of sandy arid shrubland environments: observations, process modeling, and management implications. Journal of Arid Environments 47, 123–144.

Okin, G.S., Murray, B., Schlesinger, W.H., 2001b. Desertification in an arid shrubland in the southwestern United States: process modeling and validation. In: Conacher, A. (Ed.), Land Degradation: Papers Selected from Contributions to the Sixth meeting of the International Geographical Union's Commission on Land Degradation and Desertification. Kluwer Academic Publishers, Dordrecht, pp. 53–70.

Okin, G.S., Mahowald, N., Chadwick, O.A., Artaxo, P., 2004. The impact of desert dust on the biogeochemistry of phosphorus in terrestrial ecosystems. Global Biogeochemical Cycles 18.

Owen, P.R., 1964. Saltation of uniform grains in air. Journal of Fluid Mechanics 20, 225–242.

Peters, D.P.C., Havstad, K.M., 2006. Nonlinear dynamics in arid and semiarid systems: interactions among drivers and processes across scales. Journal of Arid Environments 65, 196–206.

Plumlee, G.S., Ziegler, T.L., 2004. The medical geochemistry of dust, soils and other earth materials. In: Lollar, B.S. (Ed.), Treatise on Geochemistry. Elsevier, New York, pp. 263–310.

Prose, D.V., 1985. Persisting effects of armored military maneuvers on some soils of the Mojave Desert. Environmental Geology and Water Sciences 7, 163–170.

Prospero, J.M., Ginoux, P., Torres, O., Nicholson, S.E., 2002. Environmental characterization of global sources of atmospheric soil dust derived from the NIMBUS7 TOMS absorbing aerosol product. Reviews of Geophysics 40 Art. No. 1002.

Raupach, M.R., 1992. Drag and drag partition on rough surfaces. Boundary-Layer Meteorology 60, 375–395.

Raupach, M.R., Lu, H., 2004. Representation of land-surface processes in aeolian transport models. Environmental Modelling & Software 19, 93–112.

Raupach, M.R., Gillette, D.A., Leys, J.F., 1993. The effect of roughness elements on wind erosion threshold. Journal of Geophysical Research 98, 3023–3029.

Raupach, M.R., Woods, N., Dorr, G., Leys, J.F., Cleugh, H.A., 2001. The entrapment of particles by windbreaks. Atmospheric Environment 35, 3373–3383.

Ravi, S., D'Odorico, P., Over, T.M., Zobeck, T.M., 2004. On the effect of air humidity on soil susceptibility to wind erosion: The case of air-dry soils. Geophysical Research Letters 31 Art. No. L09501.

Retta, A., Armbrust, D.V., Hagen, L.J., 1996. Partitioning of biomass in the crop submodel of WEPS (wind erosion prediction system). Transactions of the ASAE 39, 145–151.

Reynolds, J.F., Belnap, J., Reheis, M., Lamothe, P., Luiszer, F., 2001. Eolian dust in Colorado Plateau soils: nutrient inputs and recent change in source. Proceedings of the National Academy of Sciences 98, 7123–7127.

Schlesinger, W.H., Reynolds, J.F., Cunningham, G.L., Huenneke, L.F., Jarrell, W.M., Virginia, R.A., Whitford, W.G., 1990. Biological feedbacks in global desertification. Science 247, 1043–1048.

Schlesinger, W.H., Raikes, J.A., Hartley, A.E., Cross, A.F., 1996. On the spatial pattern of soil nutrients in desert ecosystems. Ecology 77, 364–374.

Shao, Y.P., Lu, H., 2000. A simple expression for wind erosion threshold friction velocity. Journal of Geophysical Research-Atmospheres 105, 22437–22443.

Shao, Y., Raupach, M.R., 1993. Effect of saltation bombardment on the entrainment of dust by wind. Journal of Geophysical Research 98, 12719–12726.

Sheridan, D., 1978. Dirt motorbikes and dune buggies threaten deserts. Smithsonian 9, 67–75.

Sokolik, I.N., Toon, O.B., 1996. Direct radiative forcing by anthropogenic airborne mineral aerosols. Nature 381, 681–683.

Talbot, W.J., 1947. Swartland and Sandveld. A Survey of the Land Utilization and Soil Erosion in the Western Lowland of the Cape Province. Oxford University Press, Cape Town, South Africa.

Taylor, P.A., 1988. Turbulent wakes in the atmospheric boundary layer. In: Steffen, W.L., Denmead, O.T. (Eds.), Flow and Transport in Natural Environments: Advances and Applications. Springer, Berlin, pp. 270–292.

Tegen, I., Fung, I., 1995. Contribution to the atmospheric mineral aerosol load from land surface modification. Journal of Geophysical Research 100, 18707–18726.

Travis, J.R., 1975. A model for predicting the redistribution of particulate contaminants from soil surfaces. LA-6035-MS. Los Alamos Scientific Laboratory, Los Alamos, New Mexico.

Webb, R.H., 1982. Off-road motorcycle effects on a desert soil. Environmental Conservation 9, 197–208.

Wilshire, H.G., 1980. Human causes of accelerated wind erosion in California's Deserts. In: Coates, D.R., Vitek, J.D. (Eds.), Thresholds in Geomorphology. George. Allen and Unwin, London, pp. 415–433.

Wolfe, S.A., Nickling, W.G., 1993. The protective role of sparse vegetation in wind erosion. Progress in Physical Geography 17, 50–68.

Wooding, R.A., Bradley, E.F., Marshall, J.K., 1973. Drag due to regular arrays of roughness elements of varying geometry. Boundary-Layer Meteorology 5, 285–308.

Wright, R.A., Honea, J.H., 1986. Aspects of desertification in southern New Mexico, USA: soil properties of a mesquite duneland and a former grassland. Journal of Arid Environments 11, 139–145.

Wurzler, S., Reisin, T.G., Levin, Z., 2000. Modification of mineral dust particles by cloud processing and subsequent effects on drop size distributions. Journal of Geophysical Research 105, 4501–4512.

Zender, C.S., Bian, H., Newman, D., 2003. The mineral Dust Entrainment And Deposition (DEAD) model: Description and 1990s dust climatology. Journal of Geophysical Research 108, 4416.

EXHIBIT 411

Storm Precipitation in the United States. Part II: Soil Erosion Characteristics

JAMES R. ANGEL

Atmospheric Environment Section, Illinois State Water Survey, Champaign, Illinois

MICHAEL A. PALECKI

Midwestern Regional Climate Center, Illinois State Water Survey, Champaign, Illinois

STEVEN E. HOLLINGER

Atmospheric Environment Section, Illinois State Water Survey, Champaign, Illinois

(Manuscript received 16 March 2004, in final form 17 December 2004)

ABSTRACT

Soil erosion is a major global challenge. An increased understanding of the mechanisms driving soil erosion, especially the storms that produce it, is vital to reducing the impact on agriculture and the environment. The objective of this work was to study the spatial distribution and time trends of the soil erosion characteristics of storms, including the maximum 30-min precipitation intensity (I_{30}), storm kinetic energy of the falling precipitation (KE), and the storm erosivity index (EI) using a long-term 15-min precipitation database. This is the first time that such an extensive climatology of soil erosion characteristics of storms has been produced. The highest mean I_{30}, KE, and EI values occurred in all seasons in the southeastern United States, while the lowest occurred predominantly in the interior west. The lowest mean I_{30}, KE, and EI values typically occurred in winter, and the highest occurred in summer. The exception to this was along the West Coast where winter storms exhibited the largest mean KE and EI values. Linear regression was used to identify trends in mean storm erosion characteristics for nine U.S. zones over the 31-yr study period. The south-central United States showed increases for all three storm characteristics for all four seasons. On the other hand, higher elevations along the West Coast showed strong decreases in all three storm characteristics across all seasons. The primary agricultural region in the central United States showed significant increases in fall and winter mean EI when there is less vegetative cover. These results underscore the need to update the storm climatology that is related to soil erosion on a regular basis to reflect changes over time.

1. Introduction

Soil erosion is a major challenge in the United States and the world (Oldeman 1994; Pimental et al. 1995; Nearing 2001). An increased understanding of the mechanisms driving soil erosion, especially the storms that produce it, is vital to reducing its impact on agriculture and the environment. The potential for climate change, in the form of changing storm characteristics, is an additional challenge to the management of soil erosion. A recent study (Soil and Water Conservation Society 2003) discussed the implications of possible climate change and suggested the following three approaches to begin addressing the issue: 1) update the climate parameters in conservation tools, 2) investigate the damages likely to occur as a result of a changed precipitation regime, and 3) evaluate the benefits of including the risks from extreme rain events in the conservation-planning process.

Groisman et al. (2004) reviewed changes in precipitation for the contiguous United States, noting that overall precipitation had increased by 7% between 1908 and 2002. Heavier precipitation events at the 95th and 99th percentile had increased even more, by 14% and 20%, respectively. Furthermore, most of these changes occurred in the last 30 yr of record (Soil and Water Conservation Society 2003). The Groisman et al. study noted that the increases in precipitation were

Corresponding author address: James R. Angel, Illinois State Water Survey, 2204 Griffith Drive, Champaign, IL 61820.
E-mail: jimangel@uiuc.edu

© 2005 American Meteorological Society

largely confined to spring, summer, and fall, which is the period when heavier events are likely to occur. While they were focused on the more extreme daily events and the annual totals, these results have serious implications for individual storm events and their erosive potential.

Other studies have examined the potential changes in future rainfall erosivity using coupled atmosphere–ocean global climate models as guidance for climate change in the twenty-first century (e.g., Nearing 2001; Pruski and Nearing 2002). While there were regional differences in the results, Nearing (2001) found that erosion over the United States increased between 16% and 58% in projections over the next 80 yr, depending on the methodology applied. Pruski and Nearing (2002) used the Water Erosion Prediction Project (WEPP) model and output from two global climate models to examine changes in soil erosion in response to climate change. As expected, erosion increased in those areas where precipitation increased. However, the relationship became more complex in areas with decreased precipitation. For example, decreased precipitation could decrease vegetation, leading to increased erosion. In a summary of climate change and soil erosion rates, Nearing et al. (2004) noted that soil erosion rates can be expected to increase by 1.7% for each 1% increase in annual precipitation. Clearly, these studies point to the need to closely examine present-day storm erosivity in the United States and its observed change over time. Prior to this study, no such modern climatology for the United States has been produced.

Palecki et al. (2005, hereinafter Part I) examined the meteorological characteristics of storm precipitation. Our objective was to study the spatial distribution and time trends of the storm erosion characteristics of rainstorms in the conterminous United States, including the storm maximum 30-min precipitation intensity (I_{30}), storm kinetic energy (KE), and the storm erosivity index (EI). Storm erosional characteristics for each of the four climatological seasons of winter (December–January–February), spring (March–April–May), summer (June–July–August), and fall (September–October–November) were examined. The storm erosion characteristics were grouped into nine zones, representing coherent seasonal cycles of storm precipitation characteristics (Fig. 1).

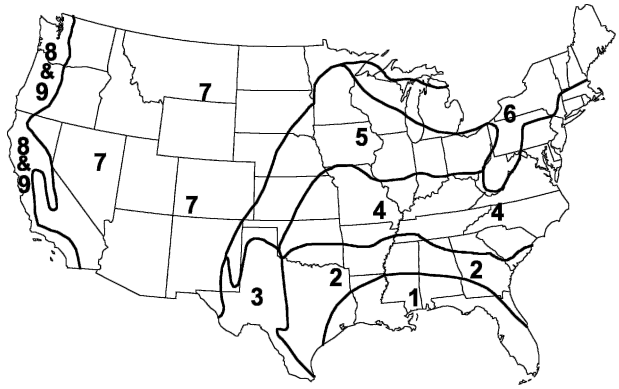

FIG. 1. Storm precipitation characteristic cluster zones. Stations in zones 8 and 9 on the West Coast are intermingled but separated by elevation (see text). For a more detailed rendering of zones 8 and 9, please see Fig. 1 in Part I.

2. Data and methods

Storm soil erosion characteristics were computed using the National Climatic Data Center (NCDC) 15-min precipitation database as measured by a network of Fischer–Porter weighing-bucket gauges (Hammer 1998). This network of unshielded gauges has remained unchanged during its operation within the period of this study (1972–2002). In a review of the U.S. climate network, Groisman and Legates (1994) examined the accuracy of precipitation measurements. They concluded that gauges underestimate the actual precipitation, largely because of wind-induced turbulence. The problem is worst in winter and northern latitudes, because the snowfall catchment is especially sensitive to wind. No attempt was made here to identify or adjust for such biases on a storm-by-storm basis. However, this inherent limitation of the data should be kept in mind while considering the results of this study, especially for winter.

While approximately 3700 stations are included in the 15-min precipitation database, many stations had missing records, and some had record lengths of less than 10 yr. The database was first screened to identify stations with a record length of greater than 20 yr and with less than 25% missing data, resulting in the final selection of 1505 stations in the conterminous United States.

Each 15-min record includes quality control flags indicating missing data, accumulated data, and data flagged by NCDC for quality control reasons (Hammer 1998). In computing the storm soil erosion characteristics, only storms that had no flags present and were separated from flagged or missing data by more than 6 h were used. The "6 h between storms" rule has been used extensively in previous work (e.g., Huff 1967; Wischmeier and Smith 1978; Renard et al. 1997).

Once each storm was identified, I_{30}, KE, and EI were computed. The I_{30} was computed by summing the precipitation in each consecutive pair of 15-min periods during a storm and multiplying the greatest 30-min total precipitation by 2 to get the rate in millimeters per hour. The resulting rate was then adjusted by 1.034 to

represent a maximum 30-min precipitation rate that would be obtained from break-point data (Hollinger et al. 2002). Break-point precipitation data are reported as time segments of an equal intensity rather than amounts at fixed time intervals, and, therefore, can capture the true 30-min maximum of a storm.

The KE, a measure of the accumulated kinetic energy of the precipitation as it strikes the ground, has been computed using a power-law equation (Uijlenhoet and Stricker 1999), a logarithmic function (Wischmeier and Smith 1958), and an exponential equation (Kinnell 1980; Brown and Foster 1987; Renard et al. 1997). In a critical literature appraisal, van Dijk et al. (2002) conclude that the exponential equation is the best estimate of kinetic energy because it places an upper limit on kinetic energy at high precipitation intensities (Hudson 1963; Barauah 1973; Carter et al. 1974; Wischmeier and Smith 1978; Kinnell 1980; Rosewell 1986; Brown and Foster 1987). The total KE (MJ ha^{-1}) is calculated after Renard and Freimund (1994),

$$\mathrm{KE}_k = \sum_{r=1}^{s} e_r \Delta V_r, \tag{1}$$

where e_r is the kinetic energy (MJ ha^{-1} mm^{-1}), ΔV_r is the precipitation depth (mm) of a given storm increment, and the summation is over the storm increments (1 to s). The number of increments (s) is determined by the storm length and data resolution. In this case where 15-min data are used, if a storm lasts 2 h, then $s = 8$. The kinetic energy e_r is computed with the continuous exponential equation from Renard and Freimund (1994), as modified by McGregor et al. (1995):

$$e_r = 0.29[1 - 0.72 \exp(-0.082 i_r)], \tag{2}$$

where i_r is the precipitation intensity (mm h^{-1}) for a particular storm increment. The McGregor et al. (1995) modification changed the exponential coefficient to 0.082 from 0.05 (Renard and Freimund 1994). The total EI (MJ mm ha^{-1} h^{-1}) is computed as

$$\mathrm{EI} = \mathrm{KE}(I_{30}). \tag{3}$$

The Fischer–Porter weighing-bucket gauge will measure snowfall events. However, the concepts of the kinetic energy of the falling precipitation and storm erosivity are not meaningful in these situations. A portion of these gauges is not collocated with climatological sites that collect temperature and snowfall data. Furthermore, those climatological sites that are collocated with gauges report only once a day, with the exact time varying from site to site. As a result, individual snow "storms" cannot be reliably identified and removed from the analysis. Therefore, the results for winter in colder climates may not always represent the potential for soil erosion.

Seasonal mean storm precipitation total, storm duration, storm intensity, and storm maximum 15-min intensity examined in Part I, as well as I_{30}, KE, and EI statistics for each of the four seasons for each station, were input into a cluster analysis using Ward's method to identify regions with homogeneous seasonal cycles of storm characteristics (Part I). This resulted in nine spatially coherent clusters or zones across the conterminous United States. (Fig. 1). Stations in West Coast zones 8 and 9 are intermixed, with zone 8 predominantly at lower elevations and interior valleys and zone 9 at higher elevations. There are also two zone 8 enclaves in northern Idaho and near Phoenix, Arizona. For a more detailed map of zones 8 and 9, see Fig. 1 in Part I.

In addition to studying the seasonal mean erosional characteristics in each zone, the statistical distribution of storm characteristics is very useful for constructing storm time series to be used in erosion modeling. The probability density function (PDF) of each storm characteristic was determined by testing the fit of two equation families to the empirical probability bins for each season and zone and finding the most appropriate fit. The first equation that is used is the double exponential:

$$y = ae^{(-x/b)} + ce^{(-x/d)}. \tag{4}$$

The coefficients a, b, c, and d are fit using nonlinear regression procedures in TableCurve 2D (SYSTAT 2002). The second equation is a more general family of curves that can be derived from the transformed general form

$$\ln y = a + bx^{\beta}(\ln x)^{\beta_1} + cx^{\gamma}(\ln x)^{\gamma_1}. \tag{5}$$

Parameters β, β_1, γ, and γ_1 define the general form of the equation, and the coefficients a, b, and c are fit using linear regression procedures from TableCurve 2D (SYSTAT 2002). Examples of the fit of these curves to the data are presented in Part I. Because of the potential usefulness of these curves, an appendix has been created with the coefficients of the best-fit curve to each empirical distribution, and the range of data where the distribution fits well.

The storm characteristics were analyzed in two ways in the following section. The nonextreme events were analyzed by the mean values and fitted distributions, while the extreme events were characterized by the 10-yr storm. The mean for each storm characteristic was calculated by season for all of the storms recorded at all of the stations in each of the nine zones. Then, the

means were compared statistically with the Student's t test to determine both regions with similar characteristics by season, and seasons with similar characteristics by region.

The mean 10-yr storm for each zone and season was derived from the 10-yr storms that were calculated for each station within the zone. The station 10-yr storms were generated by fitting the two-parameter Gumbel distribution to the annual extreme series of the storm characteristic using L-moments software (Hosking 1991). The 10-yr interval was examined because of the programmatic importance of this return frequency that is specified in government soil erosion mitigation policies (e.g., Renard et al. 1997). The mean 10-yr return interval estimate and two standard error bounds were generated for each zone and season from the individual stations.

Trends in the three mean storm erosion characteristics for each zone were evaluated using linear regression with time. The input data were annual time series of 31 values for the period of 1972–2002, derived by computing the averages of all of the sites in each zone. Using the resulting regression equations, the change in each storm characteristic from 1972 to 2002 was calculated as the regression estimate for 2002, minus the regression estimate for 1972, divided by the 1972 estimate. This is then expressed as a percent change over the 31-yr period, giving an indication of the relative size of the change.

3. Results and discussion

a. Maximum 30-min precipitation intensity

The I_{30} of a storm is a useful indicator of the storm's intensity at its peak. The mean and 10-yr I_{30} values are shown in Table 1.The highest amounts occurred in all seasons in zone 1, the one closest to the Gulf of Mexico, which is a major source of atmospheric moisture for storms and the scene of frequent tropical storms. The values generally decrease when moving farther away from the Gulf of Mexico. The lowest values are in the interior west and West Coast. In general, the lowest values occurred in winter and the highest were in summer, except for zone 9 when the higher values were in winter.

The probability density functions (PDFs) of the I_{30} for all seasons and zones are shown in Fig. 2. The PDFs illustrate the response of I_{30} in the tails of the distributions as well as the central tendencies. There is a general pattern of higher intensities in summer, largely due to the convective nature of the storms during that season. Zones 4–6 are generally skewed toward less intense I_{30} amounts. In most cases the probabilities are similar for spring, summer, and fall, whereas winter is clearly different, because nonconvective precipitation processes tend to dominate. The largest difference among the seasons can be found in zone 6 in the northern United States.

b. Storm kinetic energy

The mean and 10-yr total KE of the falling precipitation (in MJ ha^{-1}) is shown in Table 2. In general, the largest values occurred in summer and fall, and the lowest were in winter in zones 1–7. Zones 8 and 9 had higher average values in winter, reflecting their West Coast maritime climate of wet winters and dry summers.

The PDFs of the average KE for all seasons and zones are shown in Fig. 3. In most cases, there are smaller differences between the seasons than in the PDFs for I_{30}. In the east, larger KE values are found in zones 1–3, with the distribution becoming more skewed toward smaller KE values in zones 4–7 as distance increases from the important moisture source of the Gulf

TABLE 1. Maximum I_{30} (mm h^{-1}) mean and 10-yr storm interval estimate bounded by 2 times the standard error, for each zone and season. Zones with the same superscript letter in a column are not significantly different at $\alpha = 0.05$, and zones with the same superscript number for a season in the same row are not significantly different at $\alpha = 0.05$.

	Mean				10-yr I_{30}			
Zone	Winter	Spring	Summer	Fall	Winter	Spring	Summer	Fall
1	11.07	14.52	16.19	14.03	57.5 ± 1.9	81.0 ± 2.1	93.3 ± 2.2	78.5 ± 2.0
2	8.61	12.47[1]	14.89	12.56[1]	41.2 ± 1.4	69.6 ± 1.4	80.6 ± 1.5	67.9 ± 1.5
3	6.55	11.27	12.99[a]	10.75	23.4 ± 2.5	61.2 ± 3.4	73.5 ± 2.8	58.6 ± 3.1
4	6.71	9.02	13.15[a]	9.66	26.3 ± 0.9	50.3 ± 1.2	74.2 ± 1.1	52.2 ± 1.0
5	5.62	7.66	12.33	8.00	15.5 ± 0.7	43.4 ± 1.0	71.9 ± 0.9	43.9 ± 0.8
6	5.41	6.39	9.98	7.03	16.3 ± 0.6	30.9 ± 0.9	57.4 ± 1.1	36.0 ± 0.9
7	5.28	5.83	8.43	6.06	10.2 ± 0.5	21.3 ± 0.8	43.2 ± 1.6	22.5 ± 0.9
8	5.99	5.71	6.64	6.18	21.1 ± 1.2	19.1 ± 0.8	23.5 ± 1.9	21.5 ± 1.0
9	6.66	6.00	6.51	6.74	25.6 ± 1.3	21.0 ± 1.0	20.6 ± 2.0	24.2 ± 1.2

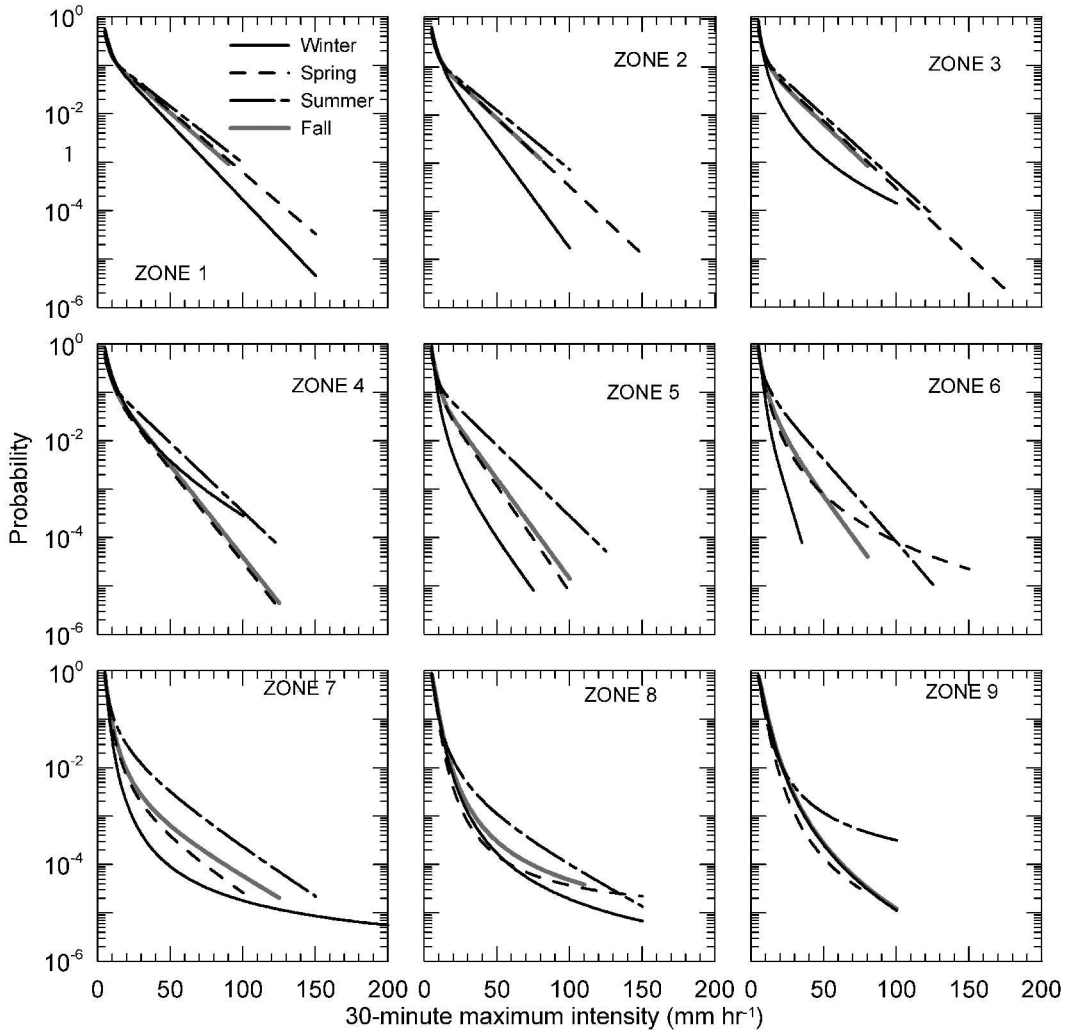

FIG. 2. Maximum I_{30} probability density distributions for all nine zones and four seasons.

TABLE 2. The KE (MJ ha^{-1}) mean and 10-yr storm interval estimate bounded by 2 times the standard error for each zone and season. Zones with the same superscript letter in a column are not significantly different at $\alpha = 0.05$, and zones with the same superscript number for a season in the same row are not significantly different at $\alpha = 0.05$.

	Mean				10-yr KE			
Zone	Winter	Spring	Summer	Fall	Winter	Spring	Summer	Fall
1	3.46[a]	3.89	3.20	3.64	25.7 ± 1.1	30.8 ± 1.4	27.3 ± 1.0	31.4 ± 1.2
2	2.78	3.23	3.08	3.50	20.0 ± 0.7	24.4 ± 0.6	23.2 ± 0.6	27.0 ± 0.8
3	1.54	2.39[a]	2.69[a,1]	2.63[1]	9.6 ± 1.1	16.8 ± 1.3	21.3 ± 1.2	19.8 ± 1.4
4	2.18	2.44[a]	2.81	2.85	14.8 ± 0.5	18.6 ± 0.4	22.1 ± 0.4	21.9 ± 0.5
5	1.33	1.90	2.63[a]	2.07	8.3 ± 0.4	14.3 ± 0.4	20.8 ± 0.4	15.6 ± 0.4
6	1.44	1.71	2.19	1.99[a]	10.2 ± 0.4	12.4 ± 0.4	17.3 ± 0.4	15.8 ± 0.5
7	1.09	1.21	1.56	1.33	5.5 ± 0.4	8.3 ± 0.3	10.9 ± 0.4	8.6 ± 0.4
8	2.22	1.54	1.38	2.00[a]	20.3 ± 1.8	13.1 ± 1.0	7.7 ± 0.6	15.3 ± 1.2
9	3.53[a]	2.21	1.62	3.00	31.4 ± 2.1	19.2 ± 1.3	9.0 ± 0.7	22.2 ± 1.5

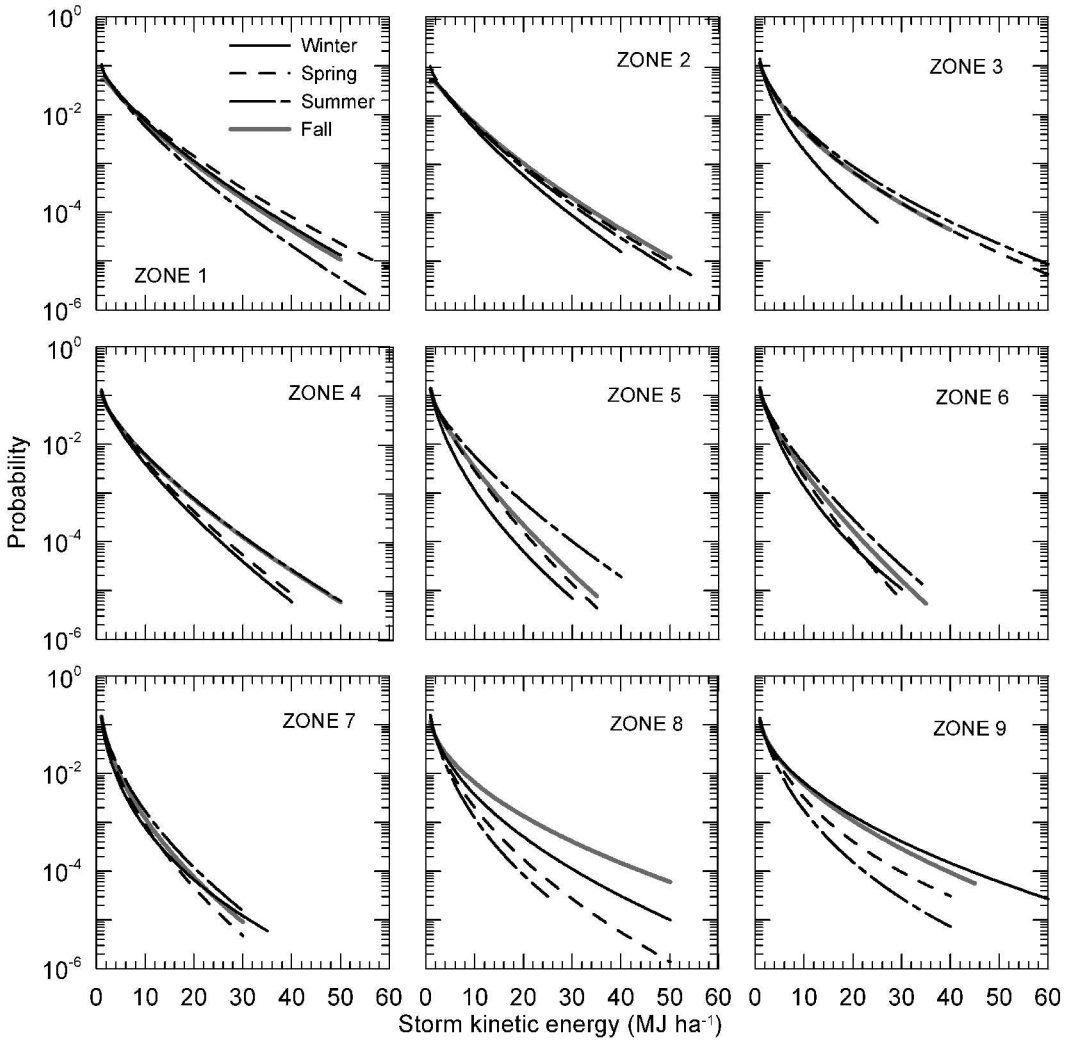

FIG. 3. The KE probability density distributions for all nine zones and four seasons.

of Mexico. In zones 1–5, summer and fall tend to have higher KE values; winter and fall are more dominant in zones 6–9.

c. Storm erosivity index

The mean and 10-yr EI (MJ mm ha^{-1} h^{-1}) is the result of multiplying the I_{30} by the KE (Table 3) and is considered to be highly correlated to rainfall erosivity (Wischmeier and Smith 1978). Spring values were slightly higher in zone 1, and summer was highest in zones 2–7. Only zones 8 and 9 had the highest values in winter.

The PDFs for EI are shown in Fig. 4. In zones 1–3, the differences between the seasons are relatively small. In zones 4–7, the differences between seasons become greater, with summer producing the highest numbers and winter producing the smallest numbers. In zones 8 and 9, the roles reverse, with summer contributing to lower amounts while fall and winter play a larger role.

The spatial patterns of storm characteristics were generally coherent. High values along the Gulf of Mexico reflect the influence of the Gulf as a source of moisture in all seasons. The influence of this moisture source region decreased away from the coast. The seasonal patterns of storm characteristics were also similar with warm season precipitation events having the largest magnitudes for all three storm erosion characteristics. The exception to this was the West Coast (zones 8 and 9), where winter events were more energetic. Most of this area is known for a West Coast maritime climate with wet winters and a dry, warm summer season. Storm erosion characteristics were lowest in magnitude in zone 7 in all seasons except summer, when zones 8 and 9 were the lowest. Zone 7 is the interior west and

TABLE 3. The EI (MJ mm ha^{-1} h^{-1}) mean and 10-yr storm interval estimate bounded by 2 times the standard error, for each zone and season. Zones with the same superscript letter in a column are not significantly different at $\alpha = 0.05$, and zones with the same superscript number for a season in the same row are not significantly different at $\alpha = 0.05$.

	Mean				10-yr EI			
Zone	Winter	Spring	Summer	Fall	Winter	Spring	Summer	Fall
1	77.3	127.1	117.1[1]	115.3[1]	1201.2 ± 81.8	2097.3 ± 146.7	2067.9 ± 100.4	1934.9 ± 111.9
2	45.3	85.9	103.7	96.8	668.5 ± 39.5	1396.5 ± 55.1	1588.8 ± 68.7	1482.0 ± 74.5
3	18.8[a]	63.6[1]	83.4	67.5	225.2 ± 44.2	939.8 ± 122.0	1376.2 ± 132.9	1026.4 ± 133.4
4	23.9	42.1	80.8	56.2	334.8 ± 23.2	758.0 ± 35.5	1371.3 ± 44.0	929.3 ± 42.1
5	10.5	26.6	71.2	32.1	129.8 ± 14.9	526.7 ± 25.3	1272.7 ± 37.1	583.9 ± 27.0
6	9.9	16.3	43.1	23.6	139.0 ± 10.6	288.9 ± 15.9	807.6 ± 35.3	433.7 ± 23.9
7	7.3	10.5	28.6[a]	13.0	61.7 ± 8.1	159.5 ± 12.4	480.5 ± 33.9	185.5 ± 17.0
8	19.6[a]	11.6	14.9	18.0	335.9 ± 47.3	190.4 ± 19.2	165.2 ± 23.9	253.1 ± 29.5
9	38.8	19.8	17.5[a]	32.1[a]	629.9 ± 62.5	322.6 ± 37.2	177.6 ± 36.7	422.9 ± 38.7

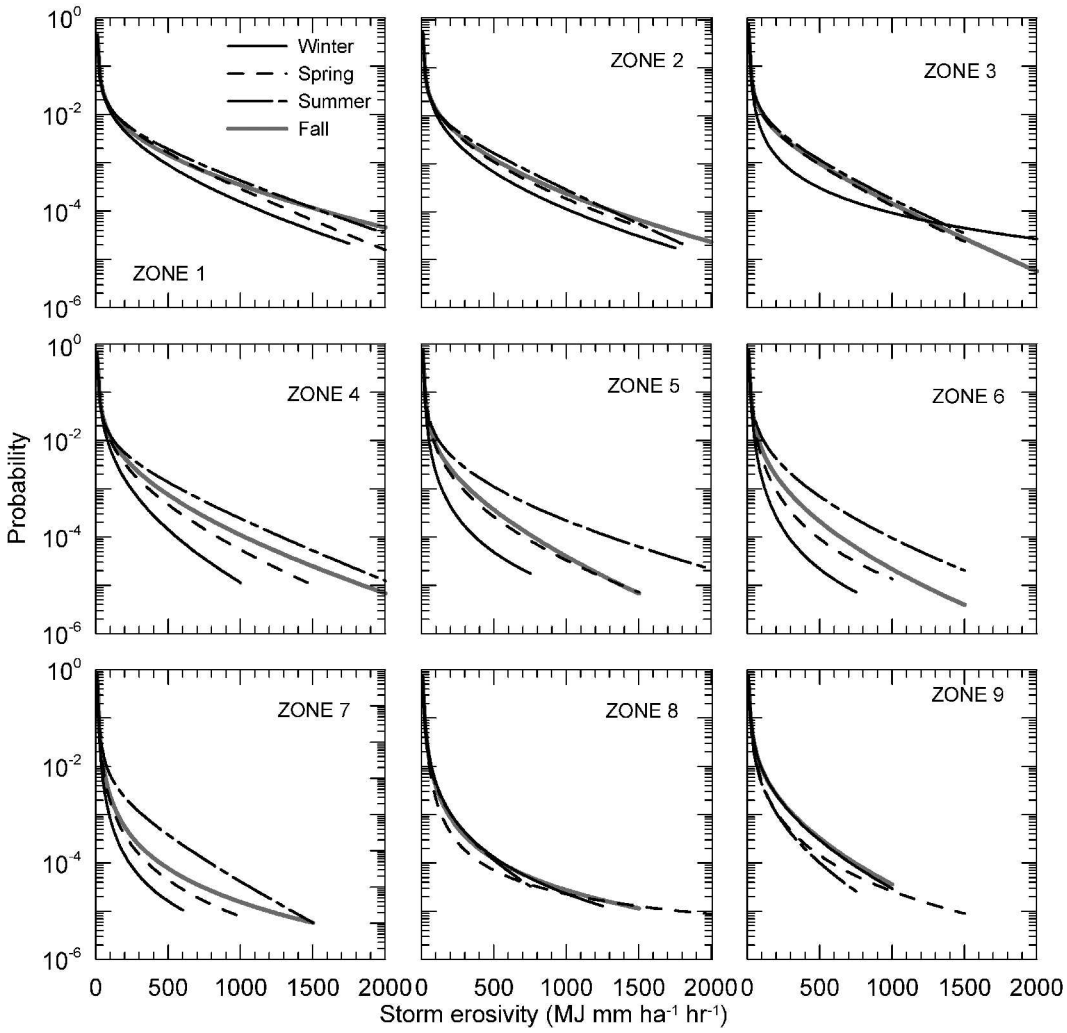

FIG. 4. The EI probability density distributions for all nine zones and four seasons.

the Great Plains—an area known for being the driest in the United States in all seasons. These storm erosion characteristic patterns are explained by the seasonal water availability from source regions, the atmospheric water vapor capacity (a function of temperature), and predominant precipitation mechanisms (convective or stratiform).

d. Trends in mean storm erosion characteristics

The results of the trend analysis of mean storm characteristics are summarized in Table 4. Mean I_{30} increased across zones 1–5 during the winter, decreased in zones 1–3 in spring and summer, and increased in zones 4–8 in spring and summer. Zone 3 winters experienced the largest percent increase during the study period, 19.5%. The three zones closest to the Gulf of Mexico showed evidence of decreasing I_{30} amounts in spring, and to a lesser extent in summer. During spring and summer, generally small increases were found in zones 4–8. Fall showed the least spatial coherence of the four seasons with little or no changes over time, except in zone 1. Zone 4 showed upward trends in all four seasons, although only the winter trend shows any statistical significance. Along the West Coast, zone 8 showed small increases in all seasons, while at the higher elevations zone 9 showed decreases in all seasons.

Mean KE (Table 4) is strongly related to storm total precipitation (Part I) as shown in Eq. (1). Eastern U.S. zones 1–5 show increasing trends in mean KE during winter, while zones 6–9 show decreases. The far southern zones 1 and 2 reverse this signal with decreasing trends in mean KE during the spring, as do zones 7–9 in the West. Summer and fall have quite varied trends across the conterminous United States. Zone 4 in the Midwest shows fairly consistent positive trends in mean KE in all seasons, although they are strongest in the winter. Meanwhile, zone 9 shows fairly large decreases in mean KE in all four seasons.

The high-elevation zone 9 is easy to analyze for mean EI trends, because both component parts—mean I_{30} and mean KE—trend negatively in every season. Therefore, mean EI trends are strongly negative in zone 9, ranging from −2.7% in fall to −26.6% during summer. With similar reasoning, zone 4 shows consistent increases across all four seasons and all three storm characteristics. Zones 1–5 also showed increases in EI in winter, as did zones 1, 3, and 4 in fall. Increasing EI trends are also apparent in zones 5–7 during spring and summer. Zone 5 encompasses the Corn Belt, and so the 26.0%, 10.2%, and 8.3% increases in storm erosivity index during winter, spring, and summer, respectively, could lead to significant impacts to agriculture and water quality. Because farm fields are less likely to be covered during these seasons, increased erosion could result. As noted in section 2, the Fischer–Porter gauge does collect snow events and, therefore, may not entirely reflect the potential for soil erosion during winter months.

The zones and seasons with consistently strong trends for all three mean storm characteristics include fall in zone 1, with large increases in I_{30} and KE leading to a 42.8% increase in EI (Fig. 5a) from 1972 to 2002 (94–135 MJ mm ha^{-1} h^{-1}, respectively). The same is true for winter in zone 3, with a 69.1% increase in mean EI (Fig. 5b) from 1972 to 2002 (from 13 to 22 MJ mm

TABLE 4. Trends in mean storm characteristics from 1972 to 2002 expressed as a percent change over the entire period. Entries marked with ** are significant at the $p = 0.05$ level, and those marked with * are significant at the $p = 0.10$ level.

Zone	1	2	3	4	5	6	7	8	9
				Max 30-min precipitation intensity					
Winter	2.3	5.2	19.5**	7.4*	4.6	−1.6	0.2	3.5	−1.0
Spring	−7.8	−7.1	−2.4	1.7	2.7	2.6	1.7	2.6	−1.8
Summer	−0.1	−6.5**	−0.1	0.4	3.2	0.7	6.1**	0.8	−5.2*
Fall	6.9*	−0.5	4.6	0.7	−1.4	−0.3	−0.3	0.7	−1.8
				Storm kinetic energy					
Winter	0.1	8.0	30.4**	9.8	16.3*	−12.7	−13.7*	−1.3	−12.6
Spring	−10.7	−11.3*	1.3	0.9	5.1	2.4	−3.7	−5.3	−14.0*
Summer	1.5	−3.8	−3.3	1.4	1.4	−2.4	4.1**	−1.1	−13.4*
Fall	23.8**	−1.7	0.7	2.7	−2.5	−2.9	−10.9**	5.0	−2.2
				Storm erosivity index					
Winter	5.1	15.7	69.1**	20.8	26.0	−17.4	−14.9**	7.2	−13.5
Spring	−18.9	−17.0	3.8	3.2	10.2	7.1	1.3	−1.5	−18.9
Summer	4.8	−10.4*	−6.0	2.1	8.3	0.5	17.0**	−0.2	−26.6**
Fall	42.8**	0.0	13.4	4.6	−5.6	1.5	−9.8	7.9	−2.7

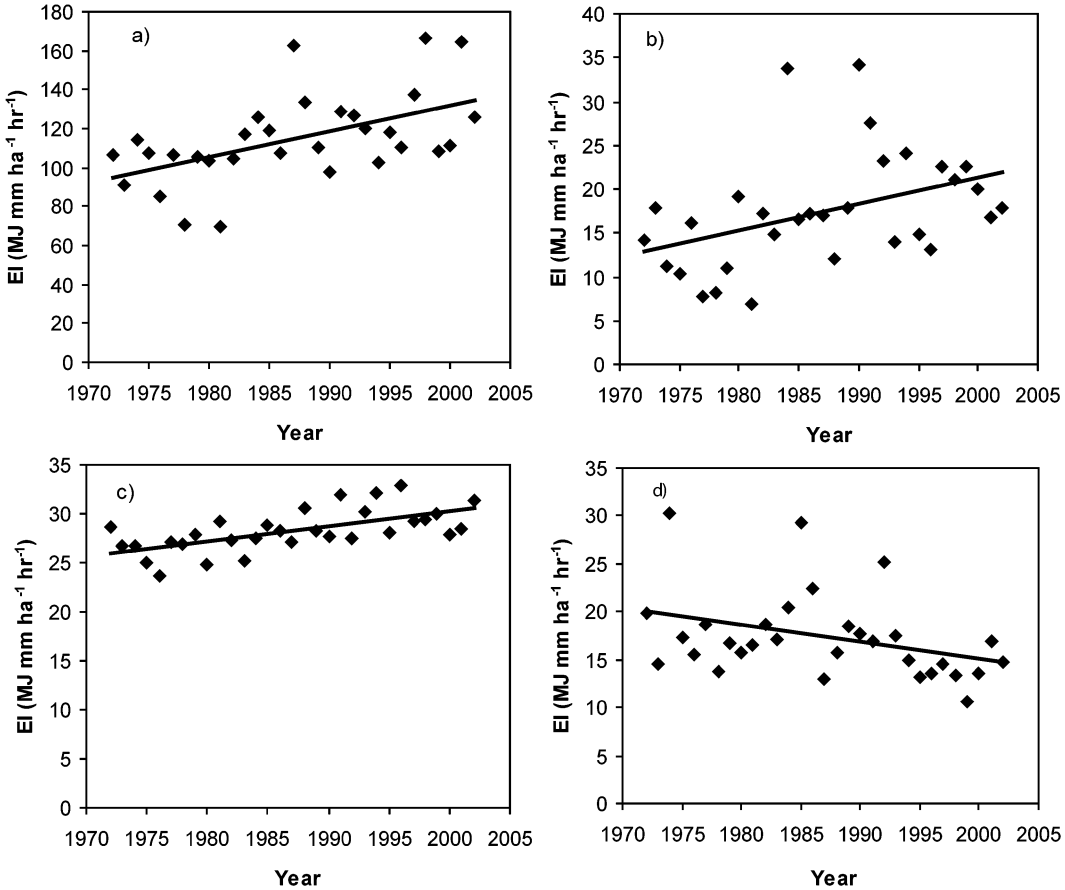

FIG. 5. Selected statistically significant trends in EI for (a) fall in zone 1, (b) winter in zone 3, (c) summer in zone 7, and (d) summer in zone 9.

ha^{-1} h^{-1}). To the west, summer in zone 7 shows increases in all three mean storm characteristics (Fig. 5c), while zone 9 shows strong decreases (Fig. 5d). The resulting changes in EI are significant—a 17% increase for zone 7 in the summer and a 26.6% decrease in zone 9 in the summer.

4. Summary and conclusions

The objective of this work was to provide a unique study of the spatial distribution and time trends of the soil erosion characteristics of individual storms, as opposed to daily or monthly precipitation, including the maximum 30-min precipitation intensity (I_{30}), storm kinetic energy (KE), and the storm erosivity index (EI). This is the first time that such an extensive climatology of soil erosion characteristics of storms in the United States has been produced.

Erosional characteristics for each of the four traditional seasons of spring (March–April–May), summer (June–July–August), fall (September–October–November), and winter (December–January–February) were examined. The storm soil erosion characteristics were computed using the NCDC 15-min precipitation database. Because of the challenges in the spatial distribution, length of record, and quality of individual stations, the storm characteristics were aggregated by zones derived from a cluster analysis to create more robust spatial and temporal patterns and to allow for the use of standard statistical testing.

The highest mean I_{30}, KE, and EI values occurred in all seasons in the southeastern United States, while the lowest occurred predominantly in the interior west. The lowest mean I_{30}, KE, and EI values typically occurred in winter, while the highest occurred in summer. The exception to this was along the West Coast, where winter storms exhibited the largest mean KE and EI values. Storm erosion characteristics were lowest in magnitude in zone 7 in all seasons except summer, when zones 8 and 9 were lowest. These storm erosion characteristic patterns are explained by the underlying physical processes that are present during the seasons.

Trends in mean storm characteristics for each zone were evaluated using linear regression. Because EI is the product of I_{30} and KE, the trends in those two parameters are reflected in EI. Previous research mentioned in section 2 has shown that EI is closely related to soil erosion. Zone 9 showed downward trends in all four seasons, while zone 4 showed upward trends in all four seasons. Mean EI increased through most of zones 1–5 in fall and winter, a time when fallow farm fields may be more vulnerable to soil erosion. Meanwhile, increasing trends in mean EI are evident for spring and summer in zones 5–7. Further examination of the physical processes driving these changes is warranted because they may lead to insights on potential future changes.

This study shows that the storm characteristics related to soil erosion (I_{30}, KE, and EI) reflect the underlying processes that also drive total precipitation, processes such as orographic features and proximity to oceans, especially the warm Gulf of Mexico. More challenging for U.S. conservation policy and practices are the significant changes in storm erosivity characteristics that have occurred during the period of 1972–2002. As a result, some portions of the country, for example, the Corn Belt located in zone 5, may be more vulnerable to soil erosion over the course of the 31-yr study period.

In addition to long-term climate variability and change, preliminary research by Palecki et al. (2002) suggests that storm characteristics are sensitive to large-scale interannual climate variability, for example, with the Pacific decadal oscillation (PDO). A further examination of the impacts of climate variability issues related to storm soil erosion characteristics is currently underway, including the influence of El Niño–Southern Oscillation events. The 31-yr record used in this study is too short to determine if the noted changes in storm

TABLE A1. Parameters for I_{30} (mm h^{-1}) valid for $5.08 < X \leq X$ max.

Zone	Season	Equation No.	a	b	c	d	β	β_1	γ	γ_1	X max
1	Winter	(4)	0.2330	13.5513	2.6383	2.7446	—	—	—	—	150
1	Spring	(4)	0.2143	17.1111	2.7738	2.3960	—	—	—	—	150
1	Summer	(4)	0.2115	18.5737	3.8609	1.9868	—	—	—	—	100
1	Fall	(4)	0.2204	16.4704	3.0699	2.3208	—	—	—	—	90
2	Winter	(4)	0.2418	10.4794	3.2609	2.7551	—	—	—	—	100
2	Spring	(4)	0.2203	15.3935	2.5227	2.6592	—	—	—	—	150
2	Summer	(4)	0.2143	17.6594	3.2439	2.1978	—	—	—	—	100
2	Fall	(4)	0.2193	15.4265	2.6582	2.5977	—	—	—	—	80
3	Winter	(5)	−1.6503	−0.3453	12.0889	—	0.0	2.0	−1.0	0.0	100
3	Spring	(4)	0.1734	15.6311	3.9561	2.4130	—	—	—	—	175
3	Summer	(4)	0.2128	15.9223	4.2545	2.1311	—	—	—	—	125
3	Fall	(5)	−2.9938	−0.0121	13.3819	—	1.0	1.0	−1.0	0.0	80
4	Winter	(4)	3.1009	−0.1609	−1.6875	—	1.0	−1.0	0.0	1.0	100
4	Spring	(4)	0.2105	11.3351	3.1175	2.8422	—	—	—	—	125
4	Summer	(4)	0.2414	15.2744	3.3806	2.2319	—	—	—	—	125
4	Fall	(4)	0.2489	11.4464	3.2582	2.6292	—	—	—	—	125
5	Winter	(5)	−3.2728	−0.4796	10.0222	—	0.0	2.0	−0.5	0.0	75
5	Spring	(4)	0.1802	9.9312	5.0738	2.4484	—	—	—	—	100
5	Summer	(4)	0.2291	14.9250	3.5074	2.3050	—	—	—	—	125
5	Fall	(4)	0.1860	10.5529	5.2869	2.3462	—	—	—	—	100
6	Winter	(4)	0.2507	4.3488	19.8545	1.6111	—	—	—	—	35
6	Spring	(5)	5.5431	−3.2417	−7.4026	—	0.0	1.0	−2.0	1.0	150
6	Summer	(5)	−4.0077	−0.0135	8.1714	—	1.0	1.0	−0.5	0.0	125
6	Fall	(5)	−5.3895	−0.0160	16.4730	—	1.0	1.0	−1.0	1.0	80
7	Winter	(5)	−14.9460	40.4600	−48.4418	—	−0.5	0.0	−2.0	1.0	200
7	Spring	(4)	−8.5420	−0.0070	26.5452	—	1.0	1.0	−1.0	1.0	100
7	Summer	(4)	−5.2372	−0.0428	11.5857	—	1.0	0.0	−0.5	0.0	150
7	Fall	(5)	−8.1429	−0.0060	25.2164	—	1.0	1.0	−1.0	1.0	125
8	Winter	(5)	−17.1216	64.8168	−71.1422	—	−0.5	0.0	−1.0	0.0	150
8	Spring	(5)	−11.8565	183.7634	−387.8300	—	−1.0	0.0	−2.0	1.0	150
8	Summer	(5)	−6.7061	−0.0346	20.9438	—	1.0	0.0	−1.0	1.0	150
8	Fall	(5)	−14.6257	47.2730	−103.5289	—	−0.5	0.0	−2.0	1.0	110
9	Winter	(5)	9.6406	−4.5609	−39.4069	—	0.0	1.0	−2.0	1.0	100
9	Spring	(5)	−26.3340	69.8979	−268.1261	—	−1.0	0.0	−2.0	1.0	75
9	Summer	(5)	−11.3187	32.9165	−55.0684	—	−0.5	0.0	−2.0	1.0	100
9	Fall	(5)	9.7045	−4.5583	−40.6869	—	0.0	1.0	−2.0	1.0	100

TABLE A2. The KE (MJ ha^{-1}) valid for $1.0 < X \leq X$ max.

Zone	Season	Equation No.	a	b	c	d	β	β_1	γ	γ_1	X max
1	Winter	(5)	−2.6089	−0.3120	0.3457	—	0.5	1.0	−2.0	0.0	50
1	Spring	(5)	−2.6811	−0.2893	0.3599	—	0.5	1.0	−2.0	0.0	70
1	Summer	(5)	−2.5687	−0.3257	0.3427	—	0.5	1.0	−2.0	0.0	55
1	Fall	(5)	−2.6224	−0.3190	−0.3561	—	0.5	1.0	−2.0	0.0	50
2	Winter	(5)	−2.5176	−0.3658	−0.3454	—	0.5	1.0	−2.0	0.0	40
2	Spring	(5)	−2.5851	−0.3247	0.3465	—	0.5	1.0	−2.0	0.0	55
2	Summer	(5)	−2.5664	−0.3358	0.3476	—	0.5	1.0	−2.0	0.0	50
2	Fall	(5)	−2.6437	−0.3138	0.3654	—	0.5	1.0	−2.0	0.0	50
3	Winter	(5)	−0.4043	−1.8560	0.2825	—	0.5	0.0	−2.0	0.0	25
3	Spring	(5)	−0.6931	−1.4768	−0.3345	—	0.5	0.0	−2.0	1.0	60
3	Summer	(5)	−0.7624	−1.4106	−0.3156	—	0.5	0.0	−2.0	1.0	60
3	Fall	(5)	−0.6984	−1.4772	−0.3298	—	0.5	0.0	−2.0	1.0	40
4	Winter	(5)	−2.5906	−0.4053	0.5512	—	0.5	1.0	−1.5	0.0	40
4	Spring	(5)	−2.5110	−0.3930	0.4824	—	0.5	1.0	−1.5	0.0	40
4	Summer	(5)	−2.6354	−0.3386	0.5217	—	0.5	1.0	−1.5	0.0	50
4	Fall	(5)	−2.6607	−0.3397	0.5387	—	0.5	1.0	−1.5	0.0	50
5	Winter	(5)	0.1740	−2.2012	−0.3100	—	0.5	0.0	−2.0	1.0	30
5	Spring	(5)	−2.4688	−0.4690	0.5078	—	0.5	1.0	−1.5	0.0	35
5	Summer	(5)	−2.6140	−0.3534	0.5228	—	0.5	1.0	−1.5	0.0	40
5	Fall	(5)	−2.5411	−0.4385	−0.5357	—	0.5	1.0	−1.5	1.0	35
6	Winter	(5)	−2.0476	−0.7982	−1.3316	—	0.0	2.0	−1.0	1.0	30
6	Spring	(5)	−2.4334	−0.5119	0.5052	—	0.5	1.0	−1.5	0.0	30
6	Summer	(5)	−2.4631	−0.4235	0.4755	—	0.5	1.0	−1.5	0.0	35
6	Fall	(5)	−2.5823	−0.4541	0.5353	—	0.5	1.0	−1.5	0.0	35
7	Winter	(5)	−3.9340	−0.6435	1.9206	—	0.0	2.0	−1.0	0.0	35
7	Spring	(5)	0.1018	−2.2541	0.2445	—	0.5	0.0	−2.0	0.0	30
7	Summer	(5)	0.0461	−2.0284	−0.2727	—	0.5	0.0	−2.0	1.0	30
7	Fall	(5)	−0.0622	−2.1077	0.2505	—	0.5	0.0	−2.0	0.0	30
8	Winter	(5)	−0.8405	−1.5086	0.3945	—	0.5	0.0	−1.5	0.0	50
8	Spring	(5)	−0.3479	−1.8569	0.3519	—	0.5	0.0	−1.5	0.0	30
8	Summer	(5)	−2.8672	−0.7286	0.9280	—	0.0	2.0	−1.5	0.0	25
8	Fall	(5)	−2.7301	−0.6215	0.7931	—	0.0	2.0	−1.5	0.0	50
9	Winter	(5)	−1.2464	−1.1972	0.2813	—	0.5	0.0	−2.0	0.0	70
9	Spring	(5)	−2.8244	−0.5556	0.8152	—	0.0	2.0	−1.5	0.0	40
9	Summer	(5)	−2.8734	−0.6582	0.9004	—	0.0	2.0	−1.5	0.0	40
9	Fall	(5)	−0.7624	−1.3369	−0.5617	—	0.5	0.0	−1.0	1.0	45

erosion characteristics are part of long-term climate change or are driven by slow oscillations in teleconnection patterns, such as PDO. However, these results suggest that the changes in the risk of soil erosion are large enough over time that climate change and variability must be actively built into soil conservation policy and practices. One way of doing this is to immediately and regularly update the climatic parameters in critical conservation planning tools and to continue to do so to reflect current climate conditions as suggested by the Soil and Water Conservation Society (2003).

Acknowledgments. This work was supported by Cooperative Agreement AG 68-7482-7-306 between the National Water and Climate Center (NWCC) of the U.S. Department of Agriculture Natural Resources Conservation Service (USDA-NRCS); and National Oceanic and Atmospheric Administration (NOAA) Cooperative Agreement NA67RJ0146. The constructive comments of and discussions with Greg Johnson are greatly appreciated. Dan Wilks provided valuable insight on fitting probability density functions to the storm characteristics. The views expressed herein are those of the authors and do not necessarily reflect those of the USDA-NRCS NWCC, NOAA, or the ISWS.

APPENDIX

Coefficients of PDF Curves by Zone and Season

In Tables A1–A3, the equations that best fit the probability distribution for each variable, season, and zone are identified as either Eq. (4) or Eq. (5) (see section 2). The appropriate parameters are identified for cases utilizing Eq. (5), and the regression coeffi-

TABLE A3. The EI (MJ mm ha^{-1} h^{-1}) valid for $10.0 < X \leq X$ max.

Zone	Season	Equation no.	a	b	c	d	β	β_1	γ	γ_1	X max
1	Winter	(5)	−6.3720	−0.0196	13.0117	—	0.5	1.0	0.0	−1.0	1750
1	Spring	(5)	−6.8382	−0.0231	14.1311	—	1.0	−1.0	0.0	−1.0	2000
1	Summer	(5)	−5.2626	−0.0203	14.3829	—	1.0	−1.0	−0.5	0.0	2250
1	Fall	(5)	−6.6006	−0.0153	13.7029	—	0.5	1.0	0.0	−1.0	2000
2	Winter	(5)	−5.5519	−0.1692	12.6588	—	0.5	0.0	0.0	−1.0	1750
2	Spring	(5)	−2.6590	−0.1880	25.2965	—	0.5	0.0	−1.0	0.0	1500
2	Summer	(5)	−5.5244	−0.0031	15.1712	—	1.0	0.0	−0.5	0.0	1800
2	Fall	(5)	−2.7913	−0.1762	26.2597	—	0.5	0.0	−1.0	0.0	2000
3	Winter	(5)	−6.7243	−0.1026	16.0673	—	0.0	2.0	0.0	−1.0	5000
3	Spring	(5)	−7.4915	−0.0263	16.2403	—	1.0	−1.0	0.0	−1.0	1500
3	Summer	(5)	−7.2078	−0.0252	15.3763	—	1.0	−1.0	0.0	−1.0	1500
3	Fall	(5)	−7.5081	−0.0255	16.2806	—	1.0	−1.0	0.0	−1.0	2000
4	Winter	(5)	−3.7411	−0.2543	12.9288	—	0.5	0.0	−0.5	0.0	1000
4	Spring	(5)	−4.8380	−0.0248	14.0378	—	0.5	1.0	−0.5	0.0	1500
4	Summer	(5)	−5.3400	−0.0239	14.9859	—	1.0	−1.0	−0.5	0.0	2000
4	Fall	(5)	−6.4222	−0.0214	13.7270	—	0.5	1.0	0.0	−1.0	2000
5	Winter	(5)	−3.9867	−0.1710	14.7318	—	0.0	2.0	−0.5	0.0	750
5	Spring	(5)	−4.3351	−0.2034	14.3340	—	0.5	0.0	−0.5	0.0	1500
5	Summer	(5)	−6.6372	−0.0175	14.0617	—	0.5	1.0	0.0	−1.0	3000
5	Fall	(5)	−4.4247	−0.0267	18.0516	—	0.5	1.0	−1.0	1.0	1500
6	Winter	(5)	6.1535	−2.7160	−17.3400	—	0.0	1.0	−2.0	0.0	750
6	Spring	(5)	−3.1782	−0.1950	8.8214	—	0.0	2.0	0.0	−1.0	1000
6	Summer	(5)	−6.3981	−0.0222	13.7727	—	0.5	1.0	0.0	−1.0	1500
6	Fall	(5)	−3.3774	−0.2361	16.0393	—	0.5	0.0	−1.0	1.0	1500
7	Winter	(5)	2.8184	−2.2462	9.5672	—	0.0	1.0	−1.0	1.0	600
7	Spring	(5)	−3.2175	−0.1815	17.2074	—	0.0	2.0	−1.0	1.0	1000
7	Summer	(5)	−6.2446	−0.0307	18.9928	—	1.0	−1.0	−0.5	0.0	1500
7	Fall	(5)	−3.2674	−0.1659	16.9335	—	0.0	2.0	−1.0	1.0	1500
8	Winter	(5)	−1.9591	−0.1841	11.0053	—	0.0	2.0	−1.0	1.0	1250
8	Spring	(5)	−21.7958	77.6075	−122.0520	—	0.0	−1.0	−1.0	0.0	2000
8	Summer	(5)	−4.0220	−0.2359	19.4217	—	0.5	0.0	−1.0	1.0	750
8	Fall	(5)	4.2909	−2.1412	0.5589	—	0.0	1.0	−1.0	0.0	1500
9	Winter	(5)	−2.8873	−0.2412	13.3532	—	0.5	0.0	−1.0	1.0	1000
9	Spring	(5)	−1.9545	−0.1817	10.8936	—	0.0	2.0	−1.0	1.0	1500
9	Summer	(5)	−3.6591	−0.2574	17.9971	—	0.5	0.0	−1.0	1.0	750
9	Fall	(5)	−3.0510	−0.2301	14.0494	—	0.5	0.0	−1.0	1.0	1500

cients for the best fit of an analytical curve to the empirical PDF are given for all of the equations.

REFERENCES

Barauah, P. C., 1973: An investigation of drop size distribution of rainfall in Thailand. M.S. thesis No. 528, Asian Institute of Technology.

Brown, L. C., and G. R. Foster, 1987: Storm erosivity using idealized intensity distributions. *Trans. Amer. Soc. Agric. Eng.,* **30,** 379–386.

Carter, C. E., J. D. Greer, H. J. Braud, and J. M. Floyd, 1974: Raindrop characteristics in south central United States. *Trans. ASAE,* **17,** 1033–1037.

Groisman, P. Y., and D. R. Legates, 1994: The accuracy of United States precipitation data. *Bull. Amer. Meteor. Soc.,* **75,** 215–228.

——, R. W. Knight, T. R. Karl, D. R. Easterling, B. Sun, and J. Lawrimore, 2004: Contemporary changes of the hydrological cycle over the contiguous United States: Trends derived from in situ observations. *J. Hydrometeor.,* **5,** 64–85.

Hammer, G., 1998: Data documentation for 15-minute precipitation data TD-3260. National Climatic Data Center, 21 pp.

Hollinger, S. E., J. R. Angel, and M. A. Palecki, 2002: Spatial distribution, variation, and trends in storm precipitation characteristics associated with soil erosion in the United States. Illinois State Water Survey Contract Rep. 2002-08, 90 pp. [Available online at http://www.sws.uiuc.edu/pubdoc/CR/ISWSCR2002-08.pdf.]

Hosking, J. R. M., 1991: FORTRAN routines for using the method of *L*-moments. T. J. Watson Research Center IBM Research Rep. RC17097, 177 pp.

Hudson, N. W., 1963: Raindrop size distribution in high intensity storms. *Rhod. J. Agric. Res.,* **1,** 6–11.

Huff, F. A., 1967: Time distribution of rainfall in heavy storms. *Water Resour. Res.,* **3,** 1007–1019.

Kinnell, P. I. A., 1980: Rainfall intensity—Kinetic energy relationships for soil loss prediction. *Soil Sci. Soc. Amer. Proc.,* **45,** 153–155.

McGregor, K. C., R. L. Binger, A. J. Bowie, and G. R. Foster, 1995: Erosivity index values for northern Mississippi. *Trans. Amer. Soc. Agric. Eng.,* **38,** 1039–1047.

Nearing, M. A., 2001: Potential changes in rainfall erosivity in the United States with climate change during the 21st century. *J. Soil Water Conserv.,* **56,** 229–232.

——, F. F. Pruski, and M. R. O'Neal, 2004: Expected climate change impacts on soil erosion rates: A review. *J. Soil Water Conserv.,* **59,** 43–50.

Oldeman, L. R., 1994: The global extent of land degradation. *Land Resilience and Sustainable Land Use*, D. J. Greenland and I. Szabolcs, Eds., Wallingford, 99–118.

Palecki, M. A., J. R. Angel, and S. E. Hollinger, 2002: Interannual variability in storm structure in the United States. Preprints, *13th Conf. on Applied Climatology*, Portland, OR, Amer. Meteor. Soc., 87–91.

——, ——, and ——, 2005: Storm precipitation in the United States. Part I: Meteorological characteristics. *J. Appl. Meteor.,* **44,** 933–946.

Pimental, D., and Coauthors, 1995: Environmental and economic costs of soil erosion and conservation benefits. *Science,* **267,** 1117–1123.

Pruski, F. F., and M. A. Nearing, 2002: Climate-induced changes in erosion during the 21st century for eight U.S. locations. *Water Resour. Res.,* **38,** 1298, doi:10.1029/2001WR000493.

Renard, K. G., and J. R. Freimund, 1994: Using monthly precipitation data to estimate the *R*-factor in the revised USLE. *J. Hydrol.,* **157,** 287–306.

——, G. R. Foster, G. A. Weesies, D. K. McCool, and D. C. Yoder, 1997: Predicting soil erosion by water: A guide to conservation planning with the Revised Soil Loss Equation (RUSLE). U.S. Department of Agriculture, Agriculture Handbook 703, 404 pp.

Rosewell, C. J., 1986: Rainfall kinetic energy in Eastern Australia. *J. Climate Appl. Meteor.,* **25,** 1695–1701.

Soil and Water Conservation Society, 2003: Conservation implications of climate change: Soil erosion and runoff from cropland. SWCS Rep., 24 pp. [Available online at http://www.swcs.org/.]

SYSTAT, 2002: TableCurve 2D 5.01 for Windows user's manual. SYSTAT Software, Inc., 672 pp.

Uijlenhoet, R., and J. N. M. Stricker, 1999: A consistent rainfall parameterization based on the exponential raindrop size distribution. *J. Hydrol.,* **218,** 101–127.

van Dijk, A. I. J. M., L. A. Bruijnzeel, and C. J. Rosewell, 2002: Rainfall intensity—Kinetic energy relationships: A critical literature appraisal. *J. Hydrol.,* **261,** 1–23.

Wischmeier, W. H., and D. D. Smith, 1958: Rainfall energy and its relationship to soil loss. *Trans. Amer. Geophys. Union,* **39,** 285–291.

——, and ——, 1978: Predicting rainfall erosion losses—A guide to conservation planning. U.S. Department of Agriculture, Agriculture Handbook 537, 58 pp.

EXHIBIT 412

DIVISION S-5—PEDOLOGY

Pedogenesis of Vesicular Horizons, Cima Volcanic Field, Mojave Desert, California

K. Anderson,* S. Wells, and R. Graham

ABSTRACT

An existing model of desert pavement formation suggests desert pavement clasts rise vertically on an accreting eolian mantle and the underlying vesicular horizon coevolves with pavement formation. Results presented here support this model and provide a mechanism whereby eolian material is transported from the ground surface to ped interiors, thereby increasing the thickness of the vesicular horizon underlying desert pavements. Basaltic desert pavements in the Cima Volcanic Field are underlain by a vesicular horizon with strong coarse columnar and strong medium platy soil structure. Peds collected from three sites along a topographic gradient were subsampled into seven ped domains to quantify physical, chemical, and micromorphological properties within peds and along the topographic transect. Ped interiors have up to 40% clay and 12% $CaCO_3$ whereas sediments adhering to ped sides have <7% clay and 2% $CaCO_3$. Argillans and siltans lining platy surfaces in ped centers and bottoms indicate desert dust is translocated vertically along the macropores between peds and horizontally along platy boundaries to ped interiors. Once soils develop a strong columnar and platy structure, translocation to ped interiors is enhanced. Calibrated radiocarbon ages between 5440 and 5045 BP for Av ped centers suggest enhanced dust flux and pedogenesis occurred during the drier middle Holocene, an inference supported by luminescence dating and correlations with regional eolian chronologies.

Vesicular soil horizons commonly underlie desert pavements in the southwestern USA. The hypothesis that vesicular soils and associated desert pavements coevolve is supported by soil and stratigraphic field studies (McFadden et al., 1984, 1986; Wells et al., 1985, 1987; McDonald, 1994), geochemical and mineralogical investigations (McFadden et al., 1987), and cosmogenic dating procedures (Wells et al., 1995; Anderson and Wells, 1997). Fine-textured eolian material accumulating below surface clasts is pedogenically altered into a vesicular horizon. Continued eolian accumulation and pedogenesis leads to cumulic soil development below accretionary desert pavements. In the California Cima Volcanic Field, fine-textured desert dust is deposited on rubbly, basalt flow surfaces (Fig. 1). Through processes such as rain splash, surface wash, and translocation, dust continually accumulates below basaltic clasts, developing underlying vesicular horizons. Thus, pavement clasts have never been buried as was once assumed, but rather they rise upwards on a vertically accreting eolian mantle (Wells et al., 1987, 1995; McFadden et al., 1987). The processes by which dust is incorporated into vesicular horizons that underlie desert pavements are poorly understood. Chemical, physical, and micromorphological data on vesicular soil peds are presented here that help identify the processes of dust translocation and $CaCO_3$ accumulation within vesicular soil peds. Combining such data with age estimates of vesicular horizons provides insights into the mechanisms and timing of accretionary desert pavement formation.

The designation of vesicular horizons as Av does not easily conform to established criteria for horizon nomenclature. For example, although vesicular horizons have been designated Av since at least 1958 (Springer, 1958) and are presently designated as such in the soils literature (Peterson, 1980; McFadden et al., 1984, 1998), the Soil Survey Manual (Soil Survey Staff, 1993) reserves v for plinthite soil horizons. In addition, Av horizons exhibit complex properties commonly attributed to B horizons, such as enrichment in salts, $CaCO_3$, and translocated clay, but they also continuously incorporate new parent material from eolian additions, so might be designated as surface C horizons. Nevertheless, to avoid confusion and maintain convention, the Av designation is used here.

Early models of pavement formation focused on the exhumation of clasts by deflation (Springer, 1958; Jessup, 1960; Sharon, 1962; Symmons and Hemming, 1968; Cooke, 1970; Cooke and Warren, 1973; Mabbutt, 1977) or the shrink and swell heave of clasts to the ground surface (Springer, 1958; Johnson and Hester, 1972; Mabbutt, 1977). More recently, the association of vesicular soils with desert pavements on many landforms in the Southwest has been shown to support an accretionary mechanism of pavement development (McFadden et al., 1986; McDonald, 1994). The shift from assuming that desert pavements are zones of erosion to the realization that they can be zones of deposition has caused studies of landscape development in the Mojave Desert to refocus on dust accumulation and soil formation (McFadden et al., 1987; McDonald et al., 1994; Reheis and Kihl, 1995). Examples of accretionary desert pavements on basalt flows of the Cima Volcanic Field include up to 2 m of relatively clast-free, quartz-rich eolian sands between basalt flows and the overlying desert pavements. The uppermost horizon, generally an Av, represents an actively accreting physically and chemically complex layer.

K. Anderson, Box 6013, Bilby Research Center, Northern Arizona University, Flagstaff, AZ 86011; S.G. Wells, Desert Research Institute, 2215 Raggio Parkway, Reno, NV 89512; R.C. Graham, Dep. of Environmental Science, University of California, Riverside, CA 92521. Received 9 Feb. 2001. *Corresponding author (kirk.anderson@nau.edu).

Published in Soil Sci. Soc. Am. J. 66:878–887 (2002).

Abbreviations: AMS, accelerated mass spectrometry; BP, before present; EC, electrical conductivity; MRT, mean residence time; TL, thermoluminescence.

Vesicular horizons were recognized by Marbut (1935) to be common in arid environments. Recently, because of the unique properties and stratigraphic position of Av horizons at the ground surface, investigations are focusing on their effects on decreasing infiltration and increasing runoff, thereby influencing plant-water relationships, soil development, surficial processes, and landscape evolution (Musick, 1973; Wells et al., 1984, 1987; McDonald, 1994). Many researchers have investigated the processes of vesicle formation. Springer (1958) reproduced vesicles from sieved Av material after only five wet and dry cycles. The original Av properties of sieved soils return after 20 to 30 wetting and drying cycles; additional cycles increase the number, size, surface area, sphericity, and continuity of pores (Miller, 1971; Figueira and Stoops, 1983; Figueira, 1984). Evenari et al. (1974) determined that vesicle formation was influenced by the following: texture, wetting front displacement of soil air, surface sealing by crusts or clasts, air trapped when wet, and thermal expansion of air bubbles. Bouza et al. (1993) found that a high exchangeable Na percentage (>15) is an important vesicle formation factor for Patagonian soils. Vesicle stability is aided by $CaCO_3$ (Evenari et al., 1971) and clay coatings (Sullivan and Koppi, 1991). Observations of Av horizons in the Cima Volcanic Field reveal strong columnar and platy soil structure, with individual peds exhibiting textural and chemical zonation from ped exterior to ped interior locations. Qualitative field properties include sandy, low-$CaCO_3$ ped exteriors, and clayey $CaCO_3$-rich ped interiors (McFadden et al., 1984). Using micromorphic, physical, and chemical analyses, Anderson et al. (1994; this study) observed that vertical and horizontal translocation of fines and solute transport within the Av horizon increase the clay and $CaCO_3$ content of ped interiors.

Radiocarbon Age Estimates

Radiocarbon age estimates based on soil organic matter can be difficult to interpret, although interpretations can be enhanced using supporting independent data. Some researchers suggest that reliable radiocarbon dating of soils is possible (Scharpenseel, 1979; Goh et al., 1977), whereas others rely on the concept of mean residence time (MRT), where a radiocarbon age on soil organic matter is the mean age of all the organic C components added to the soil over time. The MRT concept assumes that younger C is continuously added to the soil, and that older C is lost by processes of decay, translocation, and mineralization. Mean residence time dates are minimum age estimates; soils are actually older than MRT ages suggest (Birkeland, 1999).

Because of the importance of determining soil age in geomorphic, pedogenic, and archeological settings, radiocarbon dating of soils continues to be used by many researchers. Wang et al. (1996) obtained model ages based on the ^{14}C activity and rates of younger C additions. Scharpenseel (1979) determined that careful consideration of sample selection and analysis of specific organic matter fractions (humic, fulvic, humin, humic-clay, etc.) could greatly improve interpretation of the radiocarbon age. However, because of the physical and chemical variability of soil processes, it remains unclear which humus fraction is the most representative of the initiation of soil genesis for any particular soil (Stout et al., 1981). Anderson and Wells (1997) reported consistent stratigraphic trends in accelerator mass spectrometry (AMS) radiocarbon ages of vesicular soils on an alluvial fan sequence in the Mojave Desert, suggesting that an age-dependent signature may be preserved in Av soils. Because of the uncertainties of AMS ages on soil organic matter, conservative interpretations using minimum mean residence times are useful within the context of supporting data, as discussed below.

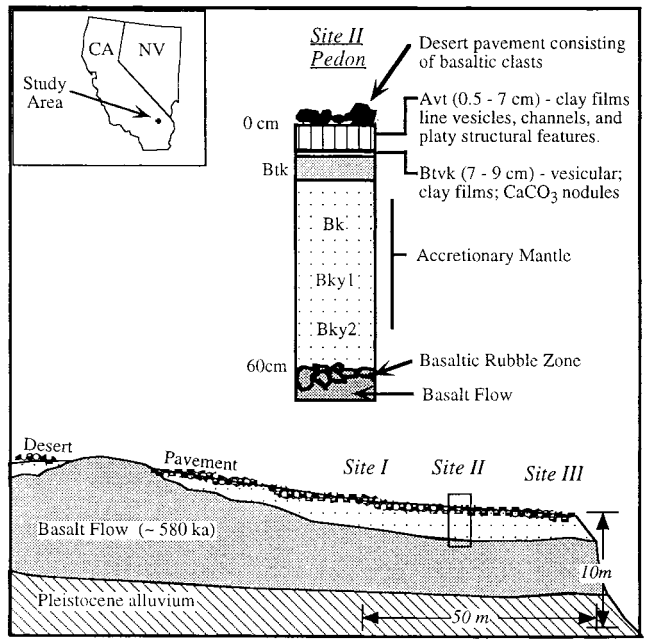

Fig. 1. Diagram showing stratigraphic and topographic relationships of Sites I, II, and III discussed in the text. Soil stratigraphy and brief descriptions of vesicular horizons show desert pavements overlying the accretionary eolian mantle. Note the location of the Cima Volcanic Field within the Mojave Desert.

The objectives of the research presented in this paper are to (i) identify the physical and chemical properties of Av peds underlying desert pavements and to (ii) determine the processes active within the Av horizon that may affect desert pavement formation. Detailed physical, chemical, and micromorphological analyses of Av peds enhance understanding of vesicular ped formation and the influence of Av horizon genesis on the development of accretionary desert pavements. Radiocarbon age estimates provide preliminary chronologic control in understanding the timing and rate of Av soil genesis for (i) comparisons with other dated soils, (ii) correlation with potentially important climatic periods, and (iii) determining whether Av horizons form during discrete periods of the geologic past, e.g., Pleistocene or Holocene.

MATERIALS AND METHODS

Site Characteristics

The study area is on a basalt flow in the Cima Volcanic Field, in the eastern Mojave Desert, that has been K-Ar dated

Table 1. Soil physical properties of Pedon II.

Horizon	Depth	Color Dry	Text.†	Structure‡	Consistence§ dry	moist	wet	HCl reaction¶	Clay films#	Pores††	Boundary‡‡	Other§§
	cm											
Typic Natrargid												
A	0–0.5	10YR 7/3	ls	m	lo	lo	sp,po	eo	na	na	as	na
Avt	0.5–7	10YR 7/3	l	3,c,cpr-2,f,pl	h	fr	s,p	e-es pin eo pex	4,n,po	3,vf-m,v+t,in	as	10YR 5/3, cl ped int.
Btvk	7–9	7.5YR 5/4	sicl	3,c,cpr-2,f,pl	sh-h	fr	s,p	es	2,n,po,br,co	3,vf-m,v,in	cs	na
Btk	9–16	7.5YR 5/4	l	1,f-m,abk	so	fr	ss,p	e mat.; ev nod.	1,n,pf	na	cw	7.5YR 8/4, vh, ev nodule
Bk	16–27	7.5YR 5/4	sl	1,f,abk	so	fr	ss,p	es mat. ev nod.	na	na	aw	7.5YR 8/4, vh, ev nodule
Bky1	27–40	7.5YR 5/6	sl	l,f,abk	lo	fr	ss,ps	eo-e	na	na	cw	asicular gypsum
Bky2	40–60	7.5YR 5/6	sl	m	lo	fr	ss,ps	ve mat. e nod.	na	na	cw	asicular gypsum

† ls, loamy sand; l, loam; sicl, silty clay loam; sl, sandy loam.
‡ m, massive; 3, strong; c, coarse; cpr, columnar; 2, moderate; f, fine; pl, platy; 1, weak; abk, angular blocky.
§ lo, loose; h, hard; sh, slightly hard; so, soft; fr, friable; so, non-sticky; po, non-plastic; s, sticky; p, plastic; ss, slightly sticky; ps, slightly plastic.
¶ eo, no reaction; ve, very slightly effervescent; e, slightly effervescent; es, strongly effervescent; ev, violently effervescent; pin, ped interior; pex, ped exterior; mat, matrix; nod, nodules.
# na, data not available; 4, many, n, thin; po, in pores; 2, few; br, bridges; co, coatings; pf, ped faces.
†† 3, many; vg, very fine; m, medium; v, vesicular; t, tubular; in, inped.
‡‡ a, abrupt; s, smooth; c, clear; w, wavy.
§§ c, common; 1, fine; int, interior; vh, very hard; ev, violent effervescent.

to 580 000 ± 160 000 yr old (Turrin et al., 1984). This flow was chosen for the following reasons:

1. Previous work provides a reliable pedologic framework (McFadden et al., 1987).
2. The thick (up to 2 m) eolian sheet and strongly developed columnar-structured vesicular horizon underlying the desert pavement provides a spectacular example of the accretionary model of desert pavement formation.
3. Age control for the underlying bedrock provides a maximum age for soil formation.

The basalt flow is 700 m above sea level and grades <2° to the west. The flow surface lies 10 m above the local base level as an erosional remnant (Fig. 1). Vegetation includes creosote bush [*Larrea tridentada* (Sessé & Moc. ex DC.) Coville], brittle bush (*Encelia farinosa*), mormon tea (*Ephedra trifurca*), and joshua tree (*Yucca brevifolia* Engelm.). Mean annual precipitation is between 12 and 25 cm and the mean annual temperature is 16 to 18°C (National Oceanic and Atomspheiric Administration [NOAA], 1978, p. 570). The basalt flow overlies Pleistocene alluvial fan gravels. A mantle of desert dust overlies the basalt flow (Fig. 1, Tables 1 and 2). Overlying the soil is a tightly interlocking desert pavement mosaic with millimeter-scale distances between well-varnished basaltic boulders and cobbles (McFadden et al., 1989). The <5-mm interclast spaces consist of basaltic fragments derived from local salt weathering of larger clasts and loose quartz-rich sand, silt, and clay eolian deposits. In some locations a thin, cohesive crust has formed. Pebble to small cobble-size clasts generally rest on the surface, whereas larger cobbles can be embedded in the Av horizon up to several centimeters. Poorly preserved pavement fabric occurs in areas where plant growth and animal activity are high. Relief across the surface is generally low, except where bedrock highs are exposed or where drainages have incised.

Sampling and Analysis

The Av horizon exhibits strong columnar parting to platy soil structure, allowing cohesive, columnar peds to be sampled individually. Three sample sites were chosen 25-m apart along a 50-m transect. Site II is downslope from Site I and upslope from Site III (Fig. 1). After pavement characteristics were described, pavement clasts were removed, which allowed collection of surface eolian material. Removal of surficial material revealed polygonal ped tops (Hunt et al., 1966; McFadden et al., 1987), ranging in both diameter and thickness from <1 to >10 cm. The soil at Site II, judged to be similar to the soils at Sites I and III, was described in detail (Soil Survey Staff, 1992, 1993); it is a Typic Natrargid consisting of Avt-Btvk-Btk-Bk-Bky1-Bky2 horizons (Fig. 1, Tables 1 and 2). The Av horizon has the following characteristics: 10YR hue, high value, and low chroma, reflecting the low organic matter content and slight oxidation; high silt and clay content; columnar and platy soil structure; horizon thickness between 5 and 10 cm; and numerous vesicular and channel pores. Ten to 12 peds from each site were collected and stored separately.

In the laboratory, ped domains were defined according to macroscopic characteristics such as Munsell color, texture, carbonate nodules, and soil structure. Peds were subsampled according to the defined domains to quantify physical and chemical variations within peds (Fig. 2). Based on variations in soil properties, the following seven distinct ped domains were identified and sampled: (1) material adhering to ped

Table 2. Soil chemical and physical properties of Pedon II.

Horizon	Depth	pH	EC†	$CaCO_3$	Sand	Silt	Clay	Silt + Clay	Texture‡
	cm		dS m^{-1}	%					
Typic Natrargid									
A	0–0.5	9.6	2.0	0.6	64	33	2	36	sl
Avt	0.5–7	10.1	3.7	6.4	33	38	30	67	cl
Btvk	7–9	9.7	10.1	5.3	na	na	na	na	na
Btk	9–16	9.1	17.2	12.7	42	37	20	58	l
Bk	16–27	8.9	18.4	5.6	53	36	11	47	sl
Bky1	27–40	8.3	24.1	8.8	53	44	3	48	sl
Bky2	40–60	8.3	23.2	16.3	na	na	na	na	na

† Electrical Conductivity.
‡ ls, loamy sand; l, loam; sicl, silty clay loam; sl, sandy loam; na, data not available.

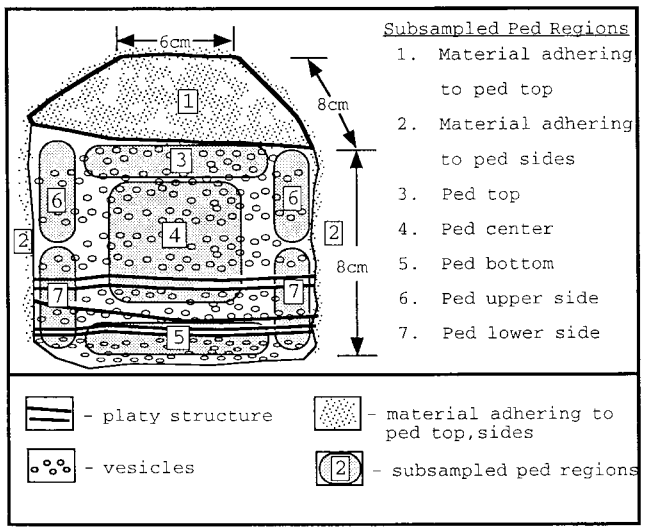

Fig. 2. Cross-section of ped interior showing vesicles, platy structure, and sampling strategy for Av peds, including subsampled Domains 1 through 7.

tops, (2) material adhering to ped sides, (3) ped top, (4) ped center, (5) ped bottom, (6) ped upper side, and (7) ped lower side (Fig. 2). Material adhering to ped surfaces (Domains 1 and 2) is generally <3 mm thick. Other sampled domains are generally between 1 and 3 cm thick, according to ped size. Subsampled ped domains from single peds provided too little material for subsequent laboratory analysis. Therefore, analyzed samples consisted of combined material from subsampled domains of several peds from each separate site. The exception to this was subsampling for the accelerator mass spectrometry radiocarbon analysis, which was performed on the center domain of two individual peds.

Particle size was determined by pipette analysis, after removal of salts and carbonate by sodium acetate digestion (Gee and Bauder, 1982). Calcium carbonate weight percentage was determined by the manometric method (Nelson, 1982). Electrical conductivity was measured on saturation extracts following Rhoades (1982). Soil pH was measured using a 1:1 ratio of soil/water paste. Large-format thin-sections (2 by 3 cm) were made on vertical sections of Av peds.

Bulk soil samples for AMS radiocarbon age determination were collected from ped centers at Sites I and II. Ped centers were sampled after trimming ped tops and sides until the center domain remained. Pretreatment for both samples included four steps: removal of macroscopic roots, acid washes in hot HCl to remove inorganic carbonates, alkali washes in NaOH to remove secondary organic acids, and final acid wash to neutralize the sample. These treatments were designed to remove the acid and alkali-soluble fraction, leaving the alkali-insoluble organic fraction for age determination. Pretreatment and analysis were performed by Beta Analytic, Inc. (Florida).

RESULTS

Micromorphology

Micromorphic analysis focused on properties of vesicles and channel pores, cutans, and carbonate accumulations. Evidence of plant and animal activity can be seen in thin sections, although rootlets, obvious animal burrows, and identifiable plant and animal remains are rare. Spherical vesicles occur in the sandy loam material that occupies exterior positions of ped tops and sides. Vesicles are not lined with clay or carbonate but are bounded by sand grains. Interior positions of ped tops, ped sides, and ped centers are dominated by irregularly shaped vesicles, compressed vertically and elongated horizontally. Many vesicles in these domains have subrounded to angular borders.

Channel pores are absent from exterior positions of ped tops and ped sides. Interior positions of ped tops, sides, and centers have interconnected channel pores, but they are commonly filled with sediment. In the lower positions of ped centers, ped lower sides, and ped bottoms, channel pores are common. Channel pores are often connected to the macropores between ped faces, forming a continuous conduit from the ground surface to interior ped domains. Channel pores in ped bottoms can be interconnected to a great extent, forming platy soil structure. Argillans and siltans commonly line the lower surfaces of platy structure, whereas the upper surfaces may have a coating of $CaCO_3$, called calcitans (Fig. 3).

Physical and Chemical Analysis

Macroscopically delineated domains within peds provide a basis for interpreting genetic processes from measured physical and chemical properties. General trends in particle-size distribution show that materials adhering to ped tops and sides have the lowest clay content, whereas ped centers have the highest (Table 3). Material adhering to ped tops and ped faces (Domains 1 and 2) consistently have the coarsest texture, sandy loam, with 2 to 7% clay. Ped top (Domain 3) textures range from silt loam to loam, having 19% clay and 45 to 50% silt, the highest silt concentration within the ped. Ped center textures range from loam to clay, with the highest clay (27 to 40%) and silt plus clay (70 to 71%) concentrations. Ped bottom textures are loam to clay loam, with generally the second highest clay concentrations. Upper-side textures are loam, with consistently low clay and high silt concentrations. Lower-side textures are clay loam and loam, illustrating an increase in clay concentration compared with upper sides.

The $CaCO_3$ content was determined for 18 subsamples, although this was not determined for material adhering to ped faces (Domain 2) because of small sample recovery (Table 3). The general trend is that material adhering to ped tops has the lowest $CaCO_3$ content and ped centers have the highest. Materials adhering to ped tops (Domain 1) have a $CaCO_3$ content ranging from 0.4 to 1.5%, and ped tops (Domain 3) range from 3.0 to 5.5%. Ped centers have a $CaCO_3$ content ranging from 6.0 to 12.1%, and those of ped bottoms are nearly as high, ranging from 6.1 to 8.6%. Upper and lower ped sides have similar $CaCO_3$ contents, with the lowest being 1.1% and the highest 3.3%.

Trends in particle-size distribution and $CaCO_3$ content also occur along the topographic transect, from Site I to Site III. The silt + clay content for material adhering to ped tops increases from 34% at the upper site (Site I) to 40% at the lower site (Site III). Similarly, the silt + clay content of material adhering to ped faces increases from 40 to 45% and the clay content for ped centers

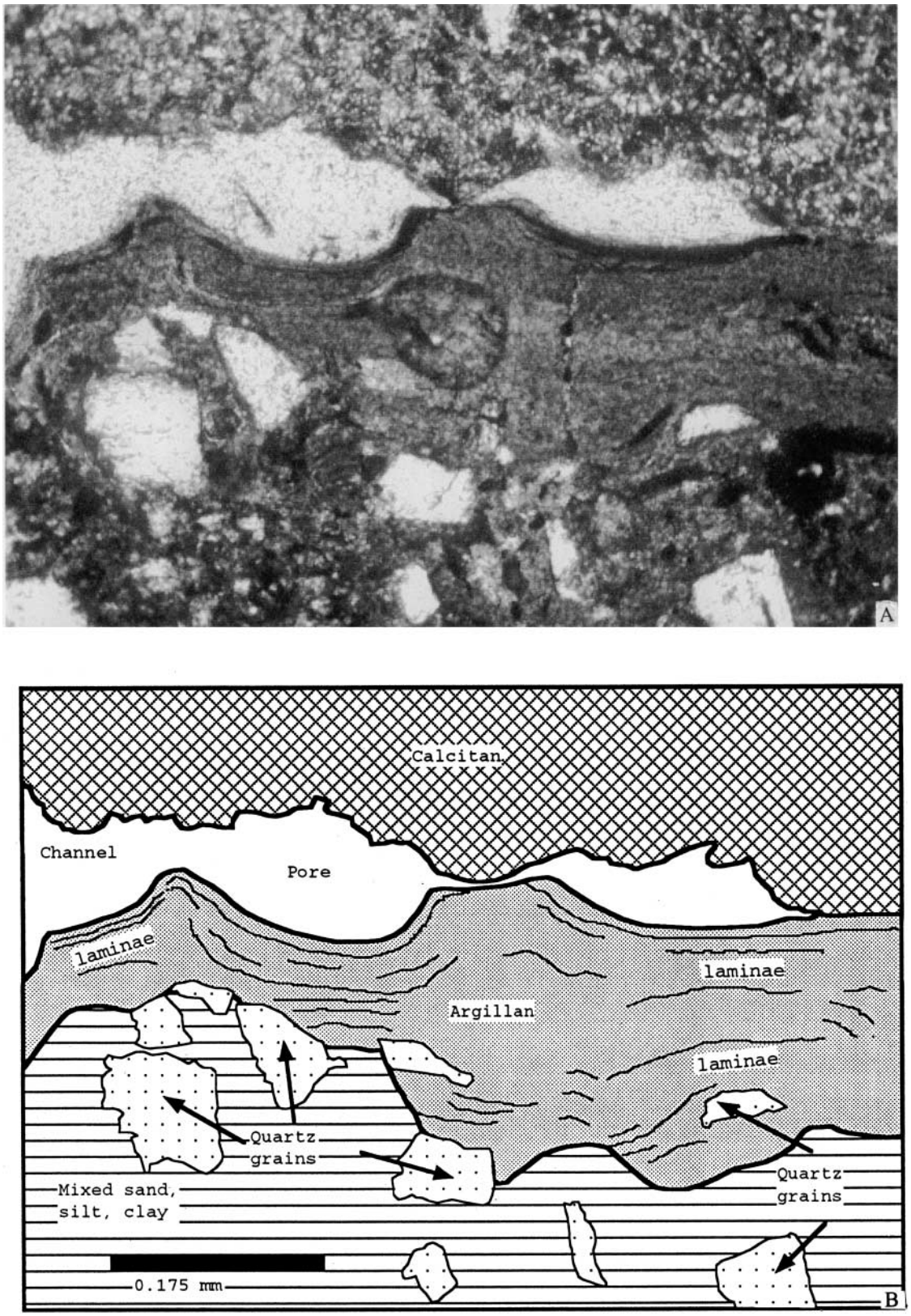

Fig. 3. (a) Photomicrograph of Av ped, with argillans indicating lateral translocation of dust to ped interiors. (b) Line drawing identifying major micromorphological features seen in Fig. 4a. See text for details.

increases from 27 to 40% between Site I and Site III. An increase in $CaCO_3$ content in downslope positions is noted for some peds in Domains 1, 3, and 4.

The results of pH and electrical conductivity (EC) analysis indicate alkaline and saline conditions (Table 3); the pH values are 9.2 or greater. No noticeable pat-

Table 3. Properties of subsampled vesicular horizon peds, Cima Volcanic Field.

Description	Domain	pH	EC†	$CaCO_3$	Sand	Silt	Slay	Silt + Clay	Texture‡
			dS cm^{-1}	%					
				Site I					
on ped top	1	9.2	1.3	0.4	66	40	4	34	sl
on ped face	2	na	na	na	60	33	7	40	sl
ped top	3	9.7	0.9	3.0	31	50	19	69	l
ped center	4	9.7	1.2	6.0	30	43	27	70	cl
ped bottom	5	9.6	1.9	6.1	34	44	22	66	l
upper side	6	9.6	2.2	2.1	31	47	21	69	l
lower side	7	9.5	1.1	3.3	32	38	29	68	cl
				Site II					
on ped top	1	9.6	2.0	0.6	64	33	2	36	sl
on ped face	2	na	na	na	58	35	7	42	sl
ped top	3	9.8	4.1	4.1	36	45	19	64	l
ped center	4	9.8	2.7	9.4	29	35	36	71	cl
ped bottom	5	9.8	2.5	8.6	33	34	33	67	cl
upper side	6	9.7	4.9	1.2	33	44	23	67	l
lower side	7	9.6	4.5	1.1	34	37	28	66	cl
				Site III					
on ped top	1	9.5	1.0	1.5	60	35	6	40	sl
on ped face	2	na	na	na	55	41	4	45	sl
ped top	3	9.8	2.1	5.5	34	48	19	66	l
ped center	4	9.3	9.4	12.1	29	31	40	71	c
ped bottom	5	9.4	7.7	7.4	32	37	32	68	cl
upper side	6	9.8	2.6	2.5	39	41	19	61	l
lower side	7	9.5	6.2	3.1	41	37	22	59	l

† Electrical conductivity.
‡ ls, loamy sand; l, loam; sicl, silty clay loam; sl, sandy loam.

tern in pH values occurred within peds or along the topographic transect. The EC values indicate saline conditions (EC > 4 dS m^{-1}) for many of the subsampled domains. Electrical conductivity of <2 dS m^{-1} occurs at all sites for material adhering to ped tops. The highest EC, 9.4 dS m^{-1}, is in the ped center of the lowest topographic position, Site III.

Radiocarbon Ages

Accelerator mass spectrometry radiocarbon analysis of fine-grained bulk soil samples from two subsampled ped centers provides similar age determinations. Conventional, uncalibrated radiocarbon ages are 4530 ± 50 BP (Beta-93902) at Site I, and 4570 ± 50 BP (Beta-91527) at Site II, 25 m apart. The two sigma (95% probability) tree-ring calibrated radiocarbon age estimate from Site I ranges from 5315 to 4995 years before present (BP), whereas the age from Site II ranges from 5440 to 5045 years BP. The calibrated radiocarbon ages, interpreted as MRTs, are comparable with a 5000 ± 1000 BP thermoluminescence age obtained from an Av horizon from a similar-aged basalt flow nearby (McFadden et al., 1998). They are also useful for discussing relationships with regional climatic (Spaulding, 1991) and eolian chronologies (Clarke, 1994).

DISCUSSION

Interpretation of Processes

The micromorphic characteristics of Av peds suggest that pore shape and continuity control the movement of material to ped interiors. Pore shapes include a variety of nonmatrix and interstructural pores (Soil Survey Staff, 1993). Nonmatrix pores occur as many very fine to medium (<0.5–5 mm) and occasionally coarse to very coarse (5–10 mm) elliptical and channel shapes. Elliptical pores may coalesce to form interconnected channels, which in turn may coalesce laterally to create platy soil structure. Platy structure in the center and bottom of columnar peds forms conduits connected to interstructural macropores between the columnar peds (Sullivan and Koppi, 1991). Interstructural pores are generally <0.5 cm wide and <10 cm long. Continuous conduits between interstructural macropores, and the channels and platy structure within the columnar peds, allow movement of sediment and water from the ground surface to ped interiors (Anderson et al., 1994). Incorporation of fine material within the ped probably occurs in two ways: transport in suspension by flowing water and matric suction. Flowing water transports the fines down vertical boundaries between peds and inward along the horizontal platy boundaries where clays accumulate as layered argillans. Further evidence for the transport of coarser material occurs in the form of microbedding, where millimeter-size channels contain deposits fining upward from sand to silt size. Matric suction draws water, solutes, and colloids to ped interiors and, as evapotranspiration dries the soil, $CaCO_3$ precipitates and clay remains. Anderson et al. (1994) indicated that sediment movement may be enhanced by the dispersive properties at the soil surface under high Na concentrations, and the flocculating properties of ped interiors and bottoms because of higher $CaCO_3$ concentrations.

Peds contain two domains of low clay and $CaCO_3$ content and five domains of higher clay and $CaCO_3$. Domains 1 and 2 have consistently lower clay and $CaCO_3$, and higher sand and silt content than the other domains. Ped centers have higher clay and $CaCO_3$ contents than all other ped domains, with up to 15 times the $CaCO_3$ concentration of exterior domains. Also, micromorphic investigations show argillans and calci-

tans lining horizontal channels and platy structural features in the lower portions of ped centers. Numerous irregular argillaceous and skeletal glaebules, and sand-filled granotubules in the upper portions of ped centers, indicate that this domain is relatively inactive with regard to the lateral translocation of sediment. Pedotubules filled with sandy material suggest that as upper ped centers become filled with sediment, the active zone of translocation shifts to lower ped domains, such as ped bottoms, where platy structures dominate.

Ped bottom domains have calcitans and layered argillans that represent distinct episodes of lateral clay translocation. Fining upward microbedding of silt and sand in ped bottoms indicates lateral sediment transport by suspension along the platy structure, which represents the active domain of lateral clay, silt, and sand translocation (see Fig. 3). Particle-size distribution, $CaCO_3$ content, and micromorphology of Av peds indicate that soluble and easily translocated constituents are preferentially removed from the outer two domains, consequently accumulating in the ped center, upper-side, lower-side, and bottom domains.

From a landscape-scale perspective, the $CaCO_3$ and clay data may provide insights into processes involved in the progressive reduction of relief on desert pavement surfaces. Incipient desert pavement landscapes have high constructional relief because of irregular topography inherited during initial emplacement, whereas mature pavement landscapes (middle to early Holocene and late Pleistocene) have reduced constructional relief (Wells et al., 1984; Bull, 1991). As pavements develop, topographic highs are reduced by salt weathering, rain splash, and colluviation, and topographic lows are filled with slopewash colluvial and eolian material. A measurable increase in both fines and $CaCO_3$ occurs from Site I to Site III (see Fig. 1). Site III, at the topographically lowest position, has consistently higher silt and clay contents for many ped domains, and clayey, $CaCO_3$-rich ped centers. Processes related to eolian deposition, surface transport of fines via overland flow, and subsurface transport of solutes to lower topographic positions may be responsible for the observed increases. The amount of clay and $CaCO_3$ incorporated into the topographically lower soils may increase the volume of material in these positions at a greater rate than slightly higher positions, thereby aiding in relief reduction of increasingly older desert pavement surfaces.

Ages of Av Peds

The processes of soil organic matter turnover and the subsequent addition of younger C to the soil system do not conform to the basic assumption that "carbon isotopic ratios have not been altered except by ^{14}C decay since the sampled material ceased to be an active part of the carbon reservoir" (Taylor, 1987). Because surface soils are an active part of the C reservoir, that is, younger C continues to be added to the soil during pedogenesis, they are very difficult to interpret. Radiocarbon ages on soils result from a mixture of material being added daily to fractions already in the soil, perhaps for thousands of years (Birkeland, 1999). Ages determined by bulk soil radiocarbon analysis are the average ages of all organic constituents in the soil, excluding those removed through pretreatment processes. In this context, MRTs do not represent steady-state systems because (i) the rates of additions and removals from the soil system may exhibit considerable temporal variation, and (ii) organic matter steady states are not attained in desert soils for a very long time (perhaps 300 000 yr) because of the relatively slow rates of organic matter additions and removals (Wang et al., 1996). Although such age determinations can be problematic (Stout et al., 1981), limited interpretations can be made using MRTs as minimum ages (Martel and Paul, 1974; Goh et al., 1977; Scharpenseel, 1979). Some researchers think that specific organic fractions can provide reliable oldest ages, and therefore the closest to the inception of soil genesis (Goh et al., 1977; Holliday et al., 1985), while others have determined that results are neither repeatable nor predictable from one soil to another (Gilet-Blein et al., 1980).

Most studies of soil radiocarbon ages identify the potential source of young organic C as continued growth and decay of in situ organic matter; few studies have attempted to account for organic matter additions from eolian sources, even though Reheis and Kihl (1995) measured up to 23.5% organic matter from dust traps in the Cima Volcanic Field and 45% in other portions of the Mojave Desert. Given that Av soils in the Cima Volcanic Field have eolian origins (McFadden et al., 1984, 1987, 1998), and that >20% of desert dust consists of organic matter, it must be assumed that a significant portion of organic matter added to desert soils is from eolian sources. Therefore, radiocarbon ages determined on any soil fraction must take this into account. Although the origin of organic C for bulk AMS analysis of the sampled Av peds remains unclear and only speculative, the possible sources, and interpretations, must attempt to explain the contributions from both in situ organic matter production and eolian additions.

A conservative interpretation of the AMS ages of Av peds can be made by comparing them with (i) an independent thermoluminescence (TL) age on Av soils, (ii) regional eolian activity, and (iii) periods of regional aridity. Preliminary inferences can thus be made regarding increased aridity, eolian activity, and enhanced vesicular soil formation during the middle Holocene.

Because the radiocarbon ages are interpreted as minimum age estimates, Av soil genesis probably began sometime prior to the 5440 to 4995 BP period. The 5000 ± 1000 BP TL age on quartz sands from an Av soil ped on a nearby 560 ka basalt flow (McFadden et al., 1998) supports these ages. The TL age on eolian quartz sand suggests an influx of eolian material onto the basalt flows in the Cima Volcanic Field during the middle Holocene, influencing vesicular soil formation by adding eolian fines to the developing Av horizon. Considering the organic matter data from Reheis et al. (1995) discussed above, it is possible that increased amounts of eolian organic matter were also added to the soil system during this time. This might explain the

correspondence between AMS and TL dating methods. Resulting ages from both methods could be interpreted as MRTs, given the dynamic processes active in the Av horizons, where organic matter and quartz grains are introduced to ped centers by the processes described earlier. Perhaps enough eolian organic matter was added during this time to lower the MRT age towards the ~5000-BP period.

The AMS and TL ages correspond to middle Holocene eolian activity at Silver Lake playa, 20 km upwind from the Cima Volcanic Field, where an eolian deposit is bracketed by 8350- and 3620-BP radiocarbon ages (Wells et al., 1989). Eolian deposits at the Kelso sand dunes, 10 km south of the project area, have been dated using optically stimulated luminescence to between 8420 and 3500 BP (Clarke, 1994). Spaulding (1991), using packrat midden data, suggested that a period of increased aridity occurred between ~8000 and 4000 BP in portions of the Mojave Desert.

The correspondence between AMS and TL dated Av horizons, with periods of increased eolian activity and regional aridity, suggests that the Av horizons investigated in this study may, in part, be influenced by a middle Holocene increase in eolian sediment and organic matter mobilization, deposition, and incorporation into surface Av soils. Wells et al. (1984, 1987) and McFadden et al. (1984, 1986) have suggested that desiccation of Silver Lake at the end of the Pleistocene dramatically increased the supply of dust to the Cima Volcanic Field, greatly affecting soil genesis and clast fracturing by increasing the amount of salt-rich eolian fines. They postulated that Av horizon development on the basalt flows in the Cima Volcanic Field may have been initiated or enhanced during the Pleistocene to Holocene transition and its increased eolian activity. The results from chemical, physical, and chronologic analyses presented above suggest that the middle Holocene may also have been a time of increased eolian deposition, affecting pedogenic development of the already formed Av horizon, with a corresponding influence on desert pavement formation.

Implications for Desert Pavement Formation

The processes of sediment incorporation below desert pavement on well-developed soils include clay and $CaCO_3$ accumulation in the upper several centimeters of the vesicular soil, causing horizon thickening and vertical accretion. Pavement clasts above this accreting Av horizon ride upward as material below continues to accumulate. Translocation and subsequent storage of eolian fines and salts in ped interiors provides a mechanism for cumulic soil development below pavement clasts, whereby material is added to the soil via lateral macropore conduits.

The initial phase of the process of eolian accumulation and pavement development remains speculative, but is probably influenced by adhesion and surface tension forces as water and sediment act to form laminar surface crusts that adhere to clast bottoms (Fig. 4). A second phase includes continued eolian influx and $CaCO_3$ accumulation, allowing formation of incipient vesicles

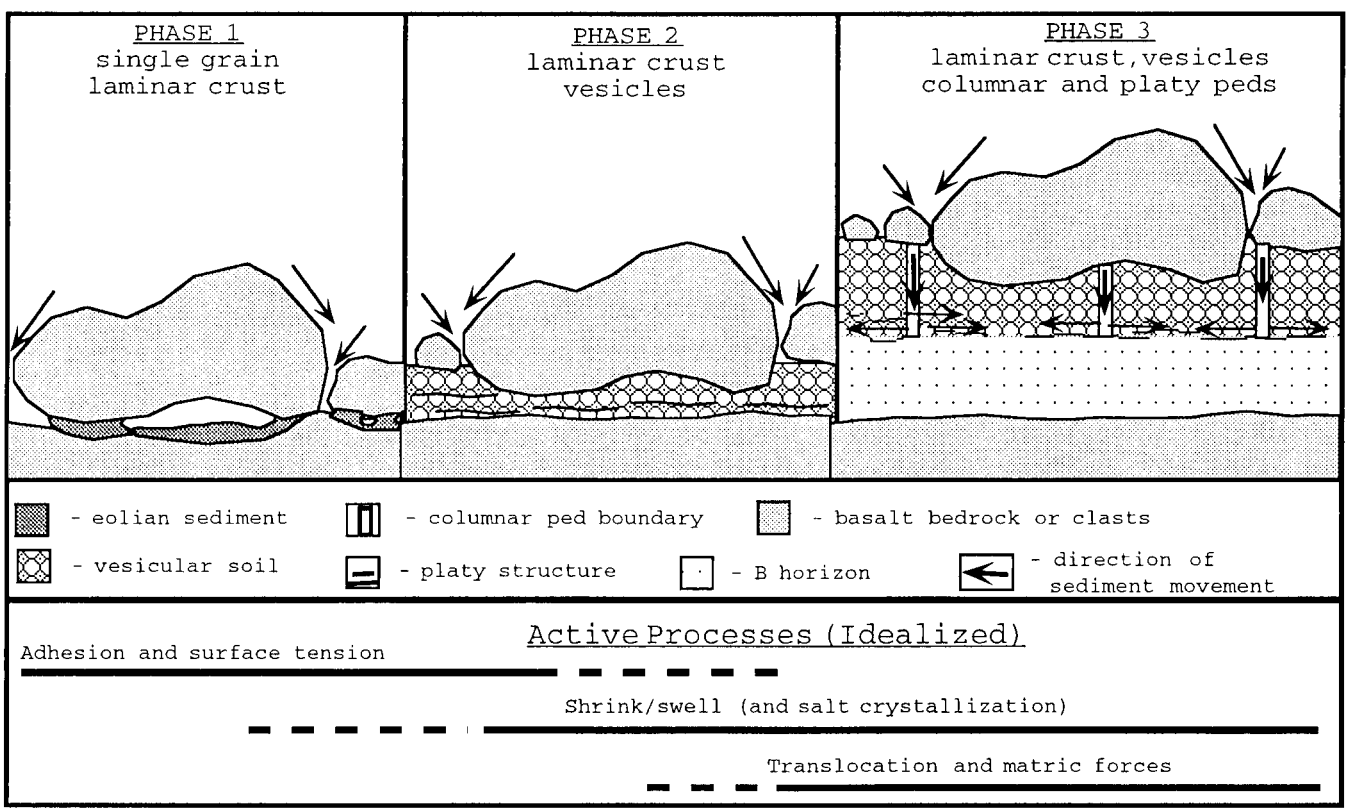

Fig. 4. Hypothesized phases of eolian accumulation and vesicular soil formation emphasizing the influence of pedogenic processes on lifting clasts and consequent formation of accretionary desert pavements. Size of largest clast shown is ~20 cm.

and pedogenic alteration. When soil properties reach certain physical and chemical thresholds—based largely on clay type and amount, and salt and Na concentration—shrinking and swelling processes may enhance clast lifting. A critical third phase of development is related to the formation of well-defined soil structure by shrink-swell activity, where vertical pores between columnar peds are connected to platy structure at ped bottoms. When this phase is attained, further eolian material can be added to both the ped tops and ped interior positions.

An increase in clay and $CaCO_3$ in Av horizons in topographic lows suggests that rates of cumulic soil development and associated pavement-clast lifting are accelerated in lower topographic positions, increasing the rate of relief reduction. In addition, as Av horizons continue to accumulate material, underlying soil horizons continue to develop as well, although the relations between Av genesis and subsoil development remain poorly understood. McFadden et al. (1987) found evidence that subsoil Btvk morphologies support the idea of the transformation of Av's to B horizons. However, increasing Av thickness with time on alluvial fan chronosequences seem to indicate rather long periods of Av stability and continued development (Anderson, 1999; McDonald, 1994). McDonald (1994) finds evidence that the Av horizon may, in fact, also rise vertically as material accumulates below both the pavement clasts and the existing Av layer.

Organic matter is continuously added to the soil by both in situ processes and eolian deposition. Preliminary interpretations of radiocarbon age estimates, and correlation with regional chronologies, suggest that the middle Holocene was a period of increased additions of datable material to the soil, notably quartz sand and organic C. Such an increase may provide enough material to cause a decrease of the mean residence time AMS and TL age-estimates, moving towards concordant chronologies. These concordant AMS and TL ages on Av peds correspond to a period of increased aridity and eolian activity throughout the Mojave Desert during the middle Holocene, with important influences on Av soil genesis and desert pavement development.

ACKNOWLEDGMENTS

This project was supported in part by National Science Foundation grant EAR-9205696, Geological Society of America student research grant, Institutional Proposal Assistance grant from the Desert Research Institute, Reno; Los Alamos National Laboratory, University of California Riverside, California State University Desert Studies Center, Zzyzx. I thank Diana Anderson and Yvonne Wood for field assistance; Eric McDonald and Les McFadden for very helpful discussions on desert pavement formation processes; and Louella Holter, Bilby Research Center, Northern Arizona University for assistance in preparing this manuscript. We also thank two anonymous reviewers for their helpful comments.

REFERENCES

Anderson, K.C., S.G. Wells, R.C. Graham, and L.D. McFadden. 1994. Processes of vertical accretion in the stone-free zone below desert pavements. p. 87. *In* GSA Abstracts with Programs 26, 7, Seattle, WA. Geological Society of America, Boulder, CO.

Anderson, K.C., and S.G. Wells. 1997. Processes responsible for the development of accretionary desert pavements in the southwestern USA. Fourth International Conf. on Geomorphology. University of Bologna, Bologna, Italy.

Birkeland, P.W. 1999. Soils and geomorphology. Oxford Univ. Press, New York.

Bouza, P., H.F. Del Valle, and P.A. Imbellone. 1993. Micromorphological, physical, and chemical characteristics of soil crust types of the Central Patagonia Region, Argentina. Arid Soil Res. Rehabil. 7:355–368.

Bull, W.B. 1991. Geomorphic responses to climatic change. Oxford Univ. Press, New York.

Clarke, M.L. 1994. Infra-red stimulated luminescence ages from aeolian sand and alluvial fan deposits from the eastern Mojave Desert, California. Quat. Geochron. 13:533–538.

Cooke, R.U. 1970. Stone pavements in deserts. Assoc. Am. Geog. 60:560–577.

Cooke, R.U., and A. Warren. 1973. Geomorphology in deserts. UCLA Press, Los Angeles, CA.

Evenari, M.L., L. Shannon, and N. Tadmor. 1971. The Negev: The challenge of the desert. Harvard Univ. Press, Cambridge, MA.

Evenari, M., D.H. Yaalon, and Y. Gutterman. 1974. Notes on soils with vesicular structure in deserts. Z. Geomorph. N.F. 18:1162–1172.

Figueira, H., and G. Stoops. 1983. Application of micromorphometric techniques to the experimental study of vesicular layer formation. Pedology 33:77–89.

Figueira, H. 1984. Horizonte vesicular: Morfologia y genesis en un aridisol del norte de la Patagonia. (In Spanish.) Cienci del Suelos 2:121–129.

Gee, G.W., and J.W. Bauder. 1982. Particle-size analysis. p. 383–411. *In* A. Klute (ed.) Methods of soil analysis. Part 1. 2nd ed. Agron. Monogr. 9. ASA, Madison, WI.

Gilet-Blein, N., G. Marien, and J. Evin. 1980. Unreliability of 14C dates from organic matter of soils. Radiocarbon 22:919–929.

Goh, K.M., B.P.J. Molloy, and T.A. Rafter. 1977. Radiocarbon dating of Quaternary loess deposits, Banks Peninsula, Canterbury, New Zealand. Quat. Res. 7:177–196.

Holliday, V.T., E. Johnson, H. Haas, and R. Stuckenrath. 1985. Radiocarbon ages from the Lubbock Lake Site: 1981–1984. Part 1. J. Plains Anthropological Soc. 30:277–291.

Hunt, C.B., T.W. Robinson, W.A. Bowles, and A.L. Washburn. 1966. Hydrologic basin, Death Valley California. USGS Prof. Paper 494-B. U.S. Gov. Print. Office, Washington, DC.

Jessup, R.W. 1960. The stoney tableland soils of the southeastern portion of the Australian arid zone and their evolutionary history. J. Soil Sci. 11:188–196.

Johnson, D.L., and N.C. Hester. 1972. Origin of stone pavements on Pleistocene marine terraces in California. Assoc. Am. Geog. Proc. 4:50–53.

Mabbutt, J.A. 1977. Desert landforms. MIT Press, Cambridge, MA.

Marbut, C.F. 1935. Soils of the United States. *In* Atlas of American agriculture. Part 3. USDA Bureau of Soils, Washington, DC.

Martel, Y.A., and E.A. Paul. 1974. The use of radiocarbon dating of organic matter in the study of soil genesis. Soil Sci. Soc. Am. Proc. 38:501–506.

McDonald, E.V. 1994. The relative influences of climatic change, desert dust, and lithologic control on soil-geomorphic processes and soil hydrology of calcic soils formed on Quaternary alluvial-fan deposits in the Mojave Desert, California. Ph.D. diss. Univ. of New Mexico.

McDonald, E.V., L.D. McFadden, and S.G. Wells. 1994. Quaternary stratigraphy of the Providence Mountains piedmont and preliminary age estimates and regional stratigraphic correlations of Quaternary deposits in the eastern Mojave Desert, California. p. 205–210. *In* S.F. McGill and T.M. Ross (ed.) Geological investigations of an active margin. GSA Cordilleran Section Guidebook, San Bernardino, CA.

McFadden, L.D., S.G. Wells, J.C. Dohrenwend, and B.D. Turrin. 1984. Cumulic soils formed in eolian parent materials on flows of the Cima volcanic field, Mojave Desert, California. p. 134–149. *In* J.C. Dohrenwend (ed.) Surficial geology of the eastern Mojave Desert, CA. GSA Guidebook, Reno, NV.

McFadden, L.D., S.G. Wells, and J.C. Dohrenwend. 1986. Influences of Quaternary climatic changes on processes of soil development

on desert loess deposits of the Cima volcanic field, CA. Catena 13:361–389.

McFadden, L.D., S.G. Wells, and M.J. Jercinovich. 1987. Influences of eolian and pedogenic processes on the origin and evolution of desert pavements. Geology 15:504–508.

McFadden, L.D., J.B. Ritter, and S.G. Wells. 1989. Use of multiparameter relative-age methods for age estimation and correlation of alluvial fan surfaces on a desert piedmont, eastern Mojave Desert, California. Quat. Res. 32:267–290.

McFadden, L.D., E.V. McDonald, S.G. Wells, K.C. Anderson, J. Quade, and S.L. Forman. 1998. The vesicular layer and carbonate collar of desert soils and pavements: Formation, age and relation to climate change. Geomorphology 24:101–145.

Miller, D.E. 1971. Formation of vesicular structure in soil. Soil Sci. Soc. Am. Proc. 35:635–637.

Musick, B.H. 1973. Barrenness of desert pavement in Yuma County, AZ. Arizona Academy of Sciences 10, Tucson, AZ.

Nelson, D.W. 1982. Carbonate and gypsum. p. 181–197. *In* A.L. Page et al. (ed.) Methods of soil analysis. Part 2. 2nd ed. Agron. Monogr. 9. ASA, Madison, WI.

National Oceanic and Atmospheric Administration. 1978. Climatologic data annual summary: Environmental data and information service. Vol. 82, No. 13. United States Department of Commerce, Washington, DC.

Peterson, F.F. 1980. Holocene desert soil formation under sodium, salt influence in a playa-margin environment. Quat. Res. 13:172–186.

Reheis, M.C., and R. Kihl. 1995. Dust deposition in southern Nevada and California, 1984–1989: Relations to climate, source area, and lithology. J. Geophys. Res. 100(D5):8893–8918.

Reheis, M.C., J.C. Goodmacher, J.W. Harden, L.D. McFadden, T.K. Rockwell, R.R. Shroba, J.M. Sowers, and E.M. Taylor. 1995. Quaternary soils and dust deposition in southern Nevada and California. GSA Bull. 107:1003–1022.

Rhoades, J.D. 1982. Soluble salts. p. 167–179. *In* A.L. Page et al. (ed.) Methods of soil analysis. Part 2. 2nd ed. Agron. Monogr. 9. ASA, Madison, WI.

Scharpenseel, W.H. 1979. Soil fraction dating. p. 277–305. *In* R. Berger and H. Suess (ed.) Radiocarbon dating. Proceedings of the Ninth International Conf., Univ. of Calif. Press, Berkeley, CA.

Sharon, D. 1962. On the nature of hamadas in Israel. Z. Geom. 6:129–147.

Soil Survey Staff. 1992. Keys to soil taxonomy. USDA Tech. Monogr. 19. USDA, Blacksburg, VA.

Soil Survey Staff. 1993. Soil survey manual. USDA Agric. Handb. 18. U.S. Gov. Print. Office, Washington, DC.

Spaulding, W.G. 1991. A middle Holocene vegetation record from the Mojave Desert of North America and its paleoclimatic significance. Quat. Res. 35:427–437.

Springer, M.E. 1958. Desert pavement and vesicular layer of some soils of the desert of the Lahontan Basin, Nevada. Soil Sci. Soc. Am. Proc. 22:63–66.

Stout, J.D., K.M. Goh, and T.A. Rafter. 1981. Chemistry and turnover of naturally occurring resistant organic compounds in soil. p. 1–73. *In* E.A. Paul and J.N. Ladd (ed.) Soil biochemistry, Vol. 5. Marcel Dekker, New York.

Sullivan, L.A., and A.J. Koppi. 1991. Morphology and genesis of silt and clay coatings in the vesicular layer of a desert loam soil. Aust. J. Soil Res. 29:579–586.

Symmons, P.M., and C.F. Hemming. 1968. A note on wind-stable stone mantles in the southern Sahara. Geog. J. 134:60–64.

Taylor, R.E. 1987. Radiocarbon dating: An archaeological perspective. Academic Press, Orlando, FL.

Turrin, B.D., J.C. Dohrenwend, S.G. Wells, and L.D. McFadden. 1984. Geochronology and eruptive history of the Cima volcanic field, eastern Mojave Desert, California. p. 88–100. *In* J.C. Dohrenwend (ed.) Surficial geology of the eastern Mojave Desert, California. GSA Guidebook, Reno, NV.

Wang, Y., R. Amundson, and S. Trumbore. 1996. Radiocarbon dating of soil organic matter. Quat. Res. 45:282–288.

Wells, S.G., J.C. Dohrenwend, L.D. McFadden, B.D. Turrin, and K.D. Mahrer. 1984. Types and rates of late Cenozoic geomorphic processes on lava flows of the Cima volcanic field, Mojave Desert. p. 116–133. *In* J.C. Dohrenwend (ed.) Surficial geology of the eastern Mojave Desert, California. GSA Guidebook, Reno, NV.

Wells, S.G., J.C. Dohrenwend, L.D. McFadden, B.D. Turrin, and K. Mahrer. 1985. Late Cenozoic landscape evolution on lava flow surfaces of the Cima volcanic field, Mojave Desert, California. GSA Bull. 96:1518–1529.

Wells, S.G., L.D. McFadden, and J.C. Dohrenwend. 1987. Influence of Late Quaternary climatic change on geomorphic and pedogenic processes on a desert piedmont, eastern Mojave Desert, California. Quat. Res. 27:130–146.

Wells, S.G., R.Y. Anderson, L.D. McFadden, W.J. Brown, Y. Enzel, and J.L. Miossec. 1989. Late Quaternary paleohydrology of the eastern Mojave River drainage basin, southern California: Quantitative assessment of the late Quaternary hydrologic cycle on a large arid watershed. p. 242–250. New Mexico Water Resour. Res. Inst. Tech. Comp. Report, Albuquerque, NM.

Wells, S.G., L.D. McFadden, J. Poths, and C.T. Olinger. 1995. Cosmogenic ^{3}He surface-exposure dating of stone pavements: Implications for landscape evolution in deserts. Geology 23:613–616.